

FINAL REPORT

January 1968

EXPERIMENT SO46

VISIBLE RADIATION POLARIZATION MEASUREMENTS

PHASE C

GPO PRICE \$
CFSTI PRICE(S) \$
Hard copy (HC)
Microfiche (MF)

ff 653 July 65

Prepared by

Space Sciences Laboratory
General Electric Company
King of Prussia, Pa.

Prepared for

University of California
Los Angeles, Calif.



FACILITY FORM 602

N 68-23527

(ACCESSION NUMBER)

(PAGES)

156
C1-65952

(NASA CR OR TMX OR AD NUMBER)

(THRU)

(CODE)

(CATEGORY)

UCLA P. O. 50772-0

NASA NAS 9-7267

FINAL REPORT

January, 1968

EXPERIMENT S046

VISIBLE RADIATION POLARIZATION MEASUREMENTS

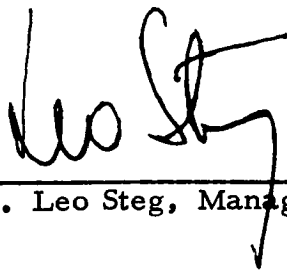
PHASE C

Prepared by:



Dr. R. T. Frost, Program Manager

Approved by:



Dr. Leo Steg, Manager

Space Sciences Laboratory, General Electric Co., King of Prussia, Pa.

Prepared for University of California, Los Angeles, Calif.

FOREWORD

This final report covers a four-month study carried out between September 7, 1967 and January 5, 1968. This work was conducted within the Space Sciences Laboratory with important contributions from Special Military Space Project and Spacecraft Department. Principal contributors to this work are listed below. This work was performed under UCLA contract number 50772-0 which was administered under the direction of the Space Science Department of the University of California, Los Angeles by Mr. Paul A. Lang.

Principal contributors were:

H. S. Blanchard
D. W. Grantham
E. L. Gray
H. W. Halsey
L. A. Lally
D. E. Lee
L. J. Napaluch
K. Pater
D. Shaw
R. W. Stanhouse
E. H. Stockhoff

TABLE OF CONTENTS

	<u>Page</u>
I. INTRODUCTION	1
II. GENERAL DESCRIPTION OF EXPERIMENT	1
A. Objective	1
B. Purpose	2
C. Advantage of Satellite Platform	2
D. Parameters to be Measured	3
E. General Instrument Requirements	3
F. Scanning Requirements	4
G. Experimental Procedures	5
III. INSTRUMENT DESIGN REQUIREMENTS	8
A. Measurement Precision	8
B. Dynamic Range	8
C. In-Flight Calibrations	9
D. Scan Accuracy Requirements	9
IV. PRELIMINARY DESIGN OF EQUIPMENT	11
A. General	11
B. Description of the Photopolarimeter Instrument	13
1. Mechanical Design	13
2. Optical Design	14
a) Identification of Optical Elements	14
b) Lenses	20
c) Lens Polarization	21
d) Window	26
e) Color Filters	26
f) Optical Beam Mixer	27
g) Photomultiplier Tube	35
h) Illumination of a Photomultiplier Cathode by a Fiber Optics Bundle	40
i) Effects of Thin Oil Films on Optical Com- ponents	49
3. Electrical Design	53
a) S046 Processor, Gain Change and Polarity Control Circuits	53

TABLE OF CONTENTS (Cont'd)

	<u>Page</u>
b) Photomultiplier Gain Stability in the Presence of Anode Current	56
c) High Voltage Supply Regulator	57
d) High Voltage Power Supply Design	59
4. Dynamic Range Considerations	63
a) Dynamic Range Calculations	63
b) Electronic Gain Settings and Gain Overlap Region	66
5. Noise and Other Measurement Errors	69
a) Statistical Noise Limitations and Other Measurement Errors	69
b) Non-Linearities, Maximum Permissible Phototube Currents, Required H. V. Regulation	74
6. In-Flight Calibrators	75
a) Internal Calibration Standard	75
b) Solar Calibrator Unit	81
c) Calibrations Based on an Integrating Sphere Method (Solar and Tungsten Lamp). Comparison with Imaging Systems	82
C. Scan Platform	90
1. Preliminary Selection	90
2. Gimbal System - Mechanical Description	92
a) Design Philosophy	92
b) Description of Gimbal Assembly	93
c) Description of Components	93
D. Pitch Scan Generator	96
1. Introduction	96
2. Simplified Block Diagram	97
3. Triangle Waveform Generator	99
4. Integrator	100
5. Squaring Circuit	100

TABLE OF CONTENTS (Cont'd)

	<u>Page</u>
6. Multiplier-Divider	105
7. Computer Operation	106
E. S046 Experiment System	111
1. Experiment Layout	111
2. Initial Weight Estimates	113
3. Initial Power Profile	113
F. Ground Support Equipment	117
1. General Description	117
2. System Requirements	117
3. Subsystem Requirements	117
a) Mechanical	117
b) Optical	119
c) Electrical	120
G. Photopolarimeter Breadboard Tests	121
1. General Description	121
2. Beam Trimming Procedure	124
3. Initial Polarization Measurements and Trimming of Breadboard Instrument	127
a) Low Polarization Source	128
b) Completely Plane Polarized Source	128
4. Scan Function Generator Breadboard	128
V. DOCUMENTATION	132
A. Preliminary Engineering Specifications	132
B. Management Plans	133
C. Functional Plans	134
D. Technical Reports	134
E. Preliminary Design Review	138
REFERENCES	140
APPENDIX (PIR 2290-41)	141

I. INTRODUCTION

This report summarizes results of a Phase C Study for AAP Experiment S046 carried out under contract with UCLA for the purpose of defining the experiment preliminary design, specifications, management plans for the flight hardware phase of the program, and providing a mockup of the experiment. The preliminary design of the experiment, critical parts of which were mocked up and tested in the laboratory, was the subject of a Preliminary Design Review held at the General Electric Space Sciences Laboratory on December 4 and 5, 1967. Engineering drawings, specifications and management plans for a Phase D contract have been submitted for UCLA approval. The primary purpose of this final report is to summarize the many technical analyses and tests which were made in a coherent form for future reference.

II. GENERAL DESCRIPTION OF EXPERIMENT

A. Objective

The objective of the experiment is to make quantitative measurements of intensity and polarization of the light emerging from the top of the earth's atmosphere as a function of wavelength and to relate these to a theoretical treatment of radiation transfer in the earth's atmosphere, including the effects of surface or cloud reflection. Recent calculations are available which predict the Stokes parameters of the emerging radiation as a function of sun angle and viewing angle when viewing extensive areas of the earth over which the reflecting and polarizing properties are reasonably uniform. These calculations depend upon detailed measurements of reflecting and polarizing properties of various materials, such as sand, clay, and grass, when illuminated by sunlight. There are sufficient data available on a few types of earth surface materials which would allow a fundamental interpretation of selected earth radiation measurements taken in space under conditions of low atmospheric turbidity. The proposed experiment would, in addition, furnish much of the cloud reflectance data required in such a quantitative program. Studies which have been performed to date show that the measurement of polarization of the radiation is quite crucial to interpreting the emergent radiation flux in terms of surface and atmospheric components. Attempts can be made to relate the measurements, in certain cases, to the effects of aerosol scattering in the atmosphere since the molecular scattering contribution may be assumed known. If sufficient data are obtained with high precision, these can serve as a basis for the development of inversion methods to deduce gross aerosol properties and distributions from satellite measurements. Initial analysis of the data can be made prior to such development of inversion techniques by determining which aerosol models give a best fit to the measurements.

B. Purpose

The purpose of the experiment is to provide experimental data for a quantitative study of the radiation emerging from the top of the earth's atmosphere over typical areas of the earth's surface. This would provide new data as a firm foundation for various applications programs such as meteorology and earth reconnaissance.

The measurements to be taken will include a number of selected targets for which "ground truth" optical measurements are available, such as deserts and grasslands in four-wavelength intervals centered at 3800, 4400, 5000 and 5800Å. The predetermined earth areas will be identified by the astronaut, who will start an automatic scan which will point the photopolarimeter continuously at the area as the space vehicle passes over, thus obtaining a continuous sweep over angles of observation at a nearly constant sun angle.

Another application of results of this program would be to furnish a quantitative experimental basis for understanding the contrast degradation caused by the attenuation and brightness of the earth's atmosphere. The work would thus support programs of multicolor photographic reconnaissance, for which atmospheric contrast degradation can become important at the shorter wavelengths or at oblique angles.

It should be pointed out that much effort has been expended recently in devising analytical and numerical schemes to extend existing solutions to the equation of radiative transfer. For instance, Sekera^(1,2) has extended the solution to the Rayleigh scattering problem for arbitrary optical thicknesses, and has also made allowance for imperfect scattering. In connection with aerosol scattering, Arking and Potter⁽³⁾ have developed computer programs to compute the intensity distribution of emergent radiation for quite arbitrary scattering phase functions. The availability of such programs makes the measurement program all the more attractive since scattering processes in a "real" atmosphere may now be more accurately described. Some theoretical studies have been initiated toward solving the inversion problem. Sekera⁽⁴⁾ has shown how independent estimates of optical thickness and albedo of a Lambert Surface can be derived from satellite measurements, assuming a molecular scattering atmosphere.

C. Advantage of Satellite Platform

Observations of clouds and other targets from a manned satellite have an advantage possessed by no other means of investigation available at the present time. An unmanned satellite (such as TIROS or Nimbus) lacks an easy visual verification of the uniformity and identity of the selected target area. Moreover, it is difficult or impossible to check the calibration of the instruments once they have been placed into orbit. While balloon measurements do allow post-flight calibration, they also are incapable of selecting a target

and keeping an instrument pointed at it. A balloon also has the added restriction of taking observations for only a short period of time, and over a limited area which may not contain suitable cloud distributions.

Use of a high altitude aircraft makes possible both the aiming and the recovery of the instrument in optimum operating condition. However, instruments at normal aircraft altitudes are not sufficient to determine completely the reflected radiation passing to space. Unless a large number of flights are made, observations from aircraft are also relatively restricted as to time and place.

Use of manned satellites as a platform for observations avoids almost all of these difficulties. The instrument may be aimed at specific targets at a series of angles; its calibration may be checked both during and after the flight; and a wide variety of surface targets and clouds may be observed over the earth for a period of time adequate to the successful conclusion of the experiment.

D. Parameters to be Measured

The parameters of the radiation to be measured are the first three Stoke's parameters I, Q, U. These parameters are to be measured in four spectral intervals once per second as the instrument is pointed continuously at a fixed target. The viewing angle is to be continuously measured.

In addition to the measured quantities, the following parameters are to be recorded:

- . Time (Spacecraft location is a derived quantity.)
- . Spacecraft Attitude.
- . Photometer filters in optical path.
- . Astronaut's spoken comments regarding target identification, obscuration, calibration, and progress of experiment.
- . A photograph taken of the target area as it passes beneath the vehicle.

E. General Instrument Requirements

The spectral intervals are defined by interference filters having a bandwidth of about 100\AA and an average transmission of about 30%. The wavelengths chosen are 3800, 4400, 5000 and 5800\AA .

The field of view of the instrument is specified to be a 3° total cone angle and sets a minimum size for the area of targets viewed over which the target optical properties should be reasonably uniform. At 250 miles altitude this gives a target area of diameter 12 miles for targets near the nadir. Interpretation of the measurements in terms of ground reflection and polarization

properties and atmospheric scattering properties will be significant if target optical properties are relatively constant over the area of target viewed. Another limitation to the size of the field of view is the necessity to associate measurements with a unique viewing direction. A complete set of measurements is made in a time interval of one second, during which time the maximum change in viewing angle will be 2° . This is consistent with a field of view of 3° . A 3° field of view in conjunction with a light collecting area of about 1 square inch gives an adequate signal-to-noise ratio when a complete set of measurements is taken in one second under the lowest illumination and albedo conditions assumed.

Since relatively small changes in polarization can be important for interpreting atmospheric scattering details, such as depolarization due to aerosols, it is necessary that the polarization measurements be made with high precision. One percent is specified when measuring polarization as small as 5%.

F. Scanning Requirements

The tracking requirements for a scan platform in order to track an earth fixed target from a satellite in low altitude orbit have been derived in an appendix. This work restricts attention to the case where targets are selected which pass directly under the vehicle track. This restriction simplifies the tracking requirements considerably. Nearly exact expressions were derived for the required tracking angles and rates in zenith angle and azimuth and from these simpler expressions were derived which are valid to an accuracy of 0.1° or so. This work includes the effects of orbit inclination, precession adjustments, eccentricity, period, target latitude and height, and earth oblateness. It is found that all these parameters can be taken account of by four adjustments to the scan mechanism.

The required instrument pointing direction in terms of nadir angle z and azimuth ξ in the local vehicle horizon system is given by:

$$(1) \quad \sin(z + \eta) = U \sin z$$

$$\text{or } \sin z = \sin \eta / \sqrt{1 + U^2 - 2U \cos \eta}$$

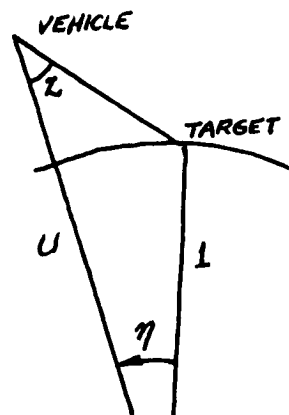
$$(2) \quad \eta = g(t - t_0) + \eta_0$$

$$(3) \quad \xi = k \sqrt{\cos^2 L_T - \cos^2 i}$$

In these equations the desired scan platform pointing direction is given by the angles z and ξ . z is the angle from the local nadir at the satellite position and ξ is the out-of-plane azimuth angle measured from the instantaneous orbit plane in inertial space.

The extreme range of z is

$$-60^\circ \leq z \leq +60^\circ$$



The orbit inclination is denoted by i . The parameter U is the ratio of the distances from earth center to satellite and earth center to target. For a circular 250 mile orbit with the target located on the surface of a spherical earth, U has the nominal value 1.06. As discussed in the appendix, it can be varied to take account of different orbit heights, orbit eccentricity, earth oblateness, and targets at a height above the geoid.

η is the angle subtended at the center of the earth between the satellite position and target position. It normally will range over the values $-7^\circ \leq \eta \leq +7^\circ$ for an orbit height 250nm during a given scan and varies linearly according to Eq. 2. g is simply the time rate of change of η and for a circular orbit and a target located on the spherical earth is a constant during the mission. An adjustment can be made in g to take account of orbit height, orbit eccentricity, earth oblateness, orbit inclination, and targets at a height above the geoid. The detailed dependence of g upon these parameters is discussed in the appendix.

$t-t_0$ is the time measured from the beginning of the scan. This will be furnished by an integrator switched on to start the scan motion. η_0 is the initial value of η at the beginning of the scan. It may vary by a few percent depending on orbit height, orbit eccentricity, earth oblateness, and for targets at a height above the geoid.

The out-of-plane pointing angle ξ is given by Eq. 3 and is essentially constant during a given scan. The orbit inclination is denoted by i and the target latitude by L_T . k is a parameter which depends upon the orbit period and inclination but is a constant in a circular orbit (see appendix). For target latitudes near $\pm i$, ξ is 0. For equatorial targets and $i = 60^\circ$, $\xi = \pm 3.5^\circ$. This fixed azimuth will be set into the scan gimbals at the beginning of each target measurement.

The photopolarimeter field of view is a 3° cone. The size and shape of the region on the earth's surface viewed will vary from a circle of diameter 12 miles to an ellipse with major and minor axes of about 48 and 24 miles respectively. In addition, vehicle stabilization is expected to be good only to about $.5^\circ$. For both these reasons the scan mechanism has been designed to give an error less than 0.5° .

G. Experimental Procedures

The predicted time of passes over the selected target areas will be relayed to the astronaut, along with a report on the local turbidity and weather conditions in the target area. The astronaut will recognize the target area as it comes into view in a view finder bore sighted with the photopolarimeter when the polarimeter is in the "start scan" position at 60° nadir angle. The astronaut can make a real time decision to select the optimum position of the target area passing behind the view finder cross hair reticule; at the selected

moment he will press a button to begin the instrument scan which has been preprogrammed to maintain the selected target area within the polarimeter field of view with the required accuracy. Besides real time astronaut judgement in optimum target selection in terms of visual observation of scattered clouds, etc., a second criterion for starting the instrument scan will be the attainment of a relatively constant reading of the unpolarized light intensity at one of the selected wavelengths displayed visually on a meter movement on the astronaut's control panel.

The instrument will make readings of the first three Stokes parameters for each spectral interval in rapid succession as the photopolarimeter continues to point at the preselected target.

Target areas will normally be selected such that the spacecraft passes nearly overhead. In this way, measurements will be obtained over nearly the full range of viewing angles relative to the surface normal. (A repetition of measurements on the same or similar areas with the sun at different zenith angles is desirable.) For low orbit heights, approximately six minutes of time will be consumed for a complete measurement. It is expected that suitable targets can be selected such that several can be observed during any single orbit. As the orbit plane precesses, some of these targets could be remeasured as the sun's angle of illumination changes.

Selection of the cloud areas to be observed will be left to the discretion of the astronauts, in accordance with the requirements for the number and types of cloud types. The astronaut will be briefed concerning the specific needs for cloud types and the location of the clouds with respect to the orbital track. During the flight, the astronaut will be advised with regard to areas which contain clouds suitable to the experiment; these advisories will be based upon forecasts derived from conventional meteorological data and from satellite photographs. The Environmental Science Services Administration maintains a meteorological support group for manned space missions, which would be supplemented by personnel associated with the experimenters for the specific support of this experiment.

A wide variety of cloud types is desired, including different types of low, middle, and high clouds; examples are low stratus, stratocumulus, cumulus, cumulonimbus, extensive layers of altostratus, alto cumulus, thick and thin cirrus, and tropical storms. It is also important that observations be obtained at radically different local sun angles.

Some liberty of action should be allowed to the astronaut to choose additional targets when time is available, and he should be trained in the selection of alternate targets. Examples would be extensive cloud covers, various regions of the sea for which current sea state information is available and extensive snow covered regions, if these can be observed in high latitude locations.

A color photograph will be taken of each area by a camera bore-sighted to the photopolarimeter. The camera can be 35 mm with an 18° field of view and should use color film. The picture will be taken automatically as the scan platform passes through zero nadir angle.

For a 30° inclined orbit, the orbit precession rate will be about 3.4° /day. During a 14 day mission, the orbit precession will total about 47° to the westward. During this same period, the sun will move eastward about 14° relative to an inertial coordinate system. Thus the orbit plane will move 61° with respect to the sun's meridian during a two week mission, exposing the targets chosen to a large range of sun angles when viewed repetitively. For a polar orbit a considerable range of sun angles on a given target position will still be achieved over longer periods due to the sun's motion on the celestial sphere. A 61° motion relative to the orbit plane will still give a sun's zenith angle variation of 61° for targets whose latitude is nearly equal to the sun's declination.

III. INSTRUMENT DESIGN REQUIREMENTS

The more important instrument design problems will be discussed in this section. Solutions have been found for all of these problems in the instrument Preliminary Design described in Section III, although careful final engineering design and testing are still required before the existing breadboard instrument model can be translated into a final flight instrument design.

A. Measurement Precision

The most difficult requirement is considered to be that for measurement of polarization with an accuracy of $\pm 1\%$ down to a polarization of 5%, leading to a limiting instrument sensitivity of $\pm 0.05\%$. To meet this requirement in a high speed instrument it is necessary to use a single detector to measure the intensity of the separate polarized beams such as A, B, and to measure the beam differences directly at the front end of the electronic data processor. This approach minimizes the effects of detector drift and reduces the precision requirements on the electronics to practical values. A system utilizing separate detectors and electronics for the separate beams A, B must preserve stability of detectors and electronics to within approximately 0.07% between calibrations. Using photomultiplier detectors and state-of-the-art space qualified high voltage supplies together with currently available signal processing techniques, such a requirement is considered unrealistic. Although the lack of such stability may be partially compensated by separate calibration for each measurement made, as in the manner of an instrument recently designed at the University of Arizona,⁽⁵⁾ such an approach is considered impractical for a high speed instrument capable of high tracking rates, such as required in the present experiment.

B. Dynamic Range

The wide dynamic range required for the instrument, coupled with a desired relative measurement accuracy of $\pm 1\%$, dictates that linear signal processing be employed with automatic electronic gain changing provided to handle the dynamic range 1660:1 expected for the beam difference signals corresponding to the Stokes parameters Q and U in the range where 1% accuracy is required. The intensity I will vary by the smaller factor 83:1 for the range of conditions assumed for lighting and albedo.

The dynamic range of the instrument has been set as 10,000:1 for the Stokes' parameters Q and U. This provides a large margin over the signal strengths calculated on the assumptions:

range of solar illumination angles	$0^\circ \leq \theta \leq 80^\circ$
range of viewing angles	$-60^\circ \leq \theta \leq +60^\circ$
range of target albedos	$0.03 \leq A \leq 1.00$
atmospheric scattering model	Rayleigh

This model predicts a maximum and minimum for the intensity I of $6.7 \cdot 10^{-2}$ and $8.2 \times 10^{-4} \text{ w cm}^{-2} \mu^{-1} \text{ ster}^{-1}$ respectively.

C. In-Flight Calibrations

To insure that data is taken with the required accuracy, in-flight calibrations will be taken at the beginning and end of each complete target scan. The calibration source will furnish a uniformly illuminated field of view to the photopolarimeter with relatively low polarization to allow calibration near zero polarization. The absolute value of the light level will be sufficient to allow intercomparison of instrument response in each of the selected wavelength intervals and will be sufficiently stable to allow reduction of the measured Stokes parameters to an absolute basis in terms of ground calibrations referred to primary calibration standards.

A low power (12 w) lamp utilizing the tungsten-iodine cycle has been selected to provide sufficient intensity and avoid problems of envelope darkening due to tungsten deposition.

In order to provide a check on the tungsten bulb calibrator, and more fundamentally, to provide a basis for direct comparison of the earth reflected fluxes with those incident from the sun, an in-flight solar calibrator is also provided. Periodically, the photopolarimeter will view the sun directly through a dense calibrated filter in such a way that the uniform flux entering the photopolarimeter will be calculable in terms of the solar flux. This will require a reorientation of the entire carrier vehicle and rotation of the photopolarimeter pitch angle to a "sun calibrate" position.

D. Scan Accuracy Requirements

Because a given target must be tracked without continuous observation and correction of the tracking error, it is necessary that the scan angle function generator deliver a precise command to the scan platform. It is desirable that the scan platform pointing not cause a large increase in the pointing errors associated with vehicle attitude motions, assumed to be limited to the order of 0.5° during the target scan period. Thus, the error contributed by the scan function generator must be significantly less than this value to allow for scan platform tracking errors.

Differentiation of the expression (1) given in Section II-F gives the error dz in scan angle z which will result from an error $d\eta$ in the angle η . For $z = 60^\circ$, $dz/d\eta = 20$. Assuming that the function generator will unavoidably generate an error as input to the circuits which simulate equation (1), we can see that the requirements stated can be written as

$$\Delta\eta = \frac{1}{20} \quad \Delta z < \frac{1}{20} \cdot \left(\frac{1}{2}\right)^0 = .025^\circ$$

This leads to a fractional error requirement for the electrical simulation of η of

$$\frac{\Delta\eta}{\eta} < \frac{.025^\circ}{6^\circ} = .004 = 0.4\%.$$

Simulation of equation (2) by means of electrical integration $\eta = g \int d(t-t_0) + \eta_0$ on an analogue compute shows that it will be easy to far exceed this specification, but that careful selection of the feedback capacitor and temperature control of critical components will be required.

In the preliminary design described in following sections, equation (1) is simulated with the aid of sine/cosine resolvers mounted on the instrument pitch axis and by use of multiplier/divider circuits which have been breadboarded and tested as part of this program. It was found that the overall accuracy of the scan motion will equal or exceed specifications.

IV. PRELIMINARY DESIGN OF EQUIPMENT

A. General

The S046 Experiments Preliminary Design is a result of numerous specialized studies, laboratory tests and tradeoff studies. Analyses supporting the design of most of the components of the experiment will be found in following Sections of this report. Figure 1 is a block diagram of the baseline system and a photograph of a mockup showing size and shape of the experiment. The three main subsystems are the photopolarimeter instrument, the mechanical scan platform, and the in-flight calibrator unit. The scan function generator is a separable segment of the Mechanical Scan Platform. As a part of the test verification of the preliminary design, a breadboard model was assembled to demonstrate the performance of the instrument and the scan function generator. The S046 experiment package is described in summary as follows:

Multispectral, Two Axis Scanning Photopolarimeter

Overall Size: Max. 12"x12"x24"

Weight: Max. 40 lbs.

Power: Max. 45 watts

Warmup: 12 watts

Average Operating: 20 watts

Total kwh: 4 kwh (14 da.)

Stokes Parameters Measured: I, Q, U

Spectral Regions:

3800 Angstroms

4400 "

5000 "

5800 "

Spectral Bandwidth (50%):

100-150 Angstroms

Field of View: $3.0^\circ \pm 0.1^\circ$

No. of Optical Barrels: 3

No. of Polarizing Prisms: 2

Optical Window Material: Quartz

Optical Aperture: Variable - 3 step

Beam Selection: Electromechanical

Color Wheel: Intermittent

(Geneva) Drive

Instrument Mechanical Drives:

Sealed Lubricated

Type of Electronics: Hybrid Circuitry

Pitch Axis Rotation: $+90^\circ$ to -75°

Pitch Axis Rate: $5^\circ/\text{sec.}$ max.

Yaw Axis Rotation: $\pm 4^\circ$

Pitch & Yaw Position Accuracy:
 $\pm 0.5^\circ$

Output Signal: Differential dc

Output Signal Accuracy: 1.0% of
reading

Number of Signal Outputs: 15

(3 Stokes Parameters x 4 Colors)

1 channel for instrument & filter
gain settings

2 channels for platform scan angles

Data Rate - Signal Outputs 16/sec.

Digitizing Requirements - 10 bits

No. of Housekeeping Lines: 20

Data Rate - Housekeeping - 2/sec.

Digitizing Requirements: 8 bits

Scan Platform Mechanical Drives:

Modified Polaris & Poisedon

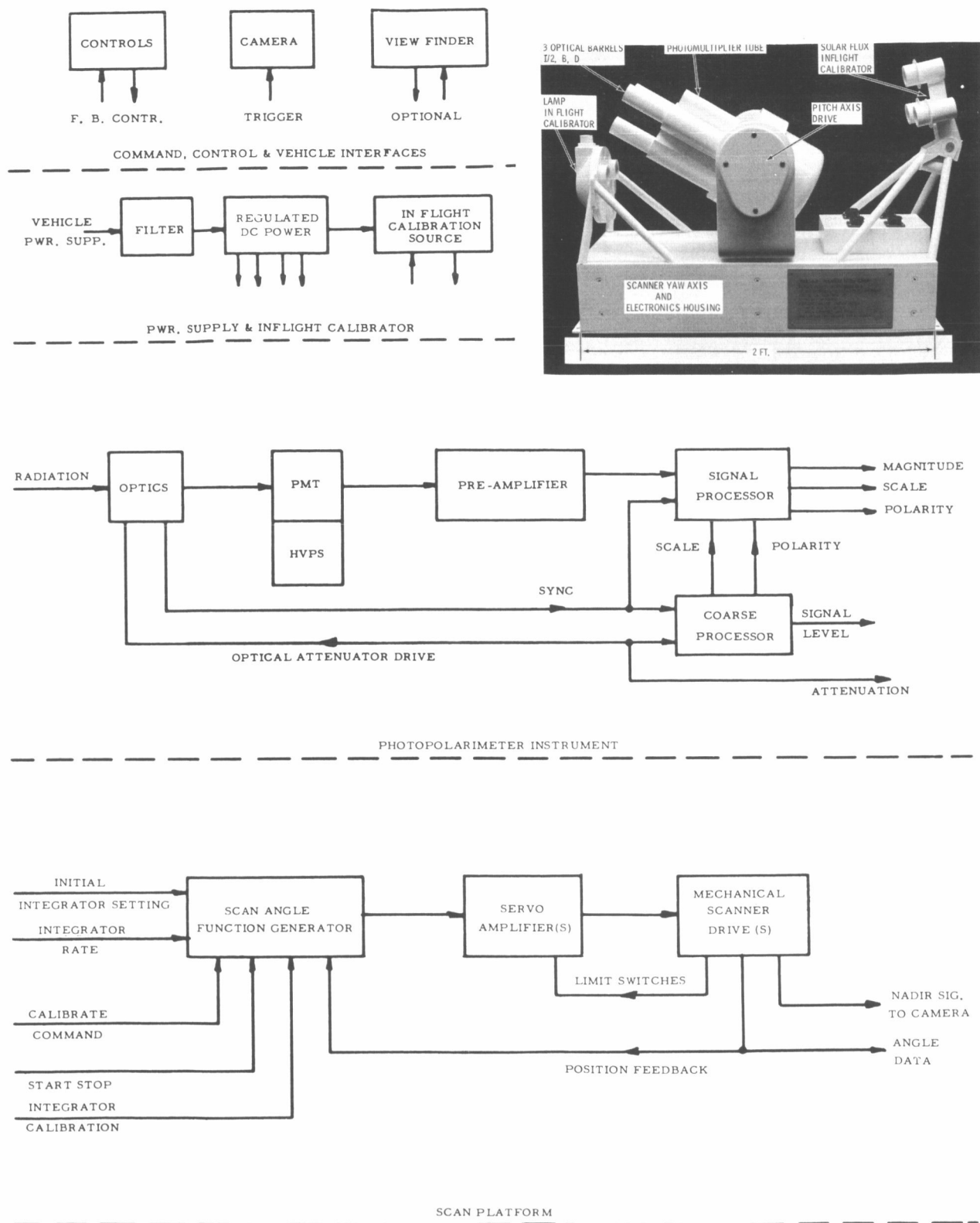


Figure 1. Block Diagram of Baseline System

B. Description of the Photopolarimeter Instrument

The photopolarimeter instrument contains three optical channels, two of which contain Glan-Thompson type polarizing prisms in the focal region of the collimating lenses. Measurement of the Stokes Parameters I, U, and Q are made by comparing the polarized beams with the unpolarized beam to obtain U and Q. Comparison of the beams is by an electro-mechanically driven beam selector wheel which is placed in the focal plane of the three collimating lenses.

Two of the barrels contain prisms oriented to accept light polarized at angles of 90° and 135° from the vertical. These polarized components are designated as B and D, respectively. The parameters Q and U are obtained as the differences $I-2B$ and $I-2D$.

1. Mechanical Design

An inboard profile drawing developed for the optical/mechanical portion of the photopolarimeter is shown in drawing 902D929. Specification drawings for important components have been given in the Engineering Specifications submitted separately. Sufficient layout work has been accomplished to provide assurance that the final mechanical packaging can be accomplished without requiring any unusually difficult or expensive production steps.

All parts of the mechanical module are mounted on a single support plate which provides good control of shaft spacing and position control of inter-related parts. Producibility and assembly are simple and straight forward and the assembly is compact and relatively unaffected by thermal gradients.

A size 11 gearhead motor has been selected to drive the beam selector wheel and the Geneva drive for the color filter wheel. The two-phase, 40 volt, 400 cycle synchronous motor will provide good speed control and maintain low armature temperature during operation under near-vacuum conditions. The electromechanical components are all contained in a sealed housing in order to insure cleanliness.

Grease lubricated mechanical components are recommended since non-lubricated parts could have a higher program risk and consequently a higher development cost.

As a result of the evaluation of the effects of lubricant deposits on the optical surfaces, a tentative decision has been made to operate the instrument in an unpressurized condition. There appears to be no strong reason for placing a requirement for pressurizing the mechanical package, and indications are that the design will be more straightforward using the

unpressurized approach. A filter will be incorporated in the vent port to prevent entry of foreign particles during normal "breathing" of the air space within the instrument cover. Assembly of the parts will be performed in a class 100,000 clean room as defined by with requirements of Federal Standard #209. The cover of the mechanical module should not be removed except in suitably clean environment.

The use of quartz windows over the ends of the fiber optics bundles will match the refractive index of the lubricant sufficiently to maintain instrument accuracy. A later section discusses the results of tests and studies in this area.

Two neutral density filters and a blank-off position have been provided in a four position wheel mounted coaxially with the color filter wheel. The four position wheel is edge driven by a separate incremental drive.

A preliminary evaluation of a Geneva drive after approximately six million cycles indicates no significant wear except for a cam follower bearing assembly. A slight design change can increase the life of this bearing assembly. An improved intermittent motion device is shown in Figure 2 with the Geneva and indications are that this drive may provide superior characteristics for use in the photopolarimeter.

2. Optical Design

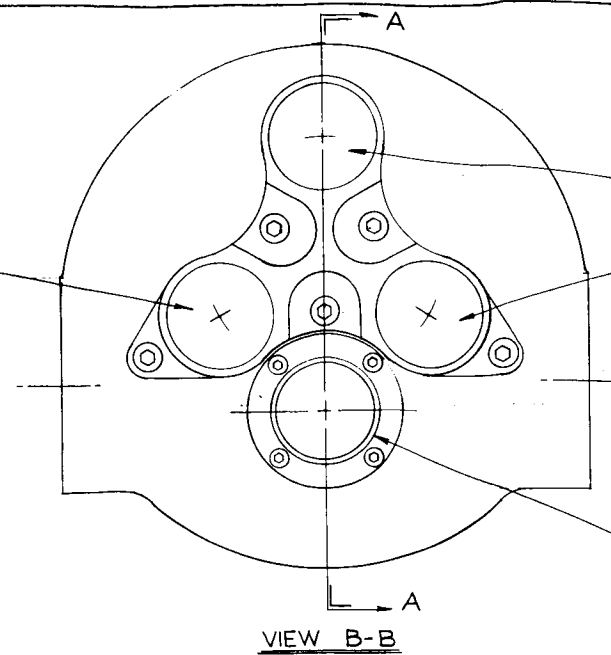
a) Identification of Optical Elements

The following summary indicates the numbers and types of elements in each optical path in the polarimeter. The sketch of Figure 3 shows a schematic layout of one barrel of the instrument through to the face of the photomultiplier. The elements are identified as follows starting at the front of the barrel.

- L - The objective whose diameter is 1.0 inch. This lens has an aperture of 0.75 inch (19.05mm) formed by the lens mounting. This lens is quartz and will be about 4 mm thick at its center.
- S - An aperture stop which is used to trim the light levels handled by each beam. This is simply a large hole in a thin plate which is placed just behind the lens. The diameter of the hole will be slightly less than 19 mm and can be determined exactly only after the instrument is built and tested.

FOLDOUT FRAME

B BARREL



OPTICS HOUSING

NEUTRAL DENSITY FILTER
174A9318-P1 1 REQD.

FUSED SILICA
PLANO/CONVEX LENS
174A9320 3 REQD.

B

B

GLAN-THOMPSON
OPTICAL PRISMS
MATCHED PAIR
DNG. NO. 174A9321
1-PAIR REQD.

NEUTRAL DENSITY FILTERS
174A9318-P2 1 REQD.
174A9318-P3 1 REQD.

HOUSING
BEAM SELECTOR DISC
FUSED SILICA WINDOWS
174A9319-P1 4 REQD.

BEAM MIXER AS
134B5793 1R

SECTION A-A

INTERFERE
FILTERS
PT. 1 THRU
174A93

4 5/8

10

1/2" BARREL

D" BARREL

FOLDOUT FRAME

ATCH AXIS

PHOTOMULTIPLIER ELECTRON TUBE
174A 9322 1REQ'D.

SY.
Q.D.

C

COVER

GENEVA MECHANISM
SIMILAR TO CAT NO EU-1
IN PIC CAT. NO. 33.

APPROX. C.G.
EST. WT. 9 LBS.

SUPPORT PLATE

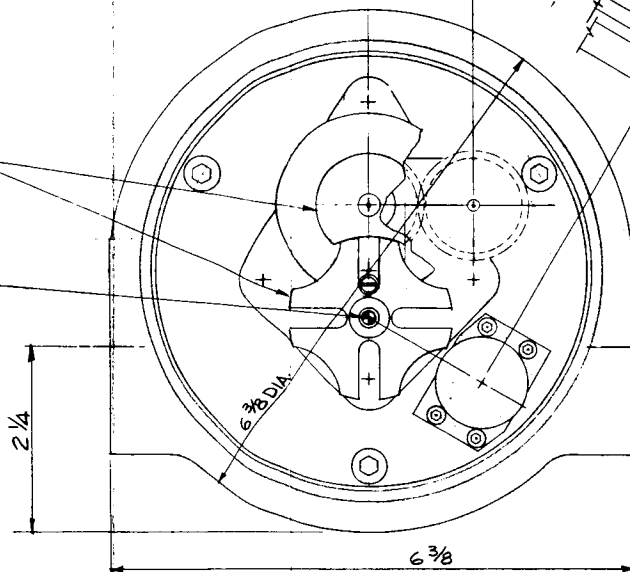
ICE COLOR
FACH OF
OF DWG. NO.

C

SUPPORT PLATE

BEAM SELECTOR DRIVE MOTOR
8000 RPM, 2 PHASE, 400 CYCLE
28 VOLTS, SIZE 11 SYNCHRONOUS
MOTOR WITH 31.5:1 GEAR
REDUCTION (254 RPM OUTPUT SPEED)

NEUTRAL DENSITY DRIVE
MOTOR. KEARFOFT
*CM 40191012



VIEW C-C

SHOWN WITH COVER REMOVED

D 902D929

UNLESS OTHERWISE SPECIFIED
DIMENSIONS ARE IN INCHES—
TOLERANCES ON:
2-PLACE DECIMALS ±
3-PLACE DECIMALS ±
ANGLES ±
FRACTIONS ±
MATERIAL—

ALL
SURF.
✓

SIGNATURES		REV	NO	VR
DESIGN	<i>R. J. [illegible]</i>	15	12	67
CHECKED				
DRAWN	<i>R. J. [illegible]</i>	15	1	67
DATE				
BY				

GENERAL ELECTRIC

DEPT LOC

S046 EXPERIMENT
INBOARD PROFILE - PHOTOPOLARIMETER

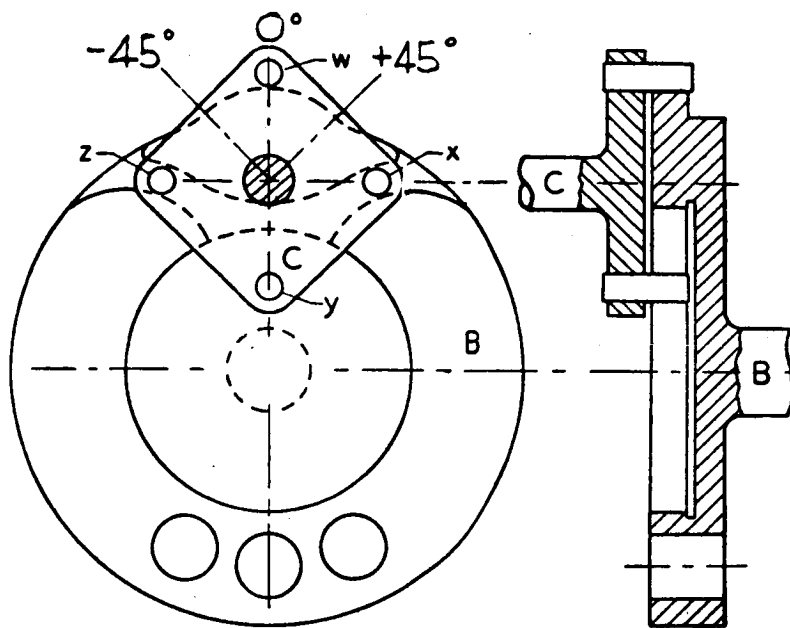
SIZE CODE IDENT NO.

D 15227

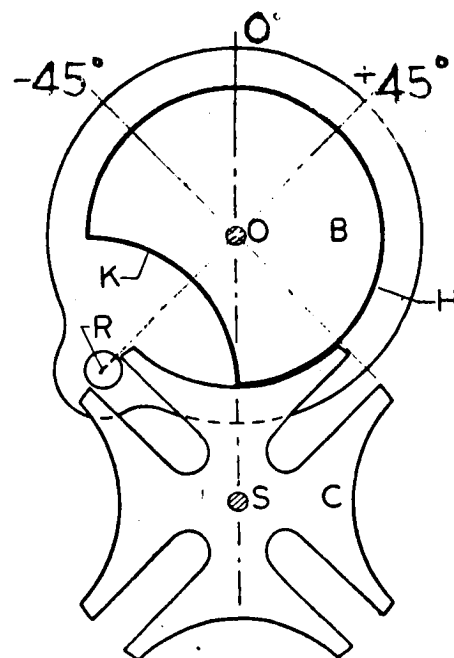
902D929

SCALE FULL

SHEET 1 OF 1



Typical Projector Feed Mechanism



Geneva Stop Mechanism

Figure 2

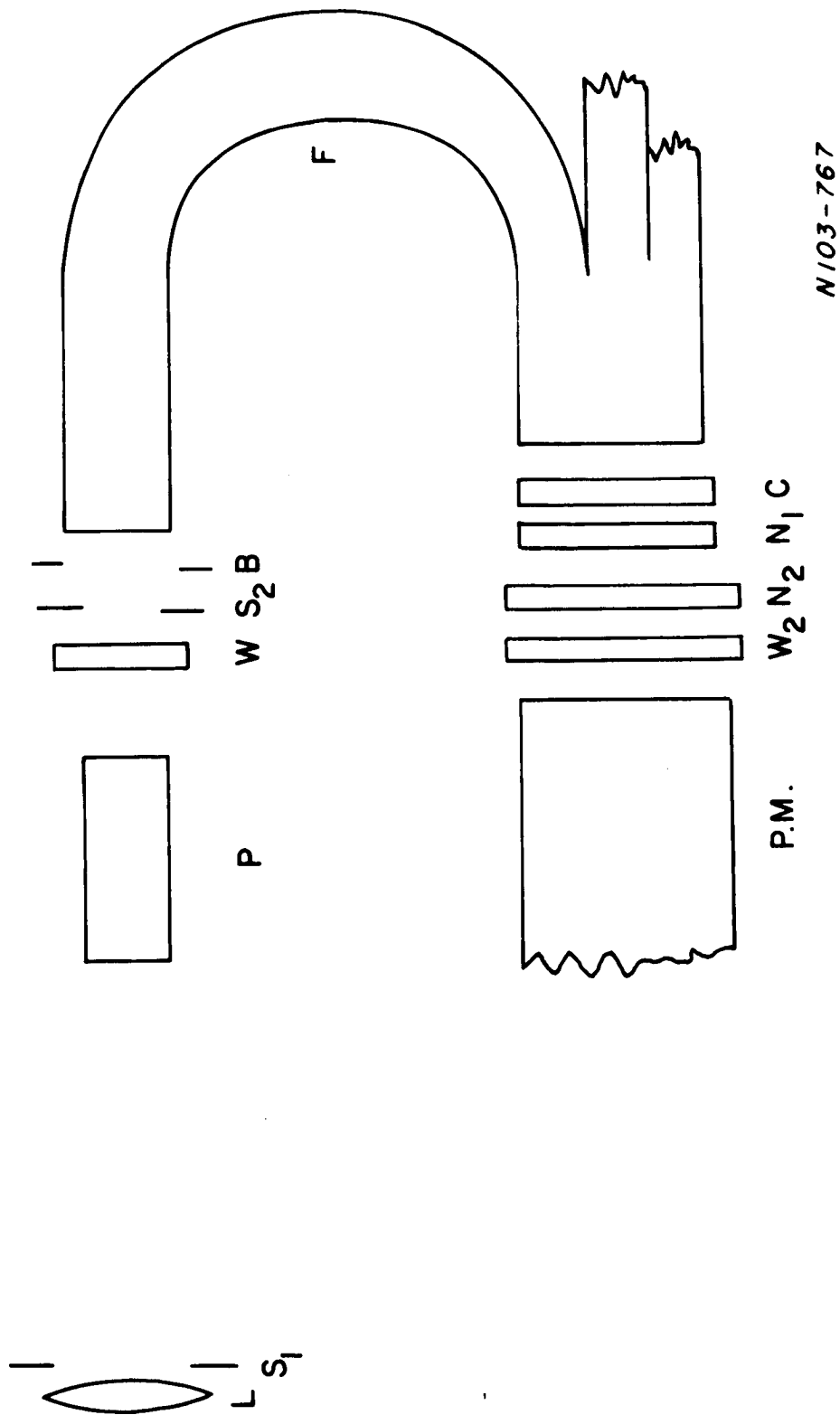


Figure 3. Schematic of One Barrel of Instrument

- P - The polarizing prism is 10 mm by 10 mm in cross section and 25 mm in length. This prism is a Glan-Thompson type made of calcite. It is mounted in a brass tube with a teflon insert and silicone rubber mounting.
- W_1 - The window between the sealed compartment and the unsealed area. This is a plane window made of quartz. The diameter is not critical except that it have a clear aperture greater than about 3/8 inch. The thickness will be about 4 millimeters.
- S_2 - A field stop to limit the field of view of the instrument. This stop is a hole approximately 5.9 mm in diameter in a thin metal plate.
- B - Beam selector wheel which selects the beams to be detected.
- F - The fiber optic bundle.
- C - The color filters are fabricated of several layers cemented with epoxy. They are about 0.6 inch in diameter with a clear aperture of about 0.5 inch. The color filters will be about 3mm.
- N_1 - A neutral density filter for trimming each color channel. This item may be provided in order to obtain the maximum dynamic range. It is expected that this filter can be deposited directly onto the color filter and covered with a thin cover glass cemented on with epoxy. Only three color channels will require this filter. The 5800 Å channel, which provides the lowest photomultiplier tube current will not require the filter.
- N_2 - The step attenuators. This is a three position attenuator containing one open channel and two channels with neutral density filters of density 1 and 2 respectively.

W_2 - The second window between compartments. This window is identical to W_1 except that it has a diameter of about one inch.

P.M. - The photomultiplier tube.

It must be noted that the sketch is representative of the two barrels containing prisms. The third barrel does not have a polarizing prism but instead is equipped with a neutral density filter just behind the lens.

b) Lenses

The lenses chosen for the polarimeter instrument are plano-convex made of fused quartz one inch in diameter and with a focal length of 100 ± 2 millimeters at 5890 \AA . These lenses are not achromatic so they exhibit different focal length at different wavelengths. The focal length of the lens is related to the index of refraction of the material and the radius of curvature of the two surfaces by the equation

$$\frac{1}{f} = (n - 1) \left(\frac{1}{R_1} + \frac{1}{R_2} \right) \quad (1)$$

where f , focal length = 100 mm at 5890 \AA
 n , index of refraction = 1.459 for quartz at 5890 \AA
 R_2 , Radius of curvature of plane side = ∞
 R_1 = Radius of curvature of convex side.

Solving the equation we find that $R_1 = 45.9$ mm. By substituting this radius of curvature back into equation (1) and solving for the focal lengths at various wavelengths, using the appropriate index of refraction we obtain the focal lengths at the four wavelengths of interest. These are tabulated in Table 1.

The polarizing prisms also have an effect on the focal length of the lens system. When the prisms are in place the focal length of the system tends to be increased since the index of refraction of the prism is greater than unity. The change in focal length is given by the relation

$$\Delta f = l(n_e - 1)$$

where Δf , change in focal length
 l , length of prism - 25 mm
 n_e , index of refraction (extraordinary ray for calcite)

By substituting the appropriate values we can calculate the change in focal length caused by the prism at the various wavelengths. The results are tabulated in Table I.

The window in the mechanical module must also be considered. This is handled in the same fashion that is used for the prism except that the indices of refraction are for fused quartz instead of calcite.

The neutral density filter in the I/2 channel must be considered and it also will be made from quartz. In the breadboard model, however, this filter is made from crown glass and so the indices of refraction for this calculation were chosen for the latter.

The focal lengths for the three lens systems can now be calculated by summing the appropriate columns of Table I. The focal length of the B and D barrels is obtained by summing the lens focal length, the change due to the prism and the change due to the window, the focal length of the I/2 barrel is obtained by summing the focal length of the lens, the window and the neutral density filter. These results are shown in Table II.

The desired field of view of the instrument is 3° . In order to achieve this the image diameter at an average focal length of 112.8 mm will be

$$\begin{aligned} d &= (\text{focal length}) (\text{field in Radians}) \\ &= 112.82 \times 0.0521 = 5.88 \text{ mm} \end{aligned}$$

A field stop with a diameter of 5.88 mm is placed at the average focal point in the system. This focal point will be 4.96 mm in front of the fiber optic bundle. This provides a small amount of beam mixing by defocusing before the light enters the fiber optic bundle.

It must be noted that the field of view changes slightly from one color to the next since the focal plane is in a slightly different place for each color. The total variation in target area from 3800 Å to 5800 Å however will be no more than 6% of the total area.

The positions of the various optical elements in each barrel are shown in the sketches of Figure 4.

c) Lens Polarization

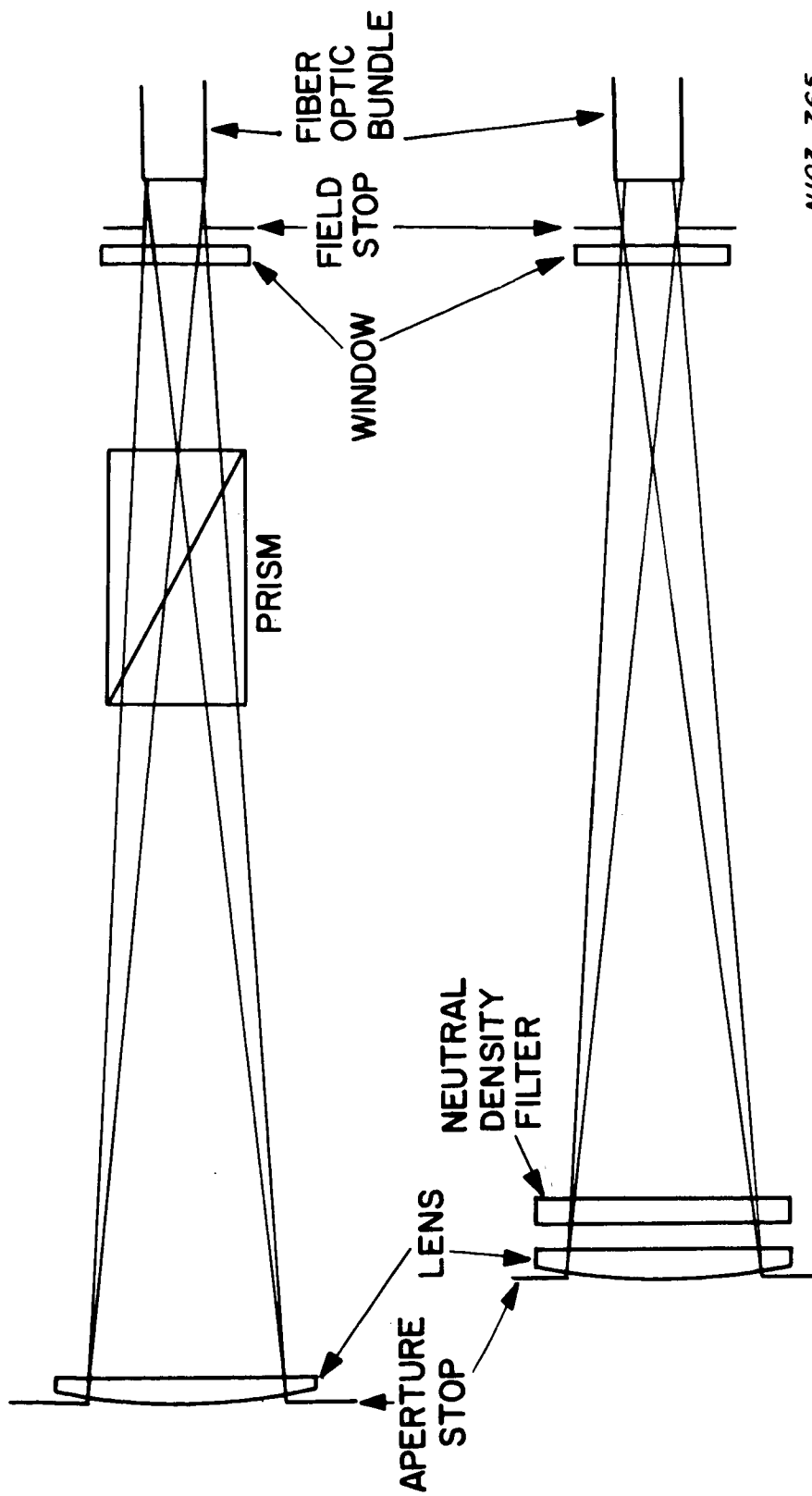
Spurious polarization will result if the lens is not used on axis. Manufacturing tolerances can be held to a fraction of a degree, thus introducing only trivial errors. Nonuniformity in the field of view is a more serious problem.

TABLE I

Wavelength \AA	Indices of Refraction			Focal Length of Lens (mm)	Changes in Focal Length		
	Fused Quartz	Calcite	Crown Glass		Prism	Window	Neutral Density Filter
3800	1.472	1.4991	1.528	97.3	+12.47	+1.89	+1.85
4400	1.467	1.4933	1.518	98.3	+12.32	+1.87	+1.81
5000	1.463	1.4895	1.511	99.1	+12.21	+1.85	+1.79
5800	1.459	1.4862	1.505	100.0	+12.13	+1.84	+1.78

TABLE II

Wavelength (\AA)	Effective Focal Length of B & D Barrels (mm)		Effective Focal Length of I/2 Barrel (mm)	
3800	111.66		101.04	
4400	112.49		101.98	
5000	113.16		102.74	
5800	113.97		103.62	
Average focal lengths	112.82		102.35	



N103-765

Figure 4. Schematic drawing of B or D barrel (above) and I/2 barrel (below)

In the worst case, all of the incident intensity would be concentrated at a point at the extreme edge of the field of view. Since the source is distant, the lens will be illuminated with parallel rays incident at 1.5° from the optical axis.

Consider a double convex lens with spherical surfaces. (It is easy to show spurious effects are nearly the same for any lens - e.g., plano convex, convex-concave with the same focal length and diameter so that on the basis of polarization the system can be designed to minimize aberrations.)

From symmetry considerations, zones of the lens for which concentric circles can be drawn about a point on a radius tipped 1.5° from the optic axis will not produce spurious polarization (Figure 5). The uncompensated area of the front of the lens will be about 44% of the total area. Maximum polarization will be produced where the angle of incidence is greatest at the top edge of the lens where $\alpha = 7^\circ 15'$. At the rear surface, the uncompensated area is 22% of the total and the maximum angle of emergence is $\beta = 13^\circ$.

Fresnel's relations for the transmitted intensities are

$$\tau_{\parallel} = \frac{\sin 2\theta_i \sin 2\theta_t}{\sin^2(\theta_i + \theta_t) \cos^2(\theta_i - \theta_t)}$$

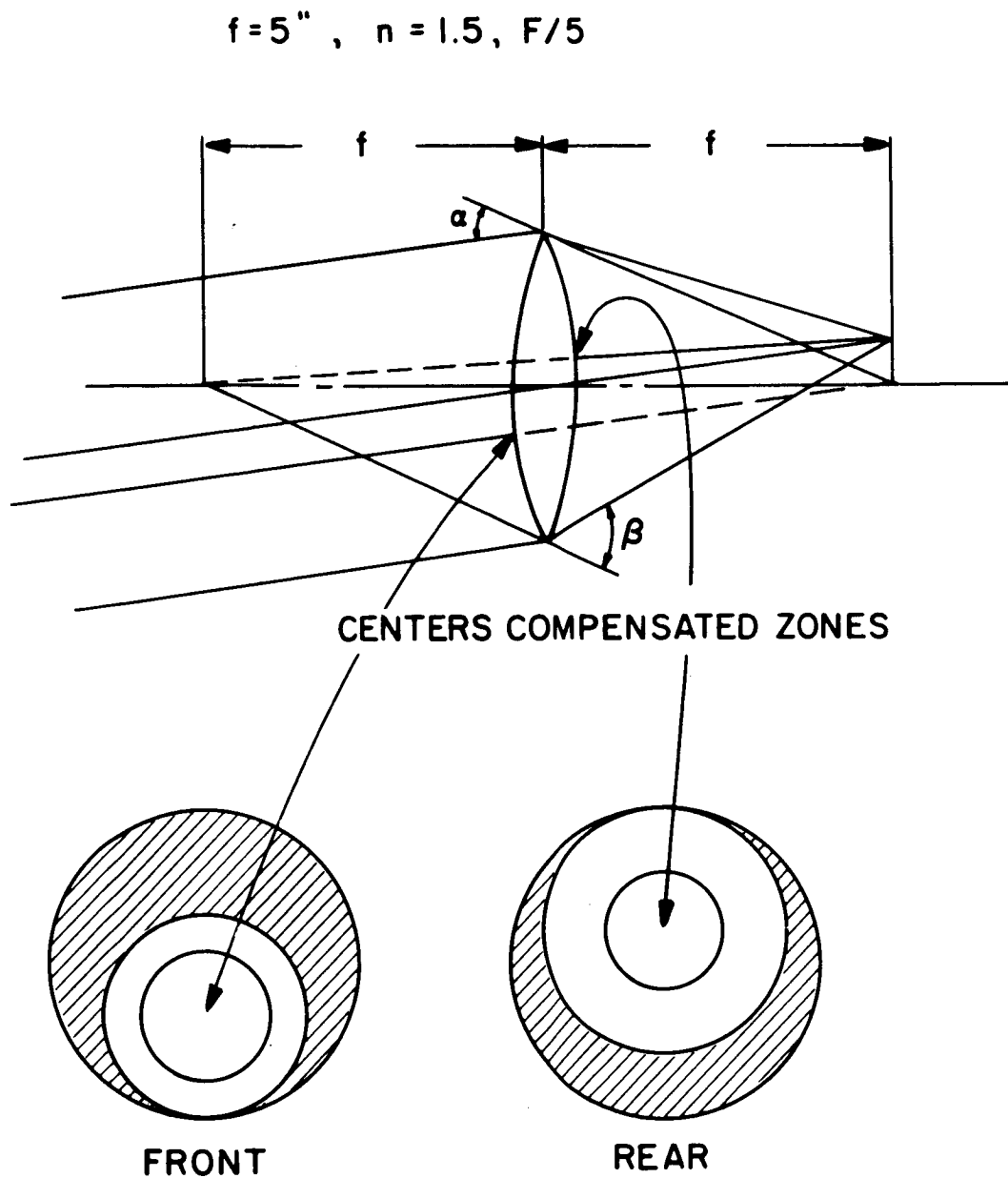
$$\tau_{\perp} = \frac{\sin 2\theta_i \sin 2\theta_t}{\sin^2(\theta_i + \theta_t)}$$

The effect over the two uncompensated zones is additive. If we assume that all uncompensated rays impinge and emerge, respectively, at $\alpha = 7^\circ 45'$ and $\beta = 13^\circ$, then lens induced polarization will be

$$.44 \left(\frac{1}{.999} - 1 \right) + .22 \left(\frac{1}{.999} - 1 \right) = .0012$$

or .13%

In a real case, the average angles of incidence and emergence are somewhat less. Nor will all incident intensity be concentrated at the extreme edge of the field of view. We conclude that lens induced polarization will be less than 1/5000.



N 103-761

Figure 5. Zones of lens (angles are exaggerated)

d) Window

In the present preliminary design, it is not planned to subject the window to a stress due to pressurization of the mechanical module. The use of quartz of the same optical quality as that used in the lens and the avoidance of excessive stress due to window mounting through the use of soft mounting gaskets should give assurance that the spurious polarization is negligible.

e) Color Filters

Evaluation of the requirements imposed by the color filters indicates that optical interference filters are available which will meet these requirements. Baird-Atomic located in Cambridge, Massachusetts, manufactures optical interference filters at each wavelength required. These filters are made by evaporating multiple layer dielectric coatings in a vacuum onto a glass substrate. A cover glass and an additional absorption filter are cemented on to the substrate with epoxy. These filters show no degradation when used in a vacuum and when properly mounted may sustain high level of shock and vibration without harm.

The filters required will be approximately 12 mm in diameter. All four filters will be about 3 mm thick.

According to Baird-Atomic they should be mounted in some resilient material so that the filter does not touch metal in order to use the filters in a high shock and vibration environment.

These filters are useable over a temperature range which exceeds that allowed for the photomultiplier tube. They are sensitive to temperature changes in that peak transmission wavelength of the filter moves toward the red about one Å per ten degrees Fahrenheit.

Our experience has shown that if the filters show no major wavelength shift after three months, they will be stable for periods of years. (Baird-Atomic concurs in this observation). The peak wavelength does shift slowly toward the blue over periods of several years. We have on hand several of these types of filters which were purchased in 1963. Periodic checks have shown that their peak wavelength has shifted about 0.1% of peak wavelength per year toward the blue. (Baird-Atomic indicated that this was normal for the filters).

It is suggested that the filters for flight use be kept on the shelf for at least three months and checked prior to installation in order to cull out the filters which have failed.

The transmission characteristics of the color filters for the advanced breadboard as received from Baird-Atomic, were checked before they were installed in the breadboard. This was done with a Jarrell-Ash, 0.5 meter, Ebert monochromator. Outputs of the monochromator were detected with a 1P28 photomultiplier and recorded on an x-y plotter.

The reduced transmission curves of the individual filters are shown in Figure 6. The tabulated characteristics of each filter are shown in Table III. The center frequency as well as the percent transmission at the peak is given. The bandwidth at half peak transmission was read directly from the transmission curves. The fourth column shows the total transmission of each filter in percent-Angstroms. The data for this column was obtained by integrating each curve with a planimeter.

This type of notation for total transmission is used since the filter curves do not all have the same shape. It shows at a glance the total amount of light transmitted by each filter.

From these data it appears that the total transmission of the 3800 Å filter should be increased. The filters for the final instrument will be adjusted by obtaining filters with the appropriate total transmission in order to insure that the signals to the processor are about the same amplitude for all colors.

f) Optical Beam Mixer

The method of illumination of the cathode is a critical factor in the use of a photomultiplier for photometry because the photo sensitivity of the cathode varies at different positions on the cathode surface.

To achieve the desired accuracy with the photopolarimeter instrument it is essential that the fluxes from the three barrels illuminate the cathode sensitive area in approximately the same manner. This could be accomplished in two ways: (a) by imaging the three scenes in exactly the same way on the photocathode, (b) by ensuring that each small element in the scene (as viewed individually by each barrel) contributes as uniformly as possible to the intensity across the complete cathode. Both methods would be satisfactory provided the targets were perfectly uniform, however method (b) has the advantage that it is able to compensate for targets with a certain non-uniformity.

A system using fibre optics (3 mil fibres) based on method (b) has been constructed and tested and is shown schematically in Figure 7. The fibres from any small area ΔC at C for example, are distributed as uniformly as possible over the end D. With this method of beam mixing, a non-uniform target produces a reasonably uniform distribution of intensities at D. Shown in Figure 7 is a photograph of end D showing the

TABLE III

Center Freq.	% Transmission at Peak	Bandwidth at Half Peak Transmission	Total Transmission in % - Angstroms
<u>3800^oÅ</u>	26.8	100 ^o Å	3090
4400 ^o Å	49.4	95 ^o Å	4770
5000 ^o Å	49.8	102 ^o Å	6220
5800 ^o Å	51.3	112 ^o Å	5900

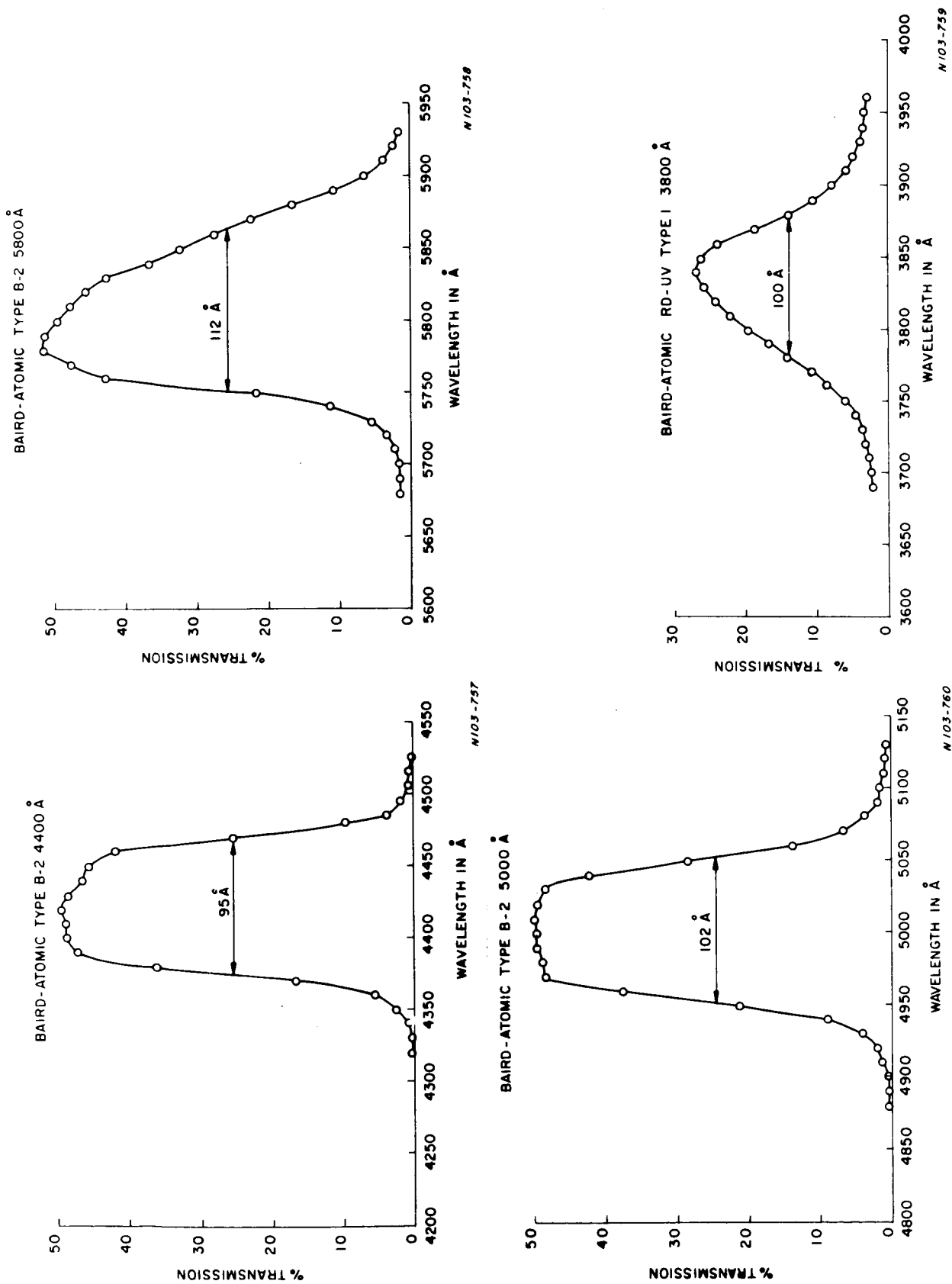
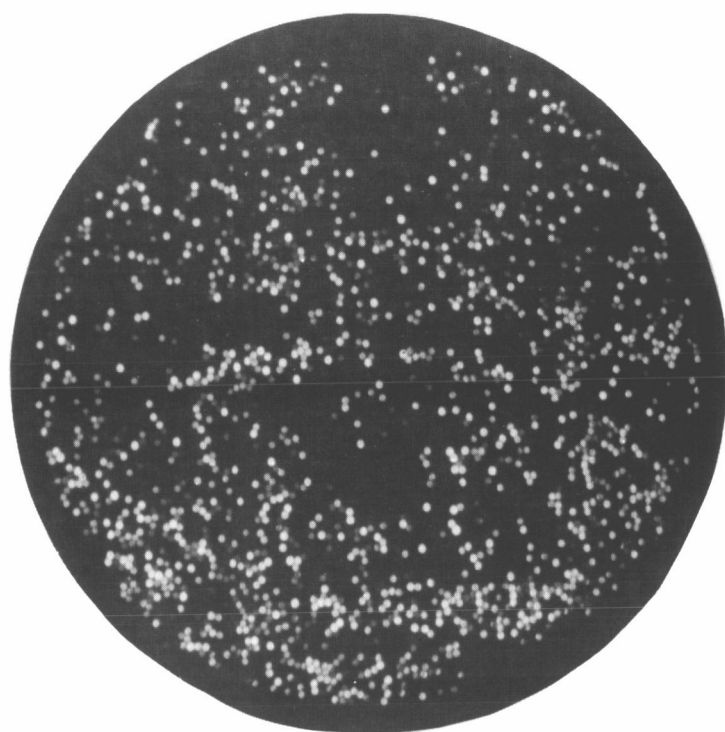


Figure 6. Transmission curves of thin-film interference filters



← OUTPUT FACE
OF BEAM MIXER

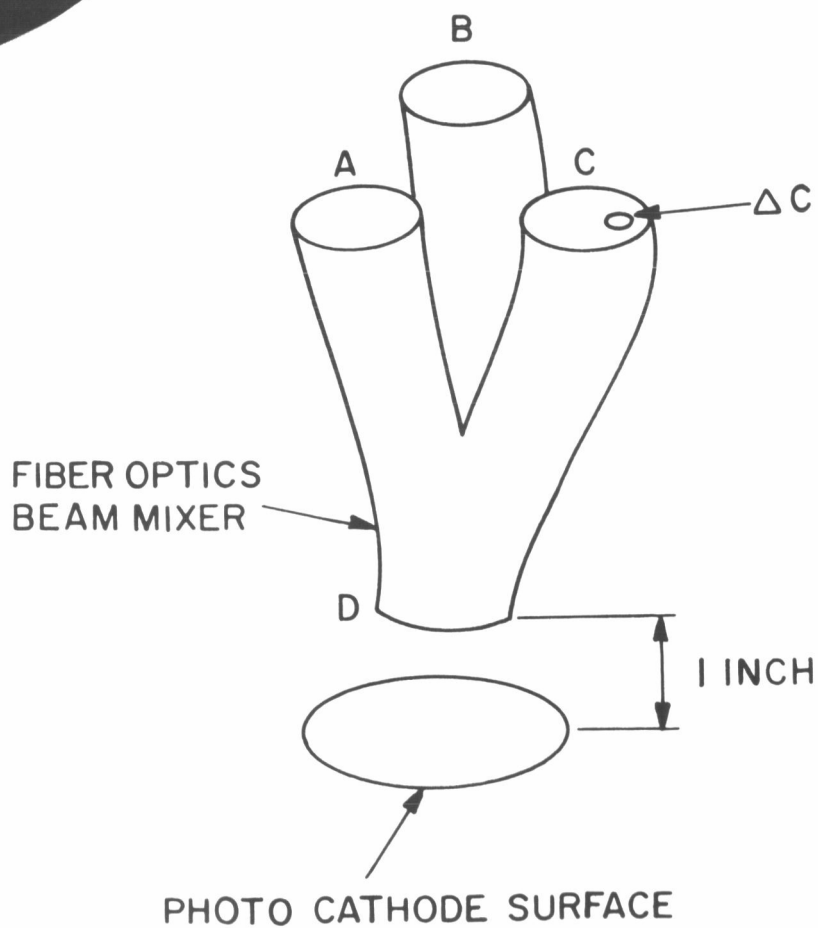


Figure 7. Fiber optics system and photograph of intensity pattern

intensity distribution over the fibres when one of the ends A, B, or C is illuminated. While this intensity pattern is not perfectly uniform, it is found experimentally that the distribution of intensity profile at a distance of 1" from end D (the proposed location of the photocathode) is very uniform. This observation results from the fact that the intensity emerging from an individual fibre has a divergence of $\sim 12^\circ$ half angle. Thus, the distribution at a distance is the result of an integration over very many fibres at D and is considerably more uniform than the apparent distribution shown to the left. A more detailed consideration of this effect is given in a following section. Results of early tests indicate that this type of mixer will provide a suitable means for illuminating the photomultiplier cathode surface.

Figure 8 shows beam mixers supplied for the breadboard tests by Bausch and Lomb. They were not supplied in time for detailed testing.

When measuring the average value of the Stokes parameters of the light emerging from a non-uniform target by comparing intensities of the different polarized components, it is important that the response of the detector or detectors be uniform for an element of the target anywhere within the field-of-view. Otherwise, although the instrument will measure an average of the polarization over the field-of-view, this average will not be properly weighted by the intensity.

As a first step toward insuring that the instrument respond in the same way to the different polarized beams, it is advantageous to utilize the same detector such that drifts in detector sensitivity have a minimum effect. This Section will establish a further requirement on the measurement system in order that the measured average polarization be properly weighted by the intensity; for example, an instrument which measured the polarization of the target averaged over the area would be useful but it is the objective of the S046 instrument design to measure average values of Stokes parameters, (e. g. $Q = IP \cos 2\psi$).

We will assume that both the intensity I and polarization P vary in an arbitrary manner across the field-of-view. A one dimensional position within the field-of-view is described by the coordinate X which has dimensions so that

$$-\pi \leq x \leq +\pi$$

We Fourier expand I and P and for brevity write only the even harmonics

$$I = I_0 (1 + a_\mu \cos \mu x) \quad \mu = 1, 2, \dots, \infty$$

$$P = P_0 (1 + b_\mu \cos \mu x)$$

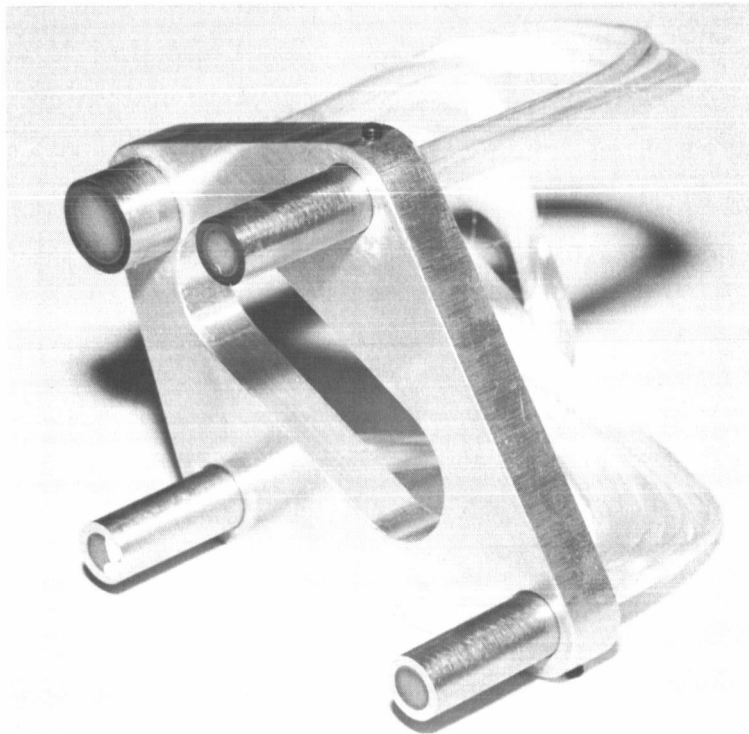
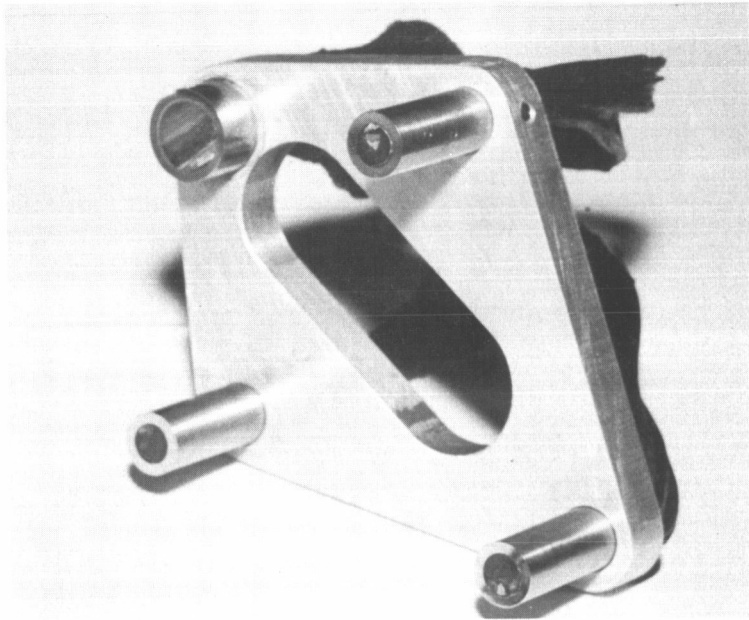


Figure 8. Beam mixers supplied by Bausch and Lomb

At the end, the more general results showing the effect of the odd harmonics will be appended.

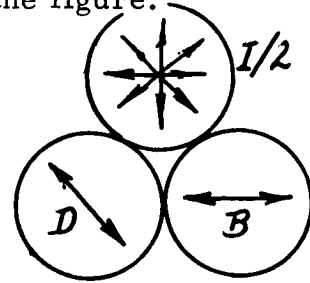
The Stokes parameters are

$$I = 2\frac{I}{2}$$

$$Q = IP \cos 2\psi = 2\left(\frac{I}{2} - B\right)$$

$U = IP \sin 2\psi = 2\left(\frac{I}{2} - D\right)$ in terms of the measured beams. The beams B and D are defined in the figure. The beam B is given in terms of I and P by

$$B = \frac{I}{2}(1 - P \cos 2\psi)$$



Assume that the phototube response to a delta function light source $\delta(x)$ in the focal plane of the objective lens is

$$R_{I/2} = 1 + c_{\mu} \cos \mu x \quad \text{for the } I/2 \text{ beam and}$$

$$R_B = 1 + d_{\mu} \cos \mu x \quad \text{for the B-beam (sum } \mu = 1, 2, \dots)$$

The instrument will then give the difference signal

$$Q_{\text{meas}} = I_{\text{meas}} - 2B_{\text{meas}} = \frac{1}{2\pi} \int_{-\pi}^{+\pi} [IR_{I/2} - 2BR_B] dx$$

Assume $I_0 = 1$ and $\psi = 0$, then

$$Q_{\text{meas}} = \frac{1}{2\pi} \int_{-\pi}^{+\pi} [(1 + a_{\mu} \cos \mu x)(1 + c_{\mu} \cos \mu x) - (1 - a_{\mu} \cos \mu x)(1 - P_0 - P_0 b_{\mu} \cos \mu x)(1 + d_{\mu} \cos \mu x)] dx$$

Now, if $a_{\mu} = b_{\mu} = 0$, $Q_{\text{meas}} = P_0 = Q$

For $a_{\mu} \neq 0$, $b_{\mu} \neq 0$,

$$Q_{\text{meas}} = P_0 + \frac{a_{\mu} c_{\mu}}{2} - (1 - P_0) \frac{a_{\mu} d_{\mu}}{2} + P_0 \frac{b_{\mu} d_{\mu}}{2} + P_0 \frac{a_{\mu} b_{\mu}}{2}$$

Assume $a_{\mu} b_{\mu} \ll 1$, then the measurement error is

$$\frac{\Delta Q}{Q} = \frac{Q_{\text{meas}} - Q}{Q} = \frac{1}{2P_o} a_{\mu} (c_{\mu} - d_{\mu}) + \frac{1}{2} (a_{\mu} + b_{\mu}) d_{\mu}$$

For small polarization P_o , the leading term is

$$\frac{\Delta Q}{Q} \cong \frac{a_{\mu}}{2P_o} (c_{\mu} - d_{\mu}) \quad \text{sum } \mu = 1, 2, 3, \dots$$

For a well-constructed instrument ($c_{\mu} \approx d_{\mu}$), or for large polarizations, the second term $\frac{(a_{\mu} + b_{\mu}) d_{\mu}}{2}$ will dominate.

Effect of Odd Harmonics

Let us now write the general case (still one dimensional)

$$I = I_o (1 + a_{\mu} \cos \mu x + \bar{a}_{\mu} \sin \mu x)$$

$$P = P_o (1 + b_{\mu} \cos \mu x + \bar{b}_{\mu} \sin \mu x)$$

$$R_{I/2} = 1 + c_{\mu} \cos \mu x + \bar{c}_{\mu} \sin \mu x$$

$$R_B = 1 + d_{\mu} \cos \mu x + \bar{d}_{\mu} \sin \mu x$$

The fractional error in measuring the Stokes parameter Q is

$$\begin{aligned} \frac{\Delta Q}{Q} \cong & \frac{1}{2P_o} [a_{\mu} (c_{\mu} - d_{\mu}) + \bar{a}_{\mu} (\bar{c}_{\mu} - \bar{d}_{\mu})] \\ & + \frac{1}{2} [(a_{\mu} + b_{\mu}) d_{\mu} + (\bar{a}_{\mu} + \bar{b}_{\mu}) \bar{d}_{\mu}] \end{aligned}$$

For $\frac{\Delta Q_{\text{meas}}}{Q} < .01$ and $P_o = .05$, we obtain the order-of-magnitude requirement

$$\begin{aligned} (1) \quad & a_{\mu} (c_{\mu} - d_{\mu}) \lesssim 10^{-3} \\ & \bar{a}_{\mu} (\bar{c}_{\mu} - \bar{d}_{\mu}) \lesssim 10^{-3} \text{ for each } \mu \end{aligned}$$

If we assume scene variations $a_{\mu} \sim 10^{-1}$, $\bar{a}_{\mu} \sim 10^{-1}$, we require

$$\left\{ \begin{array}{l} c_{\mu} - d_{\mu} \lesssim 10^{-2} \\ \bar{c}_{\mu} - \bar{d}_{\mu} \lesssim 10^{-2} \end{array} \right.$$

Equations 1 show the relation between the Fourier coefficients of the intensity distribution across the target and the Fourier coefficients which express the difference in response of the instrument to the different polarized beams. This expression is quite general and is a design requirement for all photopolarimeters in order that they measure a properly weighted average of the Stokes parameters across the target instead of some other averages depending upon the instrument. In the S046 instrument, a beam mixer is provided so that the light from the different polarized beams be distributed over the detector with nearly the same distribution. Without such a beam mixer the non-uniform response of the phototube will cause it to respond differently to the different polarized beams in the case where the illumination of the target is non-uniform.

This specification in terms of Fourier components of response of the total optical system has been resolved into separate specifications for the beam mixer and the photocathode uniformity. Although a fiber optics beam mixer procured from Bausch and Lomb Company did not meet specifications as delivered, obtaining a beam mixer which meets the specifications is not considered a major procurement problem.

g) Photomultiplier Tube

A survey of currently available photomultiplier tubes has been made with the following characteristics being required of the tubes included in the survey.

1. S-20 photocathode characteristic (see Note (d)).
2. Rugged
3. Photocathode surface diameter between 0.8 and 1.5 inches (see Note (e)).

The field was narrowed by this survey to two types of tubes which are described below.

- a). The RCA C70114C is a cylindrically shaped lime glass tube, 1.6 inch in diameter by 3.2 inches long with a minimum

(end-window) photo-cathode diameter of 1.3 inches. It has 10 copper-beryllium dynodes in a circular-cage or "squirrel-cage" structure which means the dynodes are clustered together within a cylindrically shaped cage-like structure whose longitudinal axis is perpendicular to the longitudinal axis of the glass envelope. This tube is normally supplied unpotted and without a resistor network. All wires pass through the tube wall at its base.

b). The EMR 541E-01-14 is cylindrically shaped end-window tube 1.4 inches in diameter by 4.3 inches long with a minimum photo-cathode diameter of 1 inch. It has 14 silver-magnesium dynodes in a venetian blind structure in which the hard glass spacers between the dynode plates act as the tube wall and each dynode plate extends beyond the tube wall, providing convenient weld points for the resistor network. The active portion of each circular dynode plate, which includes most of the enclosed area on it, is cut and shaped, resulting in an appearance much like that of a venetian-blind. This tube is normally supplied potted, with a resistor network, in a fiberglass shell.

The table below contains data for these tubes obtained from both RCA and EMR. In some cases data from EMR are lacking and in all cases RCA described its tube by comparison to similar RCA tubes as RCA has no data sheet for the C70114C (EMR has a data sheet for the 541E-01-14 dated March, 1966).

A brief description of several other RCA tubes is required to aid in understanding the RCA information.

4461 Formerly C70114; the only difference between this and the C70114C is the 4461 has an S-11 photo-cathode characteristic.

4464 Venetian-blind copper-beryllium dynodes (10), S-20, 2.6 inches cathode diameter, overall glass envelope non-rugged type.

8571 Circular-cage copper-beryllium dynodes (9), S-4, 0.4 inch by 0.06 inch side-window cathode, non-rugged type.

4460 In-line copper-beryllium dynodes (10), S-11, 0.5 inch cathode diameter, rugged type.

8644 In-line copper-beryllium dynodes (10), S-20, 2.6 inches cathode diameter, non-rugged type.

C70114F - Same as C70114C except with different spectral response.

<u>Items Compared</u>	<u>RCA C70114C</u>	<u>EMR 541E-01-14</u>
Space Use	<u>4461</u> -Lockheed <u>4460</u> -Lunar Orbiter C70114F-JPL (not yet flown)	<u>541E-01-14</u> ATS-D <u>541</u> Type OSO, OAO Lunar Orbiter
Environmental specifications	<u>4461</u> shock: 30g, 11 msec vib: 0.05 dia., 20-87 cps 20g, 87-2x10 ³ cps Temp: to 75°C Accel: 100g <u>4464</u> Temp: to 85°C	<u>541E-01-14</u> shock: 100g, 11 msec vib: 30 g, 20 to 3x10 ³ cps Temp: -55°C to 85°C
Average Anode Current	<u>4461</u> 1 m amp	<u>541E-01-14</u> 1 m amp
Dark Current (see note a) (unit is 10 ⁻¹⁰ amp)	<u>4461</u> <u>Typical</u> <u>Max.</u> gain=10 ⁶ 495 gain=10 ⁵ 36 140 gain=10 ⁴ 12 <u>4464</u> gain=10 ⁶ 440 gain=10 ⁵ 68 150 gain=10 ⁴ 7	<u>541E-01-14</u> <u>Typical</u> <u>Max.</u> gain = 10 ⁷ 18 gain = 10 ⁶ 2 20 gain = 10 ⁵ 0.2
Anode Sensitivity change with temperature	<u>8571</u> (extreme of six) + 65% at -46°C - 25% at 66°C <u>8571</u> (average of six) + 34 % at 46°C - 35 % at 66°C	<u>541E-01-14</u> (one) + 13% at -40°C - 18% at 60°C <u>541E-01-14</u> (average) + 14% at -40°C - 10% at 60°C
Spatial Uniformity of cathode operation (with First dynode active) (See note b)	<u>4461</u> Using a spot of light 0.05 inch in diameter, anode current com - monly varies from maximum sensitivity to approximately 10% of	<u>541E-01-14</u> Using a spot of light 0.25 inch in diameter, the anode current will not decrease to less than 50% of the maximum value. Venetial blind struc - tures usually provide

EMR 541E-01-14

541E-01-14

relatively uniform electron gathering efficiency over the face of the tube.

541E-01-14

Surface is produced by inserting and removing rf heated boats centered in the tube. Response of entire surface to light of several different wavelengths is monitored during deposition.

4461 (average)

541E-01-14 (five)

1 m amp + 10% 30
hrs
- 20% 500
hrs

0.003 m amp
±1-1/2%, 150-200 hrs

8644

541E-01-14 (six)

1 m amp - 50% is
common
total change at 500
hours

0.001 m amp
± 2%, 100-2000 hrs

4461

50% gain decrease
1 Oersted along most
sensitive axis.

Venetian blind type is less sensitive.

4461

2.2 oz, unpotted

541E-01-14

2.5 oz, unpotted
6.0 oz, potted

<u>Items Compared</u>	<u>RCA C70114C</u>	<u>EMR 541E-01-14</u>
Cost	<u>C70114C</u>	<u>541E-01-14</u>
	\$750, unpotted	\$1600 unpotted
	\$850, potted	\$1800, potted
	(no information on special aging)	(+\$300 for special aging)
Delivery	<u>C70114C</u>	<u>541E-01-14</u>
	60 - 90 days	60 days

Notes:

- a. A rule of thumb describing dark current variation with temperature is current increases by factor of two for a 10 centigrade degree increase in temperature.
- b. The cathode response to incident light is more uniform, in general, than shown by these data. These data include the electron gathering efficiency of the first dynode.
- c. Change in anode sensitivity is due to changes in dynode characteristics not in photo-cathode characteristics (if tube is not exposed to high light levels while powered).
- d. The S-20 spectral response is required to provide a suitable signal to noise ratio at 5800 Å.
- e. Preliminary design layout required photocathode diameter of at least 0.8 inch to permit filters to move between fiber optics and photomultiplier, and to permit intersecting most of the light emanating from the fiber optics. Diameters larger than 1.5 inches would have introduced no new types of tubes and would have increased weight of the S046 experiment.

On the basis of the characteristics as described in the manufacturers' data a tentative selection had been made of the 541E tube. A study of the data given above show a superiority in most areas except for a minor weight difference. A 541E-01-14 was procured and was tested prior to use in the instrument breadboard. It was found that the gain of the tube continued to change with time, despite a burn-in procedure which had been carried out by the vendor in order to stabilize gain. It was also found that the tube procured suffered from a significant non-linearity not typical for this type of tube. Further tests of available RCA tubes showed good gain stability and satisfactory linearity. This is thought to be largely due to the use of copper-beryllium dynodes. Although EMR replaced their tube with another considered

to be suitable and employing copper-beryllium dynodes, it was not received in time to be tested as part of the polarimeter breadboard. For this reason it is recommended that final choice of the photomultiplier tube be made a part of the final design choice based on further laboratory testing of both types of tubes.

h) Illumination of a Photomultiplier Cathode by a Fiber Optics Bundle

The following is a qualitative analysis of the distribution of intensity of illumination of the photo-multiplier to aid in understanding the light mixing system requirements.

Geometrical Considerations

Consider a photomultiplier cathode surface to be a distance d from the output end of fiber optics mixer bundle (see Figure 9). Each point on the cathode surface is illuminated by a portion of the mixer and the variation of the intensity across the cathode is governed by both the angular and surface distribution of light flux emanating from the fibers of the mixer. The light emitted by a single fiber has been found for normal illumination of a plane surface, to produce an intensity which may be represented approximately by

$$i = i_{\max} - rk$$

where k is a constant gradient of intensity in the direction of r and r is the radial distance from the center line of the fiber. In one dimension this distribution is triangular. Note that the intensity is zero at some maximum value of r . The angle which this maximum value of r , r_{\max} , subtends at the fiber is $\arctan r_{\max}/d$ which may be called α , the half angle of the cone of light emitted at the end of the fiber. For $f/5$ illumination of one end of the fiber, α has been found to be about 12° . The light incident upon the cathode cannot exceed an angle of incidence greater than this angle α as shown in Figure 9. Thus each point on the cathode is illuminated by the fibers in an area on the end of the mixer encompassed by a circle of radius $d \tan \alpha$. This circle is shown in the plane of the mixer output face in Figure 10.

Distribution of Intensity

The area, A , includes all the portion of the mixer which illuminates a point a distance x from the mixer-phototube axis. The intensity at this point is an integral dependent upon the area and light distribution and to a first approximation, for nearly uniform target brightness and good mixing, this intensity is nearly proportional to A . From Figure 10 it may be seen that A , or the distribution of light intensity across the cathode, rises from zero at $x = 2R$ and reach a peak at $x = 0$ as shown in Figure 11,

assuming $d \tan \alpha \approx R$.

Fluctuations

Superimposed upon this curve are random-like fluctuations caused by variation in light intensity of the areas added to or subtracted from A as x varies from -2R to +2R. These fluctuations which may vary from one moment to the next as identical distributions of light intensity are put into different inputs of the mixer, are a possible source of error in the S046 photopolarimeter if the sensitivity to light across the face of the photomultiplier is not uniform. In order to estimate the seriousness of these fluctuations, consider a mixer whose output light intensity may vary up to $\pm 5\%$ from an average as it is measured through an aperture 0.1 inch in diameter. If the mixer output face is 0.4 inch in diameter, when an area equal to that of 0.1 inch diameter is added to A and $A \approx 1/2 \pi R^2$, the increase in A is about 10%. With a number of fibers being added to a number 9 or 10 times larger, the range of possible intensity of the introduced area results in a change from $\pm 5\%$ of local mixer intensity to about $\pm 0.5\%$ of the total intensity on the photomultiplier.

Error in Photomultiplier Output

An EMR 541E-01-14 photomultiplier's cathode sensitivity will vary no more than $\pm 25\%$ when it is scanned with a 0.25 inch diameter light spot. To consider this tube with the distribution of light described above, reconsider the light received at the phototube not at a point, but in a circle 0.25 inch in diameter. This essentially adds many areas each with $\pm 5\%$ fluctuations to area A for the same small change in x, above, so that the net maximum fluctuation with all these independent areas is (0.7) (5%) or 3.5% or $\pm 0.35\%$ of the total intensity on the photomultiplier. Thus the combining of the intensity and sensitivity fluctuations can produce errors in successive photomultiplier outputs of (0.35%) (25%) or about $\pm 0.1\%$. This estimate will be improved when more detailed measurements have been made upon the photomultiplier and mixer chosen in the final design.

As part of the testing of components to go into the advanced bread-board and to aid the preliminary design studies, the branched fiber optics Figure 12 and an EMR 541A-01-14 photomultiplier were tested as described below.

Photomultiplier

A 0.25 inch diameter spot of light was moved about the photocathode surface while the anode current was recorded as a function of position. The resulting set of data is presented in Figure 13 as a map of the sensitivity of the surface in terms of lines of constant anode current. The values shown range from 80% to 120% of the average anode current, or sensitivity.

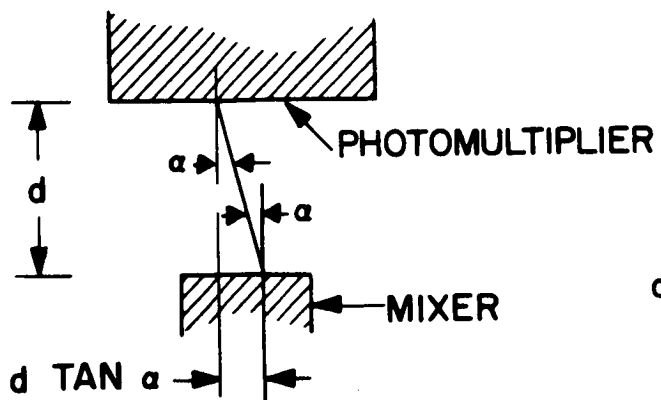


Figure 9

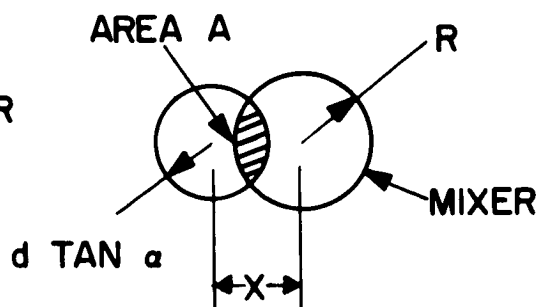


Figure 10

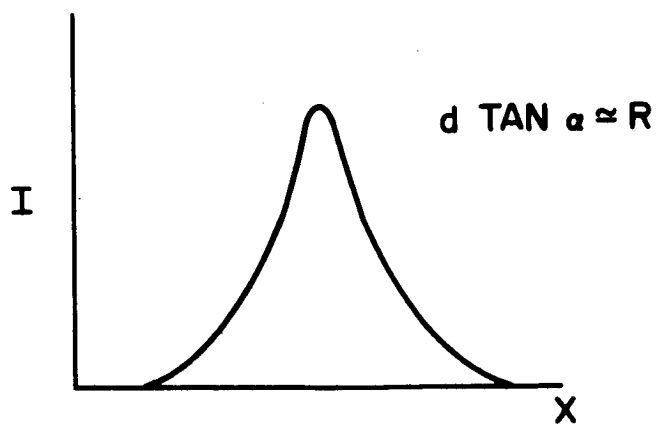


Figure 11

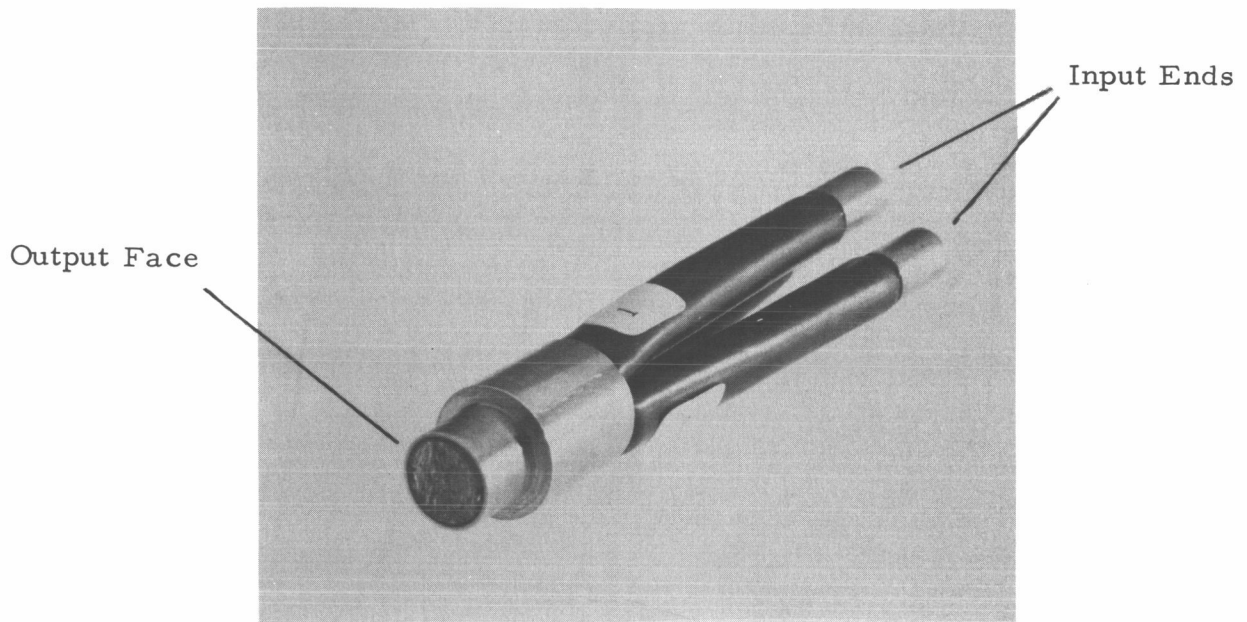
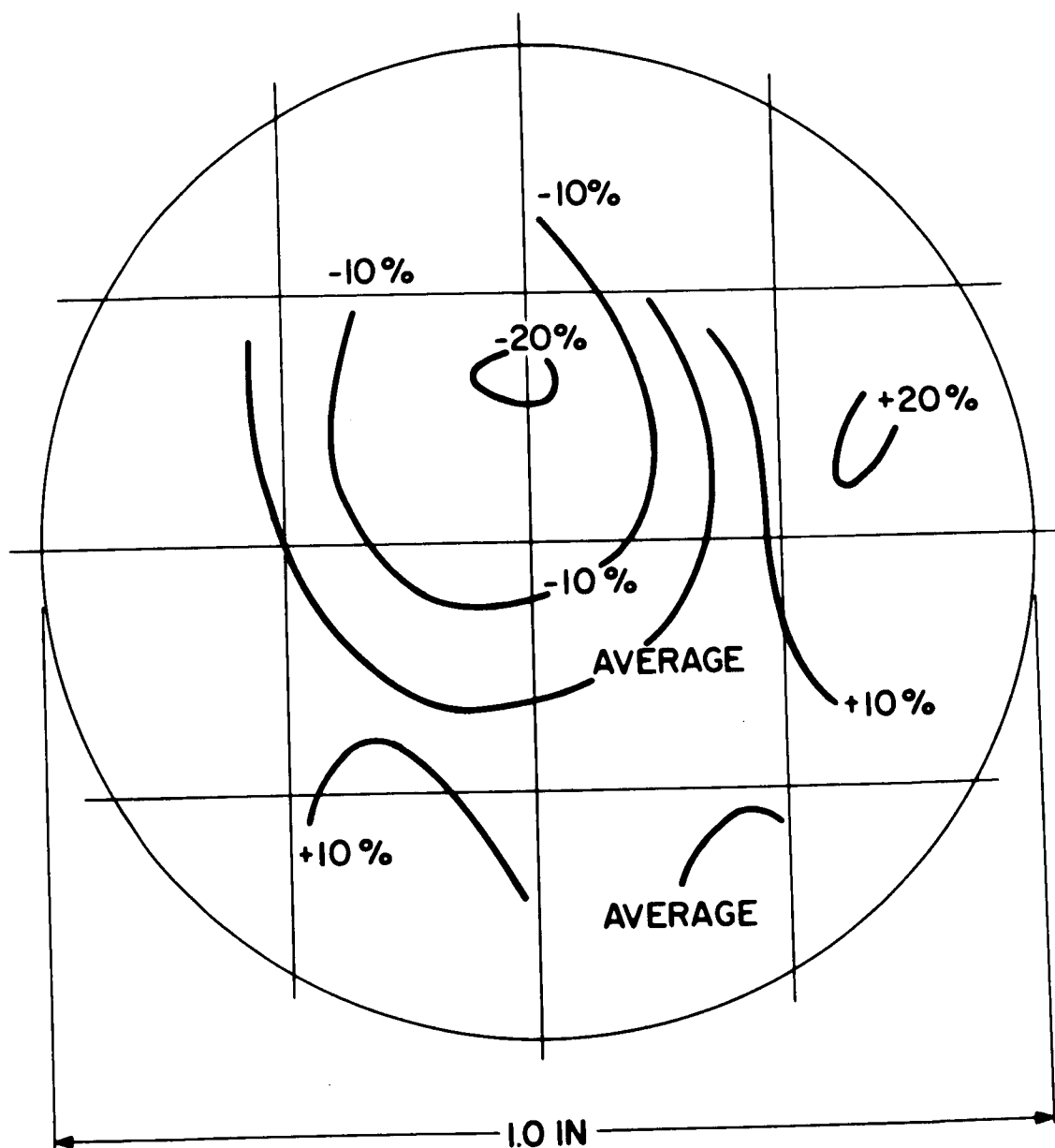


Figure 12. Branched fiber optics



Iso-sensitivity Contours for an EMR 541 A Phototube for Values Averaged over 1/4 in. dia. circle.

Figure 13

Fiber Optics - Full Illumination of Input Ends

A beam mixing fiber assembly meeting specifications was not available in time for testing. The following tests were carried out with the crude assembly available.

In a manner similar to that used above the light output from the fiber optics was measured at a distance of 1.25 inches from the output face. The average value over a 0.25 inch diameter area was measured in terms of anode current from a photomultiplier and the value of this current was recorded as a function of position of the 0.25 inch diameter area relative to the fiber optics. In performing this measurement the photomultiplier and 0.25 inch diameter aperture were held fixed while the fiber optics and source of illumination were moved. The results are shown in Figure 14 in which lines of constant anode current are again plotted. The values shown are only relative and range from the peak current or intensity down to a current 23% of this peak.

The data in Figure 14 were obtained for full illumination of branch No. 1. As may be seen in Figure 15, a corresponding plot for branch No. 2 would be centered better and that for No. 3 would be roughly complementary to No. 1, i.e., approximately a mirror image of Figure 14 about a line drawn from 10 o'clock to 4 o'clock using a clock face as a reference. Both Figures 13 and 14 are plotted viewing the plane of the 0.25 inch aperture from the source of light. The photographs of Figure 15 were taken looking toward the source of light.

Similar photographs were taken of another fiber optics beam mixer (see Figure 7) which demonstrated the ability to distribute the fibers of one input branch more uniformly over the face of the output. The small size of this bundle precluded conducting a test similar to that described above and obtaining meaningful data. Presumably if this uniformity were extended to a bundle of suitable size, the performance would be similarly improved.

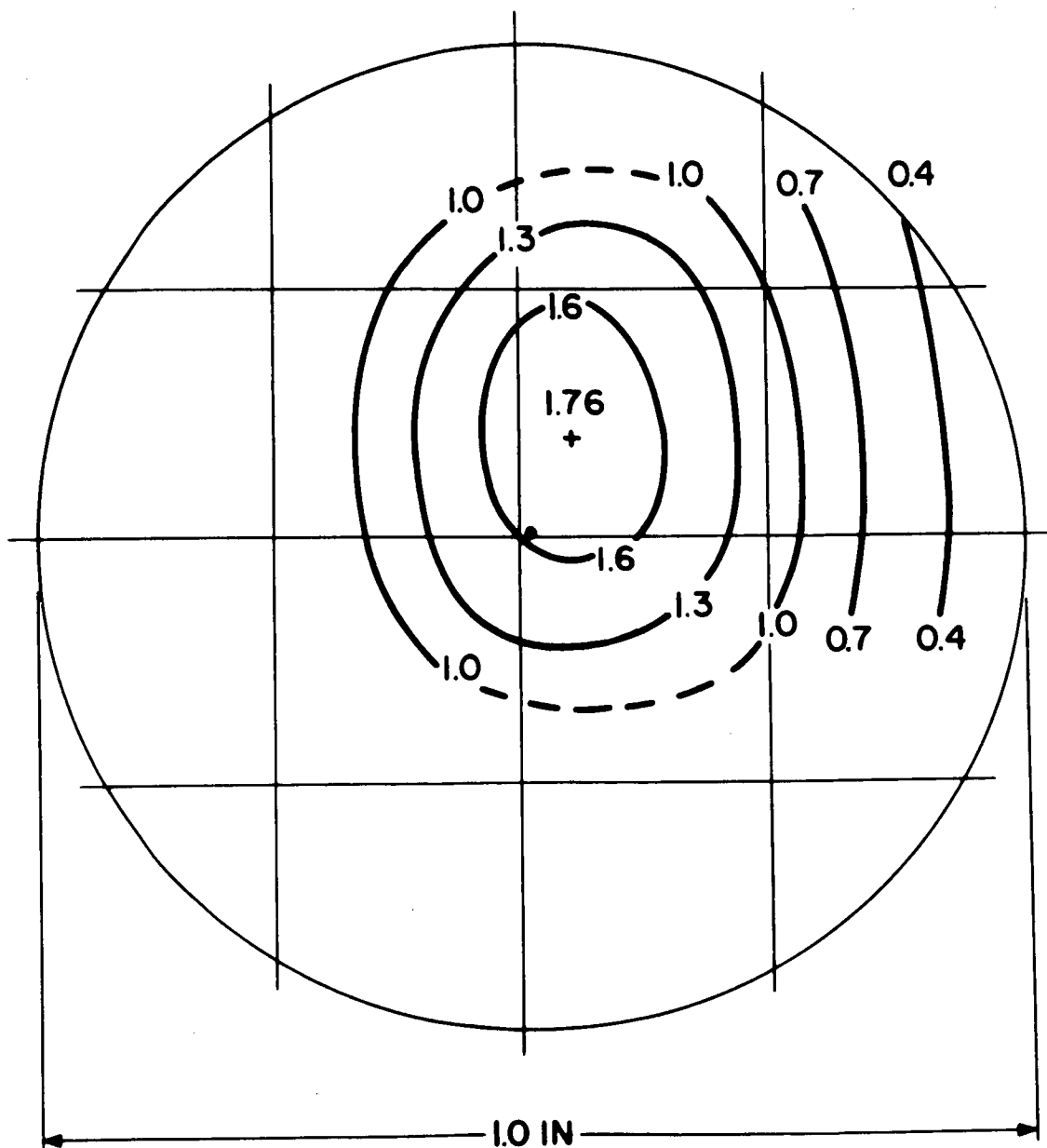
Fiber Optics - Photomultiplier Combined

The fiber optics and photomultiplier described above were combined such that their longitudinal axes were coincident, their relative orientations were approximately those shown in Figures 13 and 14 and the output face of the optics was 1.25 inches from the photocathode. Two situations were then studied.

(1) Input Areas Fully Illuminated

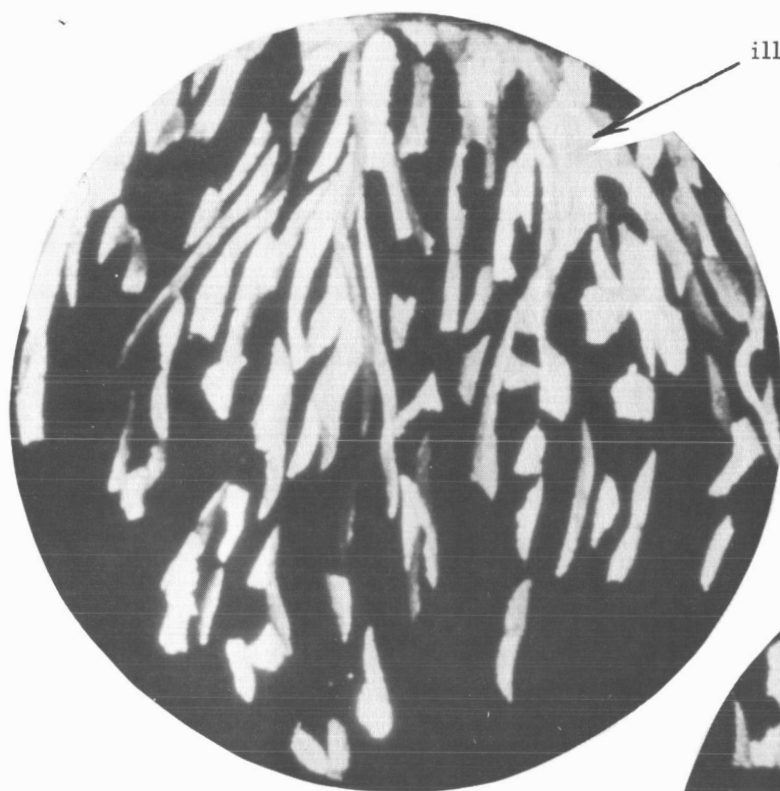
With all three input areas equally illuminated a value of anode current was obtained (approximately 0.5 microampere). Then with two inputs covered the following data (corrected for small differences in transmission) were obtained in terms of percentages of 1/3 of the above anode current.

Illumination of No. 1	111%
Illumination of No. 2	95%
Illumination of No. 3	94%



Iso-intensity Contours for Branch #1 (Light Input) of Fiber Optics for Value Averaged over a 1/4 in. dia. circle 1 1/4 in. from the Optics Output Face.

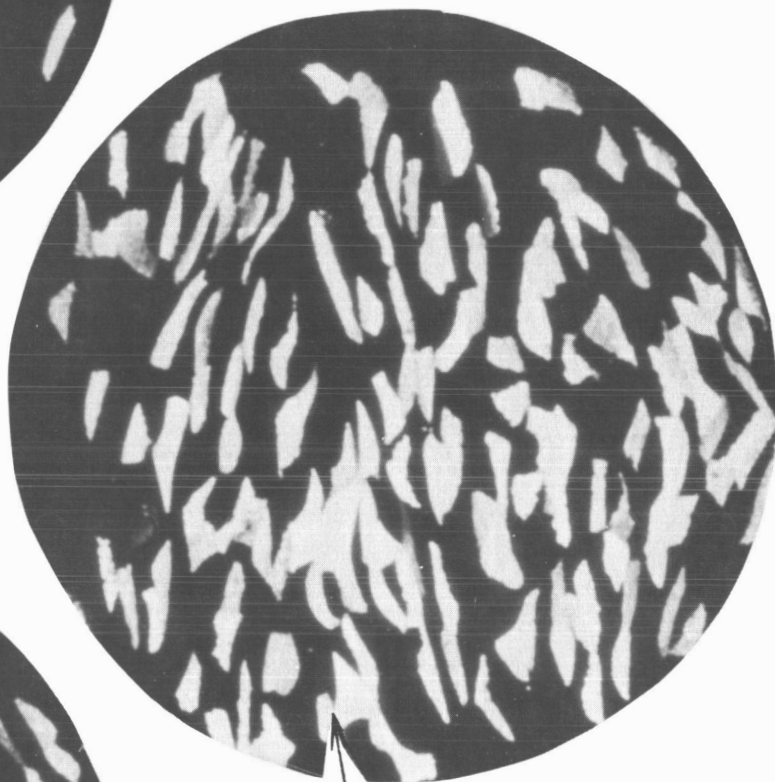
Figure 14



illuminated fibers

Branch No. 1

Branch No. 2



Branch No. 3



illuminated fibers

Output of Fiber Optics Assembly
with Full Illumination of the Input Faces

Figure 15

Thus, although the output light patterns of branches 1 and 2 are approximately complementary, their positions on the photo cathode surface were such as to emphasize the light in No. 1 by 17% over than in No. 3.

The fiber optics assembly was rotated while a constant light intensity was maintained and a peak to peak variation of 8% was found. If this were done with illumination in branch No. 2 a much smaller variation would be expected to the more uniform light distribution and if done with No. 3 a somewhat greater variation might be expected due to the greater number of fibers from No. 3 around the periphery of the output face.

(2) Input Areas Partially Illuminated

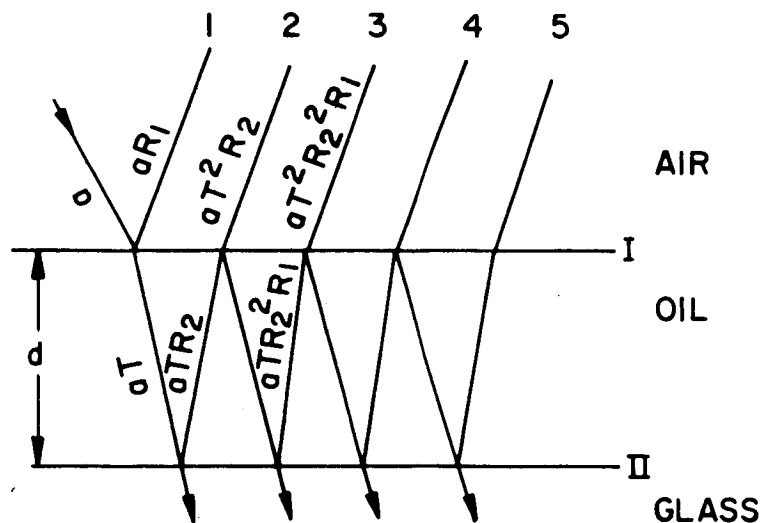
A spot of light - .10 inch in diameter was moved across the input face of branch No. 1 in 0.5 mm (0.02 inch) increments. The maximum variation of anode current from the average was 14%. No data were obtained for branches 2 or 3. But, due to the complementarity of No. 3 and the smaller variation photocathode sensitivity in the lower portion of Figure 13, similar data for No. 3 might be expected to produce a maximum variation less than 14%. Due to the more uniform distribution of light from No. 2 it might be expected to produce a maximum variation close to or somewhat less than 14%.

i) Effects of Thin Oil Films on Optical Components

A study of the change in reflective properties of an optical surface due to the deposition of a thin film has led to the conclusion that no deposition of oil can be tolerated unless the indices of refraction of the oil and glass can be matched to within ± 0.01 . The indices of refraction of two typical lubricating oils have been measured to be ≈ 1.45 . Therefore, to obtain an optical match (e.g. to the core glass $n \approx 1.62$ of a typical fibre optic system) would require fused quartz for example ($n \approx 1.45$) to be bonded to each optical surface.

Optical Effects of Oil Deposit

Consider an oil film of index n oil deposited on an optical surface of index n_g . (See sketch below)



where: a = incident amplitude
 R_1 = reflection coefficient for amplitude at I
 R_2 = reflection coefficient for amplitude at II
 T = transmission coefficient at I for amplitude

$$R_1^2 + T_1^2 = 1 \quad \text{or} \quad T = (1 - R_1^2)^{1/2}$$

The condition for maximum and minimum reflected intensities are:

$$2nd = (m + 1/2)\lambda \quad \text{min.}$$

$$2nd = m\lambda \quad \text{max.}$$

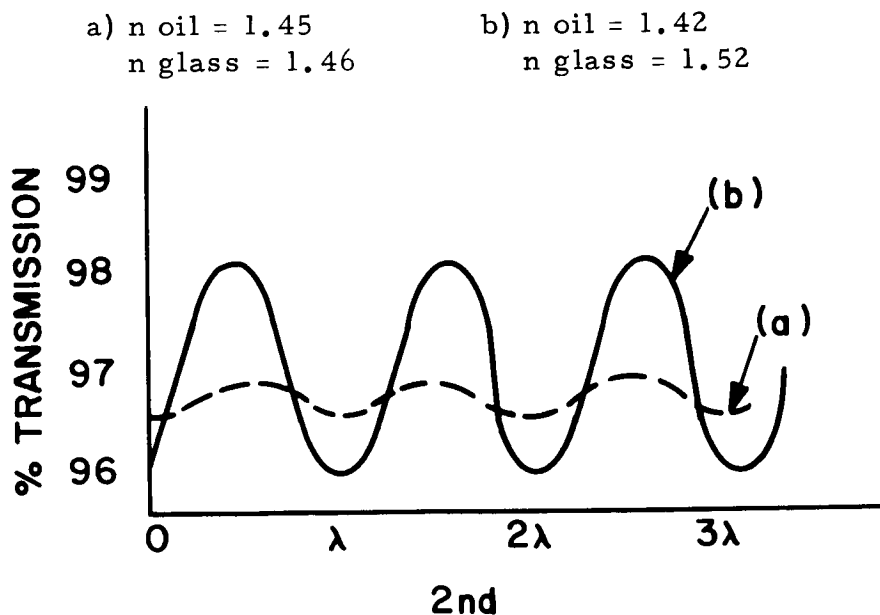
Taking into account the phase change of π at a rare dense reflection, the maximum and minimum reflected amplitudes are:

$$\text{min amplitude} = 1 - [2 + 3 + 4 + \dots]$$

$$\text{max amplitude} = [1 + 2 + 4 + 6 + \dots]$$

$$- [3 + 5 + 7 + \dots]$$

From these equations the variation of transmission as a function of the film thickness is given in sketch below for 2 cases:



It is evident that the variation in case (a) is of the order of a few tenths of a percent as the film thickness varies.

If we neglect interference effects the change in transmission with oil deposition as given by $R_1^2 + R_2^2 - R_0^2$ where R_0 is the amplitude reflectivity with no oil deposit. The % change in transmission for case (a) and (b) are $\sim 0.1\%$ and 1.2% respectively. The change in transmission for reflectivity of a thick film of oil ($n = 1.42$) deposited on glass ($n \approx 1.5$) was measured experimentally to be of the order of 1% confirming the above analysis. However, for thin films, as may be deposited in the SO46 instrument, the interference effects taken into account above are important.

b) Deposition of Vapor

In order to set an upper limit on the rate of deposition of oil on the optical surfaces, the following model has been adopted. It has been assumed that the major source of oil will be a thin film of grease on the motor shafts and bearings within the mechanical module. Under equilibrium

conditions the number of oil molecules evaporating equals the number returning to the surface. To set an upper limit, assume that all the molecules which leave surface are lost to walls of the module and the optic surfaces. Under these conditions the amount of oil leaving the surface equals the loss rate under vacuum. Assuming the oil deposits in a uniform manner in the mechanical module, then:

$$A_s LT = A_T \rho t$$

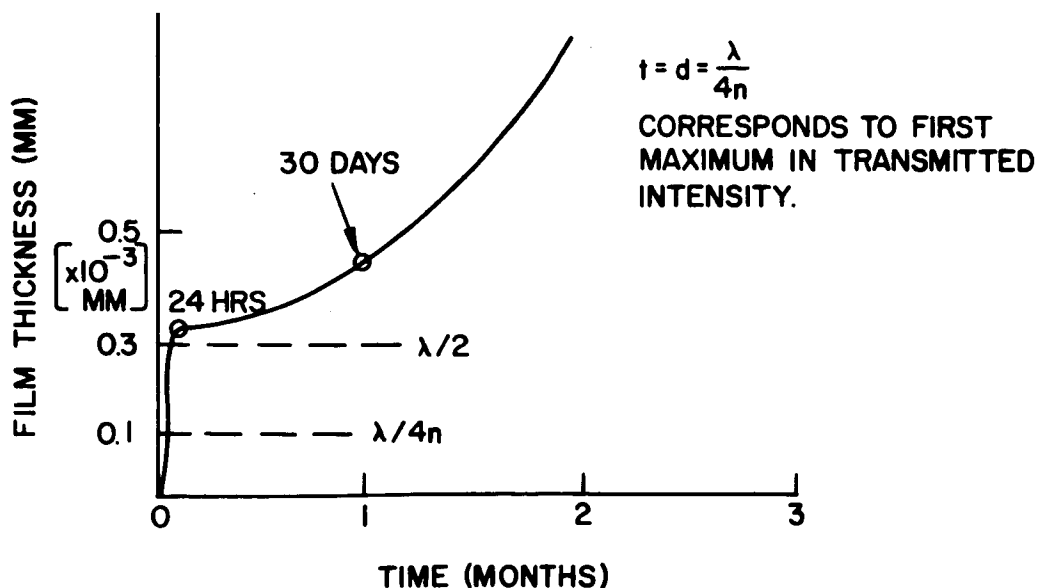
where:

$$\begin{aligned} A_s &= \text{area of shafts} \approx 15 \text{ cm}^2 & \left\{ \begin{array}{l} \text{assumed 3 shafts of } 1/4'' \\ \text{diameter and } 1'' \text{ effective} \\ \text{length.} \end{array} \right. \\ A_T &= \text{surface area of } \dot{=} 500 \text{ cm}^2 & \left\{ \begin{array}{l} \text{cylinder of } 5'' \text{ diameter and} \\ \text{mechanical module} & 2'' \text{ height} \end{array} \right. \\ \rho &= \text{density of oil } (\sim 0.8 \text{ gm/cm}^3) \\ T &= \text{time in hours} \\ t &= \text{film thickness} \\ L &= \text{evaporation rate under vacuum gm/cm}^2/\text{m} \end{aligned}$$

values adopted were taken from table II (PIR 26) for Versilube G-300 at 93°C.

In the following graph the film thickness in mm is given as a function of time. On same graph is indicated the film thickness corresponding to a one half wavelength of $\lambda = 5000 \text{ \AA}$.

Note: The growth rate given below is an upper limit.



Summary

It has been concluded that least risk is involved in providing grease lubricated bearings together with index of refraction matching by the use of fused quartz windows and quartz-coated inputs to the beam mixer. The reasons are as follows:

1. The matching of indices is almost sufficient in itself to eliminate the problem, even if one beam input has an oil coating and the other is completely free of oil. This would not be the case with wear particles from dry lubricated bearings.
2. Calculations and experiment indicate that, even if indices are not matched, layers sufficiently thick to give the same change in transmission to both beams being compared will build up rapidly and remain.
3. The use of grease lubricated bearings gives additional assurance of mechanical reliability, based on extensive Nimbus experience.
4. Use of dry lubricant would require additional testing, particularly with respect to the Geneva movement. The application of the lubricant coatings would be a significant additional cost item.

If any unexpected effects appear due to lubricant deposition with matched indices of refraction, they can be observed in the advanced breadboard testing. The use of dry lubricants will be kept as a backup.

3. Electrical Design

a) S046 Processor, Gain Change and Polarity Control Circuits

This Section describes the operation of the circuits that control the gain and polarity of the main processor (see Dwg. 125 C 1822 (Rev. A) "So46 Experiment Signal Processor Schematic").

The purpose of the gain change and polarity control circuits is to provide a unipolar output signal with a range from no less than 1 volt and no more than 10 volts for any expected input signal condition.

Figure 16 shows the inverter circuit and switches which by proper switch operation can always provide a unipolar output. The inverting amplifier A4 has unity gain and if the input polarity is opposite to the output polarity desired, switch S4 is closed and S3 is opened.

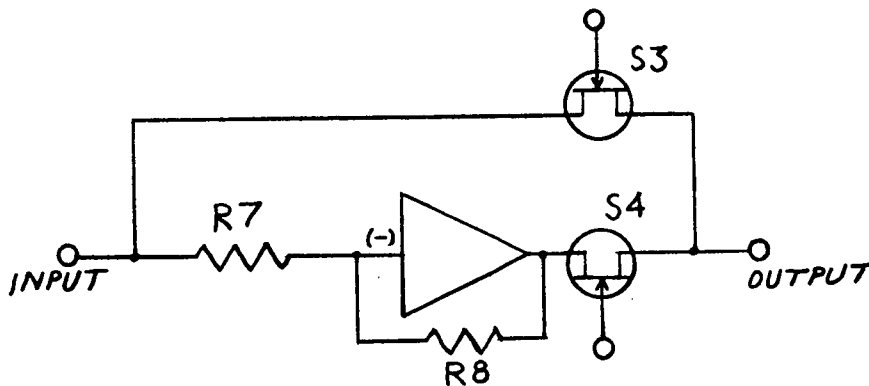


Figure 16

Figure 17 shows how the electronic gain is varied in three levels. If both S9 and S10 are open amplifier A2 has unity gain. If S10 is closed the gain is higher, given by the expression $G = \frac{R3}{R5} + 1$.

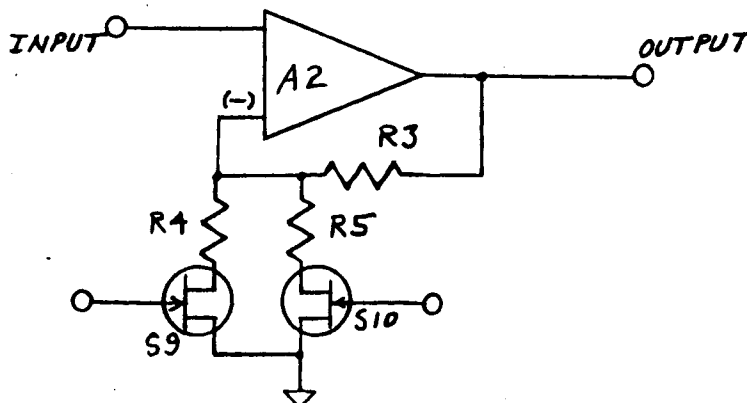
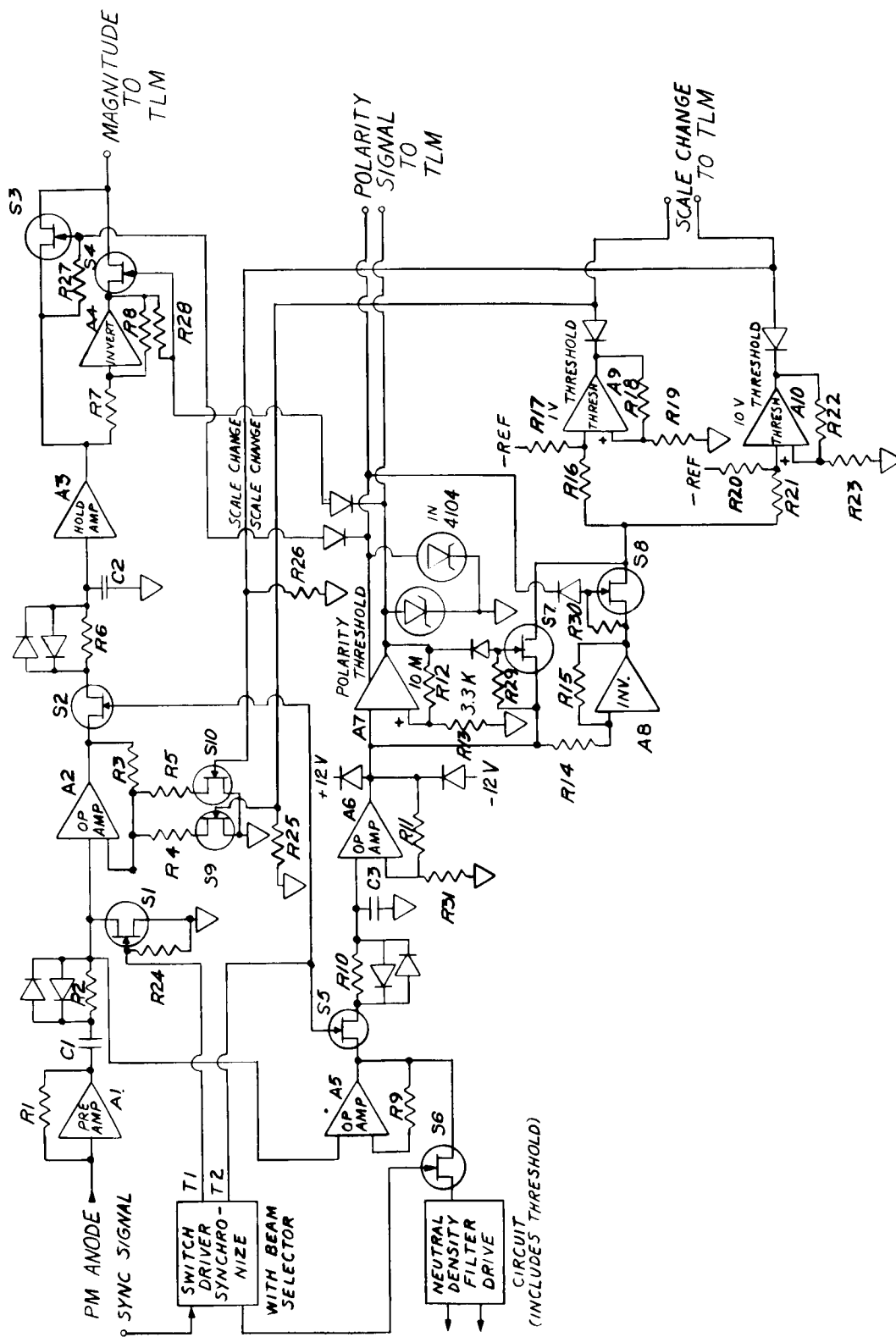


Figure 17



Dwg. 125C822. Signal Processor Schematic

If both S9 and S10 are closed the gain is highest and is given by the expression

$$G = \frac{R3}{R4} + \frac{R3}{R5} + 1 .$$

The appropriate drive signals for the switches S3, S4, S9 and S10 are provided by a separate coarse signal processor.

Figure 18 is a simplified schematic of the electronics which provides the drive signals for switches S3, S4, S9, and S10 as well as discrete telemetry information identifying the switch or switches that are actuated.

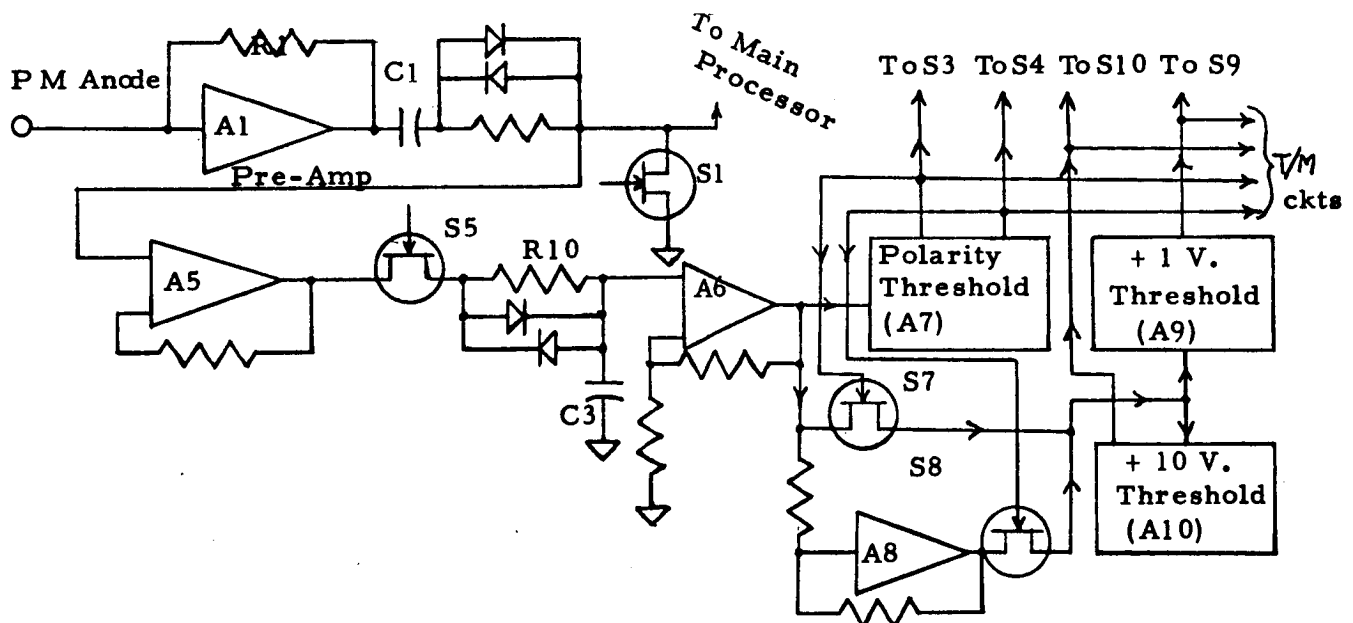


Figure 18

Capacitor C1 and switch S1 have made the ground or zero voltage the voltage of I/2 or the unpolarized signal. Through buffer amplifier A5 this signal is brought to switch S5. Switch S5 closes during the intervals when the polarized light or the background signal is present. When S5 is closed C3 charges to this signal, so the voltage on C3 is in fact the processed signal voltage proportional to either I/2 - B, I/2 - D, or I/2 - 0; depending on the position of the beam selector wheel. Buffer or hold amplifier A6 presents this signal to the polarity threshold which closes either S7 or S8 depending on whether the signal is (+) or (-). At the same time either S3 or S4 is closed in the main processor. If the signal is less than the pick-up voltage of either the +1 or +10 V threshold the processor gain must be maximum so both S9 and S10, Figure 17, are closed. Now if the

signal is high enough to pick-up the +1V threshold, switch S9 is opened reducing the processor gain. If both the +1V, and +10V thresholds are picked up then both S9 and S10 are opened giving the lowest processor gain.

The bandwidth of the coarse processor circuits A5, S5, R10, C3 and A6 can be much wider than the main processor for two reasons -

- 1). The required accuracy is not as high and
- 2). The +1V threshold only operates when the main processor output reaches +10Volts at the highest gain which is a signal +20 db higher than the minimum processed signal.

The coarse processor will have a time constant of no more than 1 millisecond, and will within about 2 milliseconds set the proper polarity and processor gain for each processed signal.

Using this method the output to the telemetry circuits will be a signal from +1 to 10 volts, a discrete signal identifying the proper polarity and a discrete signal identifying the scale factor.

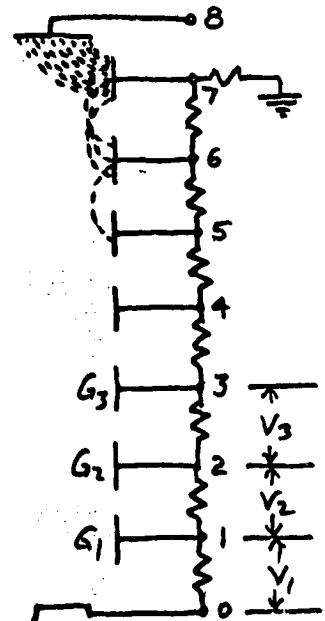
b) Photomultiplier Gain Stability in the Presence of Anode Current

At right is a schematic representation of a photomultiplier consisting of a cathode, seven dynodes, an anode and the dynode voltage divider string. The gain of dynode 1 is $G_1 = K_1 V_1$, dynode 2 is $G_2 = K_2 V_2$ etc. The total tube gain is $G = G_1 \times G_2 \times G_3 \times \dots \times G_7$, or $G = K_1 G_1 \times K_2 G_2 \times \dots \times K_7 G_7$. We may assume $K_1 = K_2 = K_3$ etc and that K does not vary with current or small voltage changes.

$$1) G = K^7 \text{ With } K_1 = K_2 = K_3 = \dots = K_7 = K, (V_1 \times V_2 \times V_3 \times \dots \times V_7).$$

If the anode current is zero and the bleeder resistors are equal,

$$2) G = K^7 V^7 \text{ where } V \text{ is the zero current interdynode voltage.}$$



If anode current flows the resistor between dynode 7 and anode will be shunted by this current and therefore its voltage will drop. In other words the bleeder current will be changed by changing each interdynode voltage so that the sum of bleeder current plus dynode current is a constant. This means the lower dynodes will operate at a higher voltage since their

dynode current is very small. The net effect, if the anode current is considerably smaller than bleeder current, is an increase in overall gain.

In order to examine the gain with anode current, equation (1) can be written as

$$G = K^7 (V + \Delta V_1)(V + \Delta V_2)(V + \Delta V_3) \dots (V + \Delta V_7) \text{ or}$$

$$(3) \quad G = K^7 \left[V^7 + \alpha_1 V^6 + \alpha_2 V^5 + \dots \right] \text{ where } \alpha_1 = \sum_i \Delta V_i \text{ and}$$

$$\alpha_2 = \sum_{i < j} \Delta V_i \Delta V_j \text{ etc.}$$

Assuming ΔV can be made sufficiently small,

$$(4) \quad G \approx K^7 \left[V^7 + V^6 \left(\sum_i \Delta V_i \right) \right].$$

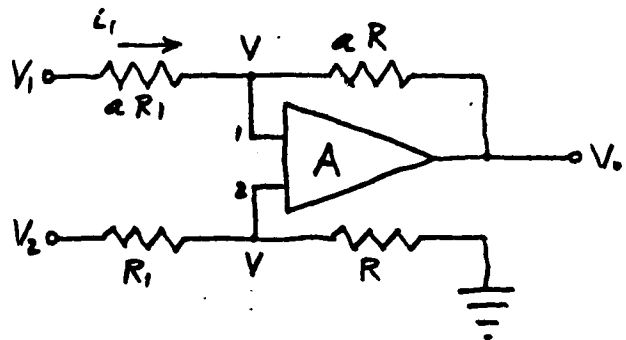
Examination of equation (4) shows that it is the gain at zero anode current plus the error term $V^6 \left(\sum_i \Delta V_i \right)$. This error term is just the sum of the voltage variation of the seven dynodes. If then the voltage from the cathode to dynode 7 is regulated the term $V^6 \sum_i \Delta V_i = 0$ and the gain with anode current becomes $G = K^7 V^7$, the same as the gain without anode current. If this is done, equation (3) becomes $G = K^7 [V^7 + \alpha_2 V^5 + \dots]$ and the new error term is $V^5 \sum_{i < j} \Delta V_i \Delta V_j$. This term can be made small without excessive bleeder current in the SO46 experiment. The following section gives the proposed regulator which is designed to regulate cathode to dynode 7 voltage.

c) High Voltage Supply Regulator

The previous section described how regulating the cathode to 7th dynode voltage greatly improves the photomultiplier gain stability in the presence of anode current. This section describes a regulator designed to accomplish the desired regulation.

In the sketch at right, A is a high gain d.c. amplifier so the voltage at input 1 is equal to the voltage at input 2.

To derive the equation for output voltage V_o , assume inputs 1 and 2 require no current.



Differential Amplifier

$$V = \frac{R}{R_1 + R} V_2 \text{ at input 2.}$$

Because V at input 1 is equal to V at input 2,

$$V_o = V - i_1 aR. \quad i_1 = \frac{V_1 - V}{aR_1} = \frac{V_1}{aR_1} - \frac{1}{aR_1} \frac{R}{R_1 + R} V_2$$

Substituting,

$$V_o = \frac{R}{R_1 + R} V_2 - aR \left[\frac{V_1}{aR_1} - \frac{RV_2}{aR_1(R_1 + R)} \right] = \frac{RV_2}{R_1 + R} - \frac{RV_1}{R_1} + \frac{R^2 V_2}{R_1(R_1 + R)}$$

Note that "a" may have any value. This means the currents from V_1 and V_2 need not be the same.

$$V_o = \frac{RR_1 V_2 - RV_1(R_1 + R) + R^2 V_2}{R_1(R_1 + R)} = \frac{V_2 R(R_1 + R) - V_1 R(R_1 + R)}{R_1(R_1 + R)}$$

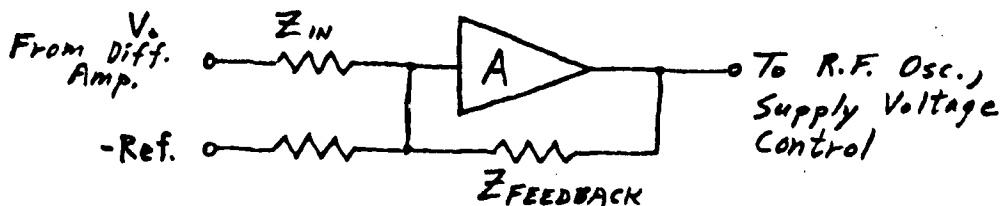
$$V_o = \frac{R}{R_1} (V_2 - V_1).$$

Making $V_o = 10$ volts with $V_1 = -1400$, cathode voltage and $V_2 = -200$, the 7th dynode voltage,

$$10 = \frac{R}{R_1} (-200 + 1400), \quad \frac{R_1}{R} = 120.$$

The sketch below shows the reference subtracted from V_o with a high gain amplifier whose output then controls the R.F. oscillator voltage and hence the high voltage output level.

The input and feedback networks Z_{in} and $Z_{feedback}$ will be determined by supply output impedance, regulation requirements and stability.



Comparator

d) High Voltage Power Supply Design

This section describes the preliminary design of the High Voltage Supply for the photomultiplier tube. This circuit has been bread-boarded and tested in the laboratory. See Figure 19.

The power supply can be broken down into five functional circuits as follows:

1. Amplifier A1 is the differential amplifier.
2. Amplifier A2 is the error amplifier.
3. Q1 and Q2 are the current limiting driver stages.
4. Q3 is the radio frequency (50 KC) oscillator.
5. The string of diodes and capacitors is the 8 stage voltage multiplier.

These circuits will be described in the order given.

The Differential Amplifier

Referring to the previous section and sketch of differential amplifier, the output voltage of A1 is

$$V_o = \frac{R}{R_1} (V_2 - V_1), \text{ where}$$

$$R = 220K, R_1 = 30 \text{ Meg}, V_2 = -200V, V_1 = -1600V.$$

Therefore

$$V_o = \frac{.22}{30} (-200 + 1600) = \frac{.22}{30} (1400) \approx 10 \text{ volts.}$$

This voltage can be measured at the test point provided.

The capacitors C1 and C2 in this circuit reduce the ripple and pickup that may come from the high frequency oscillator and voltage multiplier. C2 also is used to slow the -200 volt signal, which by itself is regenerative through the loop, to match the time constant of the -1600 volt signal. Without the lag of C2 the supply would have an undesirable overshoot for a stepped load current out of the 7th dynode.

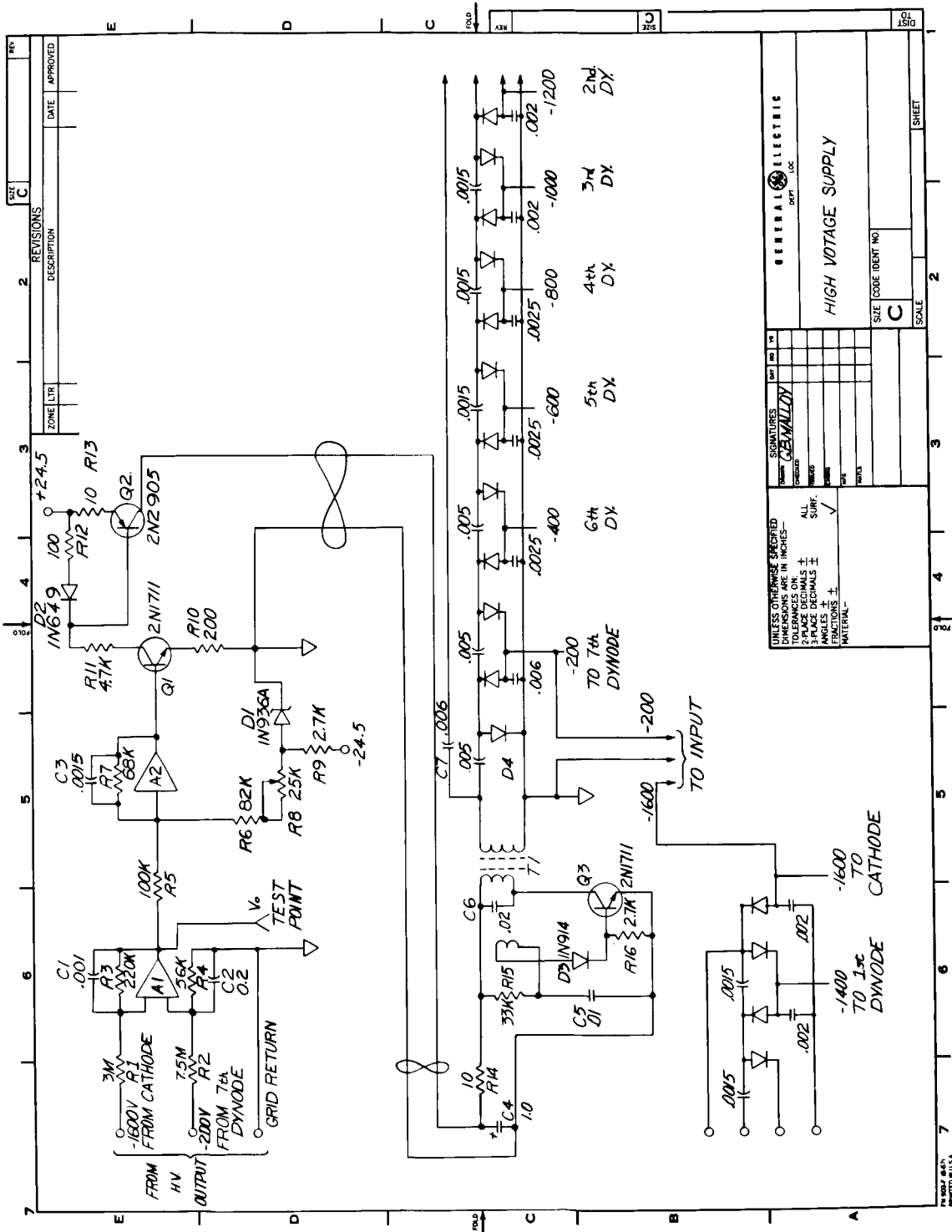


Figure 19. Schematic of high voltage supply

The Error Amplifier

The output voltage V_o of the differential amplifier delivers a signal current toward the input of A2 through R5 which then splits up into a reference current through R6 and an error current through R7. If the error current is not zero it produces an output voltage into the driver stage Q1. The result is to change the R.F. oscillator voltage which changes the signal current until the error current is nearly zero. Capacitor C3 filters undesirable noise and ripple. The signal current is $\frac{V_o}{R5}$ and the reference current is $\frac{9.15 \text{ volts}}{R6 + R8}$ and because the loop will make these currents nearly equal, the variable resistor R8 can control the output of the power supply.

Current Limiting Driver

An input voltage into Q1 base from the error amplifier produces a collector current in Q1 of $I_c = \frac{V}{R10}$. This produces a voltage drop across R12 at the input of Q2 of $\frac{V}{R10} \times R12$. Q2 acting here as an emitter follower puts this voltage across R13, so a collector current flows through Q2 of $\frac{V}{R10} \times R12 \times \frac{1}{R13}$. This is the output current which drives the R.F. oscillator. We shall now describe how this current is restricted to some maximum value.

In the collector of Q1 is R11. The maximum current that can flow in Q1 is $I_{\max} \approx \frac{24.5}{R10 + R11 + R12}$, neglecting the small diode drop and transistor saturation drop. This current produces a maximum voltage across R12 and, via Q2, across R13 of $V_{R13} = \frac{24.5}{R10 + R11 + R12} \times R12$. Therefore the maximum current through R13 and Q2 is $\frac{24.5 \times R12}{R10 + R11 + R12} \times \frac{1}{R13}$. With the values given, this current is

$$I_{\max 2} \approx \frac{24.5 \times 100}{200 + 4,700 + 100} \times \frac{1}{10} = \frac{2450}{10 (5,000)} \approx 50 \text{ Ma.}$$

Of this current the oscillator and high voltage multiplier consume 20 Ma., so the maximum excess power is $(50-20) (24.5) = 30 \times 24.5 \approx 750$ milliwatts. Assuming this is due to a high light level on the photomultiplier, the anode current cannot exceed about 2 milliamperes. This exceeds the guarantee value but is by no means destructive. The major effects are to produce a temporary reduction in gain which affects immediate processing accuracy, and to age the tube which is a permanent reduction in gain.

Other than a possible aging of the photomultiplier, no damage will be sustained by any part as a result of high load current out of the high voltage power supply.

The R. F. Oscillator

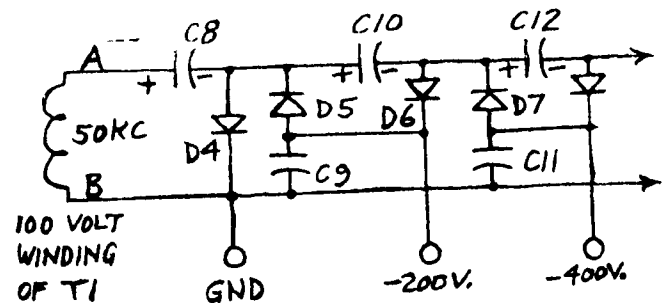
The 20 volt primary of T1 and capacitor C6 are resonant at about 50 KC with a Q of about 25. The 5 volt secondary provides positive feedback to Q3 forcing it to oscillate at 50 KC. A 100 volt winding delivers the 200 volt peak to peak voltage to the high voltage multiplier. Capacitor C4 and resistor R14 serve to decouple the 50 KC current pulses from the driver stages.

The 100 volt winding isolates the High Voltage Multiplier from the oscillator so that the ground return of the high voltage, which is the photomultiplier anode current return, can be used as the signal return of the processor.

The Voltage Multiplier

A schematic of the first two stages of the voltage multiplier is shown below.

Assume the voltage at point A is going to +100 volts. Capacitor C8 will charge through diode D4 to 100 volts with the polarity shown. In the next half cycle point A will go to -100 volts. This -100 volts added to the -100 volts across C8 puts the cathode of D5 at -200 volts hence capacitor C9 charge to -200 volts. When point A again goes to +100 volts the downstream side of C10 is tied to C9 which is at -200 volts so C10 charges up to 200 volts with the polarity shown. Now when point A again goes to -100 volts, this -100 volts added to the 100 volts of C8 and the -200 volts of C10 drive the cathode of D7 to -400 volts. This charges C11 to -400 volts.



There are eight such stages each with an output of 200 volts more negative than the previous stage. Lines are brought out from C9, C11, etc., to the 7th. dynode, 6th. dynode, etc., until the last stage which goes to the cathode. The -200 and -1600 volt lines also go to R2 and R1 respectively as feedback to the differential amplifier.

With a maximum anode current step of 30 microamperes, the supply voltage ($V_2 - V_1$) varies by approximately 1.0 volt. This represents

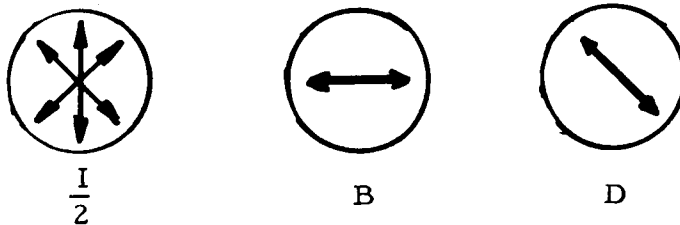
about 1/2% processor error. The transient period is completely over in 10 milliseconds and will not affect the processor accuracy. The low frequency noise content measured less than 0.07 volts which represents about .005%. It will not significantly affect processor accuracy. No shielding effective at 60 and 120 cycles was used with the breadboard.

Total power consumed was about 1 watt divided equally between the oscillator-voltage multiplier and regulating circuits.

4. Dynamic Range Considerations

a) Dynamic Range Calculations

The instrument is designed to measure the relative intensities in three beams, each of different polarization characteristics but which cover the same field of view, and perform difference measurements between electrical signals which correspond to these intensities. The polarization characteristics of the three beams are best described in the sketch below.



The quantities obtained by the instrument are

$$I = 2\frac{I}{2} = 2\frac{A+B}{2} \text{ (The } \frac{I}{2} \text{ channel has a neutral filter of density 0.301)}$$

$$Q = 2 \left[\frac{A+B}{2} - B \right]$$

$$U = 2 \left[\frac{A+B}{2} - D \right]$$

In order to assess the dynamic range of the instrument it is necessary to look at the maximum and minimum signals to be expected in any channel. In the case of maximum signal let us look at the $\frac{I}{2}$ channel. In the extreme case when A is zero then $I = 2\frac{B}{2}$ and the signal seen by the $\frac{I}{2}$ channel is $\frac{B}{2}$, while the signal seen by the B channel is B. In the case of minimum signal, both the B and the D channels are subtracted from $\frac{I}{2}$. The lower limit of sensitivity will be shown in a later section to be limited

by the statistical noise in the $\frac{I}{2}$ channel. It follows that the maximum signal to be observed is in the B or D channel and is B(max) or D(max) and the minimum signal for which 0.07% clamping accuracy is required is that seen in the $\frac{I}{2}$ channel as $\frac{I}{2}$ (min).

In order to evaluate the range of values to be expected from B(max) to $\frac{I}{2}$ (min) we have assumed a range of illumination angles ranging from $\mu_o = 1.0$ to $\mu_o = 0.1$ ($\mu_o = \cos\theta_o$ where θ_o is the zenith angle of the sun), and a range of albedos from unity to 0.03. The Coulson, Dave, Sekera Tables were used as a basis to find the maxima and minima of the quantities desired over the range of look angles expected. Since $B \leq I$, values of I max were computed utilizing these tables.

The accompanying table shows the steps used to calculate the currents for the photomultiplier from the values of I(max) and $\frac{I}{2}$ (min). The first column gives the center wavelength while the second column gives the relative intensity components of I(max) and $\frac{I}{2}$ (min). The third column gives the ratio of solar flux at that wavelength divided by π , since the Sekera et al calculations are for π units of incident flux. The fourth column, target intensity is given by,

$$\text{Target intensity} = \left\{ \begin{array}{l} I(\text{max}) \\ I/2(\text{min}) \end{array} \right\} \frac{\text{Solar flux}}{\pi} \text{ watts cm}^{-1} \mu^{-1} \text{Ster}^{-1}.$$

The next columns give the field of view of the instrument (ϕ = three degrees $\sim 2.14 \times 10^{-3}$ steradian) and the aperture of the objective lens ($A = 0.75$ inches = 2.85 cm^2). The filter bandwidths are given in microns for the types of filters chosen. The next column is the light power in watts incident on the objective lens in the filter bandwidth which is calculated by,

$$W = (\text{Target Intensity}) \phi A(B.W.)$$

The transmission of the optical system is now tabulated at each color and the light signal incident on the photomultiplier is calculated by

$$W_p = WT$$

The nominal sensitivity of the photocathode (S = amperes/watt) at the various wavelengths is tabulated and the nominal gain of the photomultiplier is listed as 10^4 . The anode current is calculated in the next column without attenuators. The next two columns give the values for the step attenuator and the fixed attenuators in each color channel. The last

TABLE IV

Wave-length (μ)	I (max)	Target Int. Solar Flux π cm ⁻² ster ⁻¹	Solid Angle of Inst. (° Ster.)	Aperture (A cm ²)	Filter Band Width (BW μ)	Watts Incident on system (W)	Trans-mission of optics (T)	Watts Incident on P. M. (Wp)	Sensitivity of Cathode (S amps/watt)	Gain of P. M. (G)	Anode Current (i _a μamps)	Fixed attenuator density (ratio)	Step attenuator density	Anode Current with attenuators (micro amperes)	Signal dynamic range expected in each channel
0.38	1.0870	0.04456	0.04844	2.14×10 ⁻³	2.85	0.0105	3.102×10 ⁻⁶	0.056	1.74×10 ⁻⁷	0.060	10 ⁴	0.02572 (1.061)	1	9.77	75:1
0.44	1.0584	0.05857	0.06199	2.14×10 ⁻³	2.85	0.0105	3.970×10 ⁻⁶	0.102	4.05×10 ⁻⁷	0.065	10 ⁴	0.34830 (2.23)	1	11.8	91:1
0.50	1.0400	0.06494	0.06754	2.14×10 ⁻³	2.85	0.0118	4.861×10 ⁻⁶	0.102	4.96×10 ⁻⁷	0.052	10 ⁴	0.25018 (1.779)	1	14.5	119:1
0.58	1.0250	0.05921	0.06069	2.14×10 ⁻³	2.85	0.0138	5.108×10 ⁻⁶	0.102	5.21×10 ⁻⁷	0.037	10 ⁴	0	(1.00)	19.3	148:1
$\frac{I}{2}$ (min)															
0.38	0.0144	0.04456	0.000642	2.14×10 ⁻³	2.85	0.0105	4.111×10 ⁻⁸	0.056	2.30×10 ⁻⁹	0.060	10 ⁴	0.02572 (1.061)	0	1.30	
0.44	0.0117	0.05857	0.000685	2.14×10 ⁻³	2.85	0.0105	4.387×10 ⁻⁸	0.102	4.47×10 ⁻⁹	0.065	10 ⁴	0.34830 (2.23)	0	1.30	
0.50	0.0093	0.06494	0.000604	2.14×10 ⁻³	2.85	0.0118	4.347×10 ⁻⁸	0.102	4.43×10 ⁻⁹	0.052	10 ⁴	0.25018 (1.779)	0	1.30	
0.58	0.0069	0.05921	0.000409	2.14×10 ⁻³	2.85	0.0138	3.442×10 ⁻⁸	0.102	3.51×10 ⁻⁹	0.037	10 ⁴	0	(1.00)	1.30	

column gives the maximum and minimum values of the anode current to be expected in any color channel under the condition specified in the table.

b) Electronic Gain Settings and Gain Overlap Region

The previous section has discussed the dynamic range requirements for the experiment in terms of the unprocessed signals. It is the purpose of this section to discuss dynamic range considerations including the voltage range limitations of the preamplifier, the electronic gain settings of the gain switching amplifier, and the overlap regions in which the electronic or optical gain settings can have either of two values depending upon whether the signal level is increasing or decreasing.

The variable aperture provides optical attenuation settings of $A = 1, 0.1, \text{ or } .01$ relative to the situation with no optical attenuation in the light path. The first two attenuator settings are capable of handling the signal intensities expected according to the assumption of Lambert reflection, Rayleigh scattering, and the specified range of surface albedos and solar angles. Alternate insertion or removal of the factor 10 attenuations will restrict phototube anode currents to the range $0.65 \text{ to } 13 \mu\text{amps}$. Such a restriction is required to satisfy photoelectron statistics on the one hand and reasonable power supply size and phototube linearity on the other hand. The anode current is also restricted because of the requirement to restrict the preamplifier voltage to the range $50 \text{ mV to } 10 \text{ volts}$. This restriction follows from the requirement for 1% signal processing accuracy at the low end and the avoidance of amplifier saturation at the high end.

Electronic gain setting of 1, 5, and 25 are recommended in order to restrict the experiment output voltages to the vehicle storage and telemetry system to the range 1 to 10 volts. This section will show that these gain settings are satisfactory and provide sufficient overlap so that normal noise should not cause a change in gain setting for signals near the gain switch threshold.

The dynamic range for the experiment can be represented as a two-dimensional figure in which the total intensity is chosen as abscissa and a typical processed signal such as Q is shown as ordinate. Since neither Q nor U can exceed I , this ordinate scale can be thought of as representing any of the three processed Stokes parameters $I, Q, \text{ or } U$. In order that the preamplifier output voltage limitation be taken account of in determining the overall dynamic range, this ordinate scale can be expressed in the corresponding voltage. This voltage, when multiplied by the gain of the gain switching amplifier, will give the voltage input to the vehicle data handling system. Figure 20 shows the two-dimensional representation of the dynamic range in terms of photomultiplier anode current and preamplifier output voltage. The abscissa scale is labeled alternately in terms of the absolute radiant flux as

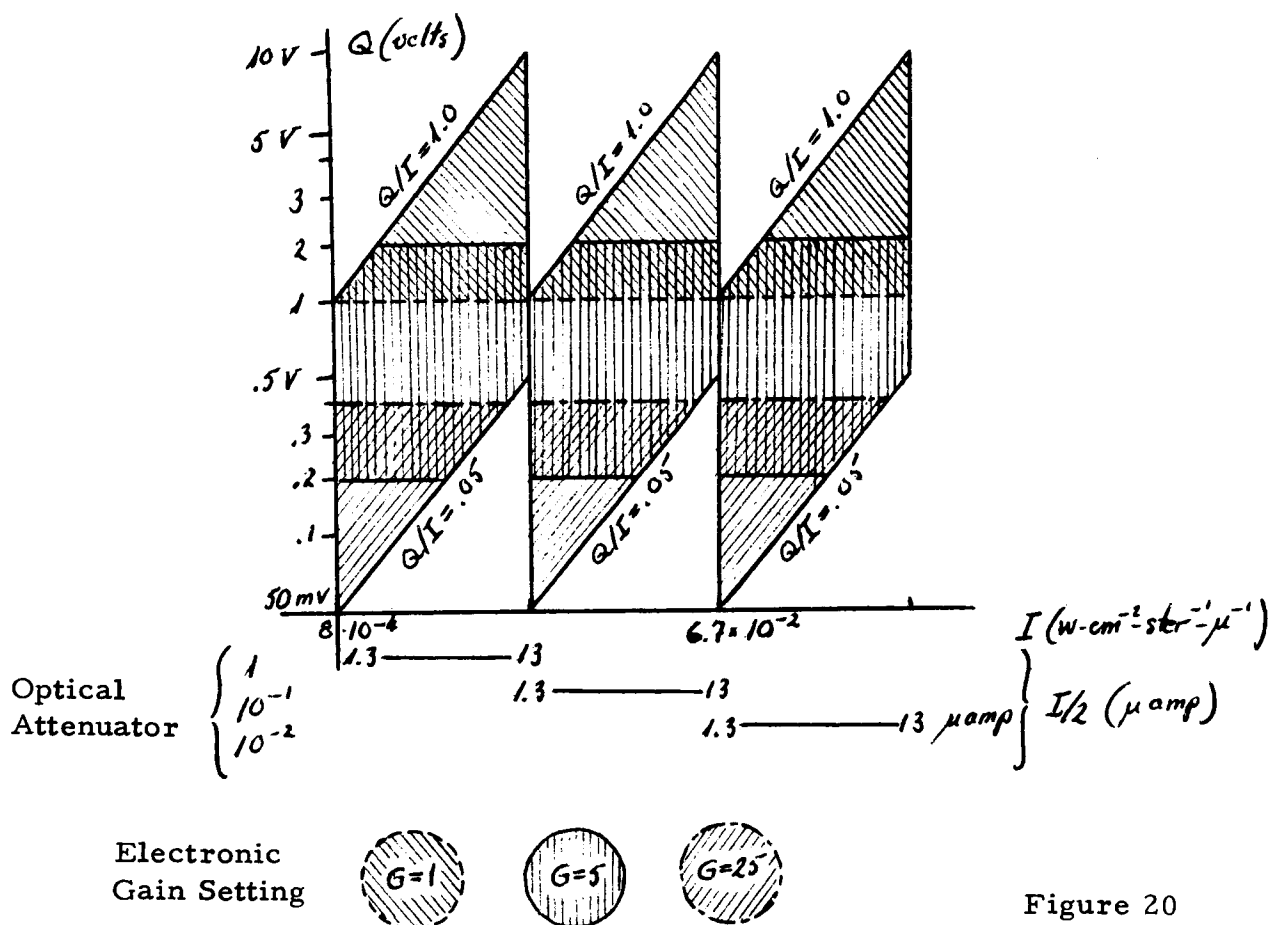


Figure 20

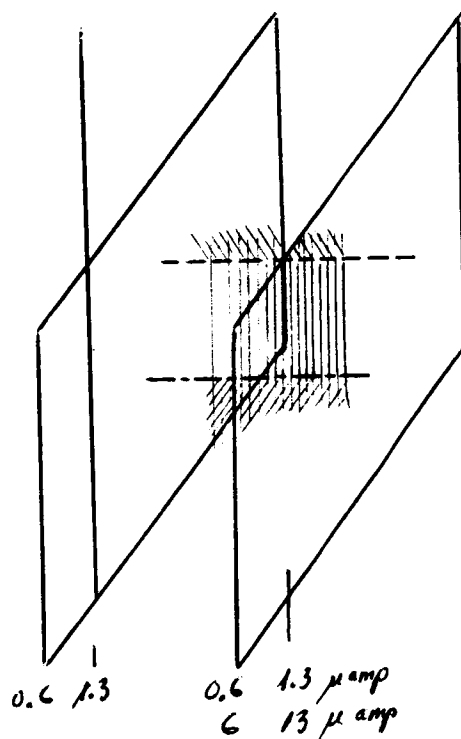


Figure 21

taken from the previous section, which ranges between 8×10^{-4} and 6.7×10^{-2} $\text{w} - \text{cm}^{-2} - \text{ster}^{-1} - \mu^{-1}$ and in terms of μ amps anode current. The effect of the introduction of the two neutral density filters restricts the variation in tube current to a single decade, although thereby three decades are actually covered. The scales of absolute flux and current are not uniquely relateable because of the fact that the phototube efficiency, optical transmission and filter bandwidth varies for the different spectral interval measured.

The region within which 1% accuracy in measurement of the Stokes parameters is specified is included between the pairs of lines labeled $Q/I = .05$ and $Q/I = 1.0$. It can easily be seen that the restriction on the buffer amplifier voltage to the range 50 mV to 10 volts automatically restricts the phototube current range to a factor 10. This follows because the dynamic range in processed signal is the product of the dynamic range in I and Q/I . The figure shows that another decade of readable signal strength is available above the maximum level predicted in the previous section. For a wavelength of 5000 Å the corresponding radiant flux would be $0.67 \text{ w} - \text{cm}^{-2} - \text{str}^{-1} - \mu^{-1}$.

For simplicity, Figure 20 does not show the required overlap in the I regions in which the aperture settings can have either of two values, depending upon whether the signal level is increasing or decreasing. Such overlap (hysteresis) is necessary to prevent jitter due to noise. Figure 21 shows the overlap between two such regions of different optical gain setting for the case where a neutral density filter is introduced at a phototube current of 13 μ amps but removed only if the current falls below 0.6 μ amps. The regions of the dynamic range in which the electronic gain is set to particular values in Figure 20 are shown cross-hatched as illustrated in the key below the diagram. It can be seen that, with gain choices of 1, 5, and 25, there is an overlap factor of two between the point at which the amplifier gain is either increased or decreased, depending on whether the signal is increasing or decreasing. Multiplication of the buffer amplifier voltages shown on the ordinate by the electronic gain settings shows that with this arrangement the gain will be increased whenever the voltage input to the data handling system falls below one volt and will be decreased whenever the voltage exceeds 10 volts.

Careful consideration of Figure 20 shows that with this particular choice of currents, voltages, gain settings, and gain thresholds, a problem still exists in balancing these factors over such a large dynamic range as 1000 to 1 in I with all of the other constraints apparent from the detailed design. This can be seen by considering that the largest voltage in the preamplifier output will not be a processed signal voltage, but either of the unprocessed signals B or D under conditions where the polarization is a maximum. For 70% polarization the unprocessed signal B or D can attain a value 70% greater than the signal $I/2$. In order to prevent saturation of the preamplifier within the small part of the dynamic range where this can occur, it is recommended

that the processed signal voltage be allowed to fall below 50 mV to a value 30 mV. This would introduce a small portion in the dynamic range diagram for which signal processing accuracy was not as good as 1%.

5. Noise and Other Measurement Errors

a) Statistical Noise Limitations and Other Measurement Errors

It is the purpose of this section to discuss the noise due to photo-electron statistics in the S046 experiment and its effect on the statistical variance in the processed signals. Other sources of error are also discussed.

Statistical Noise: The variance $\delta(A-B)$ in the quantity A-B due to statistical fluctuations in the photocathode currents corresponding to beams A and B can be written as

$$\frac{\delta(A-B)}{A-B} = \frac{\sqrt{(\delta A)^2 + (\delta B)^2}}{A-B}$$

where δA and δB are the statistical variance in the separate quantities A and B. If we denote the ratio B/A as f this can be written

$$\frac{\delta(A-B)}{A-B} = \frac{\delta A}{A} \frac{\sqrt{1+f}}{1-f}$$

since $\delta B = \sqrt{f} \delta A$.

More generally, we can consider that A represents the more intense of any pair of beams being compared. For a polarization of 5%, $f = .90$, and the fractional variance in A-B will be approximately $10 \times \sqrt{2}$ times as great as the fractional variance $\frac{\delta A}{A}$ of the more intense of the two beams. For larger polarizations,

the fractional variance in A-B approaches $\frac{\delta A}{A}$. For the worst case, that of 5%

polarization, a requirement, for example of 1% statistical accuracy in A-B requires a statistical signal to noise ratio $\frac{\delta A}{A}$ in the more intense of the two

beams of 1400:1. In the limit of low intensity and small polarizations, statistical noise will be the dominant error in the system. RMS errors due to digitalization range from a maximum of 0.4% for one volt signals fed to the A/D converter to a minimum of .11% for the 10V maximum signals fed to the A/C converter. Compounding of this error with the 1% random error due to statistics for the special cause of minimum intensity and minimum polarization would lead to a combined error of 1.12%. We could, of course, improve the statistical error with larger lenses but feel that since the error becomes rapidly smaller with increased intensity and polarization this is not worthwhile.

$$Q$$

$$P \cos \psi = \frac{A-B}{A+B}$$

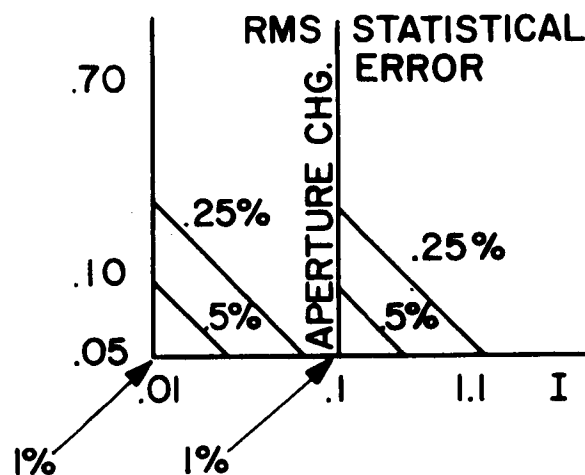


Figure 22

We have focussed attention on the "one sigma" errors; the probability that the error would be less than 2 sigmas would be approximately 95%. Figure 22 illustrates the manner in which the purely statistical error is expected to vary with light level I and polarization P . As the intensity of the light is increased from its minimum value, a level is reached at which the variable aperture will introduce a factor 10 attenuation in the optical signal to the phototube. At this point the statistical errors will again equal their value for the minimum light signals but will then again decrease as we go to higher levels. Due to the "hysteresis" (factor 2) to be provided for the automatic change in optical aperture, the aperture will operate at a different point depending upon whether the light level is increasing or decreasing. The two dimensional plot of statistical error shown in our diagram will thus be a double valued function in

the region near the middle of the dynamic range in I. We do not show this complication in the figures here. The sketch shows only a part of the total dynamic range. This extension of the dynamic range of I would introduce another region in the I-Q plane. The variation of statistical error within this third region will be exactly as in the other two regions. Using the present specifications on the optical system and phototube, it is calculated that the 1% maximum statistical error occurring in the sketch will be reached for a signal level one half the minimum computed on the basis of 3% ground albedo, sun elevation 6° , and vertical viewing through a Rayleigh atmosphere. At the bottom of the expected dynamic range of signals, then, the statistical error should be 0.7%.

Digitalized Error: We consider a linear system with automatic gain change so that the voltage fed to the A/D converter lies in the range 1 to 10V for polarizations greater than 5%. We further consider the use of a 10 bit A/D converter which divides the range 0-10V into 1024 equal increments of approximately 10mV each. An input signal voltage anywhere within a given 10 MV range will be transformed into the binary number

$$S_R = b_1 2^0 + b_2 2^1 + b_3 2^2 + \dots b_{10} 2^{10}$$

The error due to digitalizing arises from two sources. The first is a 10 mV offset error due to the quantizing process and the second is an approximately 0.1% slope error. A 10 bit converter divides the input voltage range, 0-10 volts into $1024 = 2^{10}$ equal parts of 10 m volts each. A signal input which is greater than 1V by an arbitrarily small amount can be written as 1.00^+ . This will be quantized to a converter output of 1.01 volt. An input signal that was smaller than 1.00 volts by an arbitrarily small amount and which we can denote by 1.00^- would be quantized to the next higher step 1.00. If a converter output signal of 1.01 volts is assumed to correspond to an input signal of 1.005 volts then the error incurred by this assumption is only 1/2% corresponding to an input voltage uncertainty of 5 mV. In our preliminary instrument design we have arranged so that the smallest signals for which 1% accuracy is required corresponds to 1 volt input to the A/D converter. For larger signals to the A/D converter the maximum percentage error will decrease inversely with the input signal. For a voltage input of 10V the maximum percentage error due to offset, or quantization error, will be only .05%. Since for an ensemble of measurements leading to a given A/D output, the inputs would be uniformly distributed over the range $S_R - 10V/2^n$, the distribution of probable error about the level $S_R - 10V/2^{n+1}$ can be considered uniformly distributed from $-10V/2^{n+1}$ to $+10V/2^{n+1}$. The RMS value from the mean is $0.5\% / \sqrt{3} = 0.3\%$.

In addition to the offset error, there is a maximum slope error corresponding to 0.1% of the signal input. Combining the offset and slope error gives an RMS expected error of about 0.5% for the minimum 1 volt signal to a value 0.11% for the maximum 10V signal.

Since an input signal of 1 volt to the A/D converter can correspond to different optical signal levels depending on the gain settings of the instrument, the map of digitalizing errors as a function of the intensity I and $P \cos 2\psi$ exhibits a maximum digitalizing error of 0.5% in the lower left hand corner in each of the rectangular areas corresponding to voltage input corresponding to the A/D converter of one volt. The addition of the density 2 filter to the system has the effect of adding two more rectangular regions to the sketch shown in the I, Q plane. The variation of digitalizing error within these additional regions is exactly the same as in the other regions and hence has not been shown.

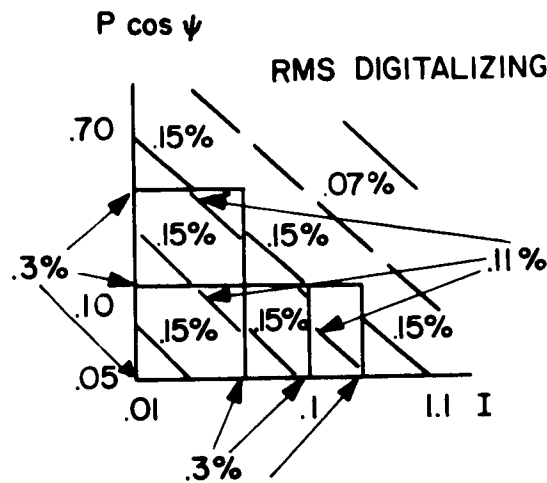


Figure 23

Systematic Error due to Power Supply Voltage Change due to Load Changes: A predictable systematic error will arise from changes in phototube gain due to changes of power supply voltage with changes in phototube load current. The high voltage power supply is designed for a short term (30 m sec) voltage stability of 1/6th volt due to a load change of one microampere. This would correspond to the difference in anode currents when changing between beam 1/2, and beam B under conditions of 5% polarization with $\psi = 0$ and under conditions of maximum intensity. This requirement arises from the requirement for .07% stability in phototube gain in order to measure the polarization to the required accuracy under these conditions. Although the systematic error due to this voltage change can be "calibrated out" of this system, or even computed with reasonable accuracy, our objective is to design an instrument in which corrections for systematic errors such as non-linearities is not required. This objective is highly desirable in terms of simplifying final calibration for the instruments which may have to be carried out in conditions of limited available time.

A 1/2 volt change in power supply voltage over the 30 m sec period of comparison of the successive beams A and B will give rise to an

approximately .1% change in phototube gain due to the load change in signals A and B. This will lead to a 1% systematic error in the measurement of the difference A-B under conditions where $B = .9A$, or where the polarization is 5%. This systematic error increases linearly with the intensity I and is independent of P. The map shows the variation of this systematic error as a function of I and $P \cos 2\psi$ (Figure 24).

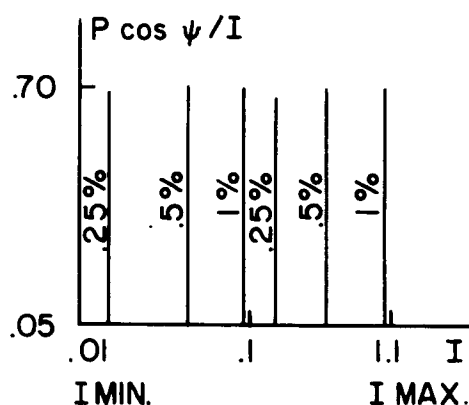


Figure 24

Systematic Errors due to Misalignments, Differential Thermal Expansions and Long Term Changes in Optical Transmission: It is expected that there will be small systematic errors due to these effects which can to a large extent be calibrated out prior to the actual flight experiment. The performance of periodic "on board" calibration of the response of the instrument to a secondary standard will permit a correction for any slight changes in these effects which may occur during the actual flight. The degree to which such changes can be taken account of depends to a large extent upon the accuracy, frequency and the number of intensity levels at which the in-flight calibrations can be performed. The use of a highly linear system (non linearity much less than 1%) will permit a reliable extrapolation of these calibrations over the entire dynamic range of the instrument provided in-flight calibrations are done at 2 or 3 light levels covering the full dynamic range of the instrument. The objective will be to calibrate out the systematic errors to a relative accuracy of about 1/2%. The map of these systematic calibration errors in an I vs. P plot as we have been using would show a uniform value of 1/2%.

Compounding of Errors: We assume that the error in data recording and/or transmission is negligible in comparison to the errors discussed above. Since the data can be recorded and transmitted digitally, such errors will be random errors in which an occasional bit is in error. This matter needs a separate discussion when details of the data storage and transmission system are known. Techniques exist for rendering such errors negligible compared to those discussed above (e.g. error coding bit).

The various errors obey distribution laws as follows:

- | | |
|---|---|
| 1. Statistical noise | Gaussian |
| 2. Digitalizing noise. | Uniform within band width of 10mV.
(+ slope error) |
| 3. Error due to HV changes | Systematic. |
| 4. Errors due to misalignment,
temperature differentials,
transmission changes. | Systematic. |

Since each separate source of error is relatively small, an exhaustive error analysis in terms of the overall distribution of errors is not considered warranted. Examination of the diagrams discussed above shows that a maximum error will occur at two values of illumination at minimum illumination and at about 1/2 scale and 5% polarization.

b) Non-Linearities, Maximum Permissible Phototube Currents,
Required H. V. Regulation

It is desired that corrections to the data not be required to take account of non-linearities in any part of the photopolarimeter system. We explore here the requirement on the degree of linearity which is imposed by the demand that the quantity A-B be measured to an accuracy of 1% without such corrections.

The non-linearities expected from the phototube and the H. V. supply are such that the phototube output current i , instead of being simply proportional to the optical signal A or B as expressed by the equations

$i_A = kA$ and $i_B = kB$, has an additional quadratic term as expressed by

$$(1) \quad i_A = k_0 (A + \beta A^2) \text{ and } i_B = k_0 (B + \beta B^2)$$

due to the fact that the "gain" k sags with increasing signals in a manner expressed by

$$(2) \quad k = k_0 (1 + \beta A) \quad k = k_0 (1 + \beta B).$$

Such a change in gain can be caused by imperfect voltage regulation in the H. V. supply with load changes, or non-linearities in the phototube current at a fixed power supply voltage. The latter changes are expected to be negligible at reasonable phototube gains ($G = 10^4$). The changes in phototube gain with H. V. changes are expected to dominate, since a given percentage change in H. V. leads to a percentage change in phototube gain approximately five times as great.

If we require that the phototube current difference $i_A - i_B$ measuring the difference in the optical signals A and B be within 1% of the value

expected with perfect equipment linearity, this can be expressed as

$$\frac{\delta Q}{Q} = \frac{\delta(i_A - i_B)}{i_A - i_B} \leq 0.01$$

From equation (1), which expresses the nonlinearities, we then obtain

$$\left| \beta \frac{A^2 - B^2}{A - B} \right| \leq 0.01, \text{ which implies}$$

$$(3) \quad \frac{\delta Q}{Q} = \beta |(A + B)| \leq 0.01.$$

Equation (2) shows that βA is the percentage departure of the gain from its linear value when the signal attains the level A. (3) then shows that, since B and A may be approximately equal, the maximum value of βA or βB should not exceed 0.005, or 0.5%. Since the H. V. regulation must be five times better than this, we obtain a requirement of 0.1% for H. V. regulation when the phototube current is varied from its maximum value down to the dark current level. This precise regulation is required only over the short time periods of 30 ms when two consecutive signals are being compared.

Data taken on RCA #4461 and #7265 phototubes show 1% linearity up to a current of approximately 25 amps. Data furnished by EMR Corporation showed similar linearity up to currents of 100 μ amps but our tests of two of their tubes fail to confirm this. It is believed that tube selection is required in order to achieve such a high degree of linearity.

Since the dynamic gain measured is a measure of the slope of the curve of phototube current vs. input light level, a measurement of 1% slope change at 25 microamps corresponds to a gain reduction at 25 microamps on the order of 1/2%.

6. In-Flight Calibrators

a) Internal Calibration Standard

Mechanical arrangement and important design parameters for both in-flight calibrators have been shown on the S046 Experiment General Layout Drawing No. 895D192.* Significant design features of the on-board lamp calibration include the selection of the tungsten iodine lamp No. 1973 and the provisions for adjustment of lamp and lens position to provide alignment and balancing of the three output beams of the calibrator. The lamp socket provides four degrees of freedom (3 positional plus rotation) and the three lens retainers provide axial positioning of the lenses to balance the flux output of each of the three beams.

*See Section E.

Significant design features of the on-board solar flux calibration system include a single operation deployment device operated by a torsion spring and a release mechanism consisting of a non-contaminating pyro technic/mechanical actuator. Sun shades and debris protection shields are provided on all barrels of the solar flux calibrator. The solar flux calibrator unit is mounted from the base of the experiment package, and provisions can be made if desired to provide a guide or latch to assure positive alignment of the photopolarimeter instrument during solar flux calibration.

A weight of two pounds has been allowed for each of the in-flight calibrator units in the initial experiment weight estimate (Section 8). Preliminary design results indicate that a significant reduction may be possible in the weight of these units.

The use of a 2.5 watt tungsten lamp operating at 2150°K appears to be adequate for calibration of the photopolarimeter over approximately $1/2$ of its dynamic range at 3800\AA and the complete range at other wavelengths. An area of concern, in addition to the reduced output at 3800\AA is the bulb darkening which will occur during the lifetime of the S046 experiment. This darkening will undoubtedly be non-uniform due to the internal geometry of the lamp and it will be extremely difficult if not impossible to distinguish between this non-uniform bulb darkening and changes in the performance of the photopolarimeter instrument.

A new 12 volt tungsten iodine cycle lamp (GE No. 1973) can provide a significant improvement over the 2.5 watt tungsten lamp in increased lamp life and radiant output at 3800\AA if sufficient power can be made available for calibration purposes. Present indications are that the operating power for the other parts of the S046 experiment will be considerably less than originally expected and it may therefore be possible to calibrate after each scan with the 12 volt tungsten lamp source by allowing the calibration lamp to warm up during the scan period. Periodic calibration checks before and after each run could be made to verify the stability of the entire system.

The actual operation of the solar calibration unit will require consideration by the integration contractor of experiment and vehicle systems interactions to establish the extent to which the crew can be used for performing a sun calibration of the S046 experiment. Design studies show that mechanical arrangements will allow the scan platform to be driven to a stop position beyond the maximum scan angle to view the solar calibration unit. The vehicle orientation can then be controlled by the pilot to "aim" the S046 Solar Calibrator unit within one or two degrees of the earth-sun line.

The photopolarimeter will be calibrated in flight in a "parked" position where each barrel will receive radiation from the standard source in

as uniform a manner as possible. Four important conditions must be fulfilled:

- (a) Any source polarization must be small and constant.
- (b) The intensity should be divided uniformly between the three beams.
- (c) The beams should be spread over the 1/4" diameter cross sectional area of the fiber optic aperture as uniformly as possible.
- (d) The system must provide sufficient intensity to allow a calibration over the whole or at least a sufficient part of the dynamic range.

The system proposed consists of an incandescent filament (assumed to have a maximum linear dimension of 1/8") lamp and three symmetrically placed plane mirrors and lenses to define three equal intensity beams (Figure 25). The position of the filament relative to the lens is chosen to provide sufficient mounting clearance yet maximum solid angle of acceptance by the lens in order to meet the intensity requirements. The focal length of the source lenses is chosen to focus the filament five inches behind the focal plane of the polarimeter entrance lenses (Figure 26).

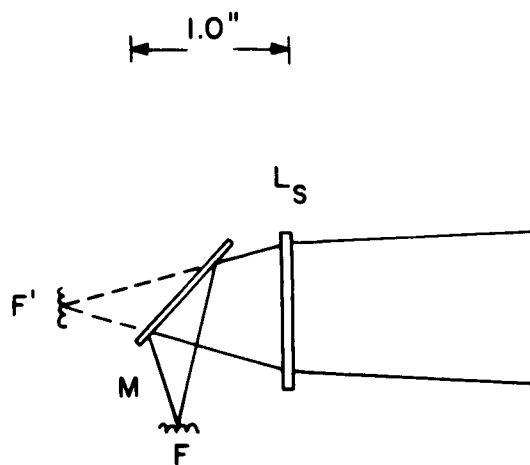
With this arrangement, the fractional area of the total beam cross section accepted by the fiber optic aperture (located five inches behind the lens) is $1/4 = T$, the transmission for any position on the filament, neglecting optical losses.

An assessment of the performance of this source can be made from a consideration of conditions (a), (b), (c), and (d) above.

(a) Polarization: In order to meet this condition, plane mirrors having a high reflectivity ($> 90\%$) in the range 3800 to 6000 Å will be used. For this reflectivity the maximum degree of polarization would be a few percent and would be stable.

(b) Uniformity of the division of intensity between the three beams: By careful positioning of the filament relative to the source lenses, it should be possible to meet this requirement.

(c) Beam cross-section uniformity: Neglecting any variation in reflection losses at the lenses for different angles of incidence, the beam cross section from any point on the filament aperture is uniform. This results from the fact that the radiant energy per unit solid angle is constant and the variation in the projected areas for two extreme, infinitesimal cones intersecting the fiber optic aperture is very small. To minimize any non-uniformity arising from reflection effects, the lenses of the source should have high quality anti-reflection coatings.



F - FILAMENT
 F' - IMAGE OF FILAMENT BY M
 M - PLANE MIRROR
 L_s - LENS

Figure 25

F - FILAMENT (.125" MAX. LIN. DIM.)
 L_s - SOURCE LENS
 L_p - POLARIMETER LENS
 F' - IMAGE OF F BY L_s
 F'' - IMAGE OF F' BY L_p

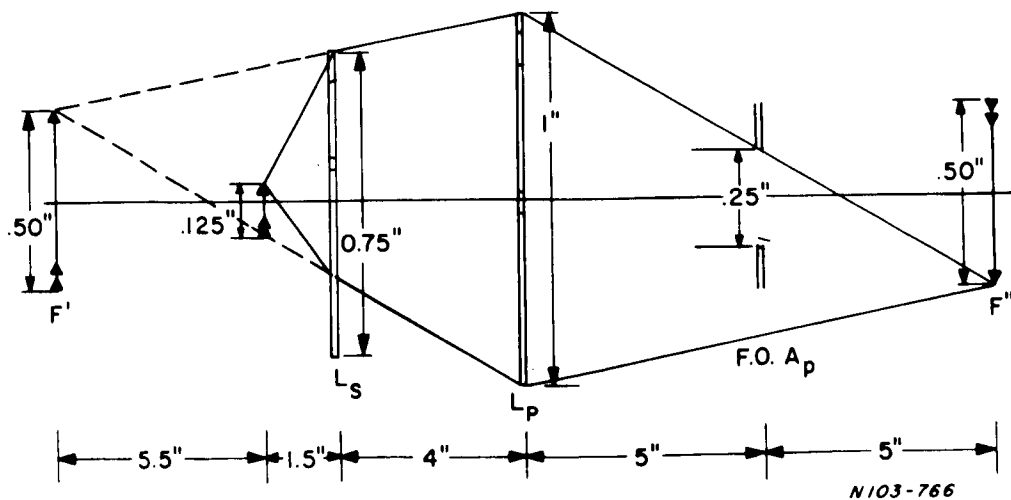


Figure 26

(d) Calibration intensity requirement: If the greatest intensity received by the polarimeter corresponds to a target with a Lambert surface of albedo 0.8 and a radiance of 3.3×10^{-4} watts/cm²sterad. / 100Å = R_T , the calibration source must be able to supply the equivalent radiation at 3800Å as well as the three longer wavelengths which present less of a problem. If Ω_P and Ω_S are the solid angles of the polarimeter, A_P is the aperture area of polarimeter, A_S is the source filament area and R_S is the radiance of the source, the powers received by the polarimeter are:

$$\text{from target, } W_T = R_T A_P \Omega_P = 3.3 \times 10^{-6} \text{ watts/100Å}^\circ$$

$$\text{where } \Omega_P = 2 \times 10^{-3} \text{ ster.}$$

$$A_P = 5 \text{ cm}^2$$

$$\text{and from source } W_S = R_S \Omega_S A_S T$$

$$\text{where } T = 1/4, \Omega_S = \frac{\pi(0.40)^2}{(1.5)^2} = 2.2 \times 10^{-1} \text{ sterad.}$$

By equating W_T and W_S , we get

$$R_S A_S = 6.0 \times 10^{-5} \text{ watts/ster/100Å}^\circ.$$

For a standard 2.5 watt conventional incandescent lamp of filament area $A_S = 0.1 \text{ cm}^2$, the radiance R_S required is:

$$R_S = 6.0 \times 10^{-4} \text{ watts/ster/cm}^2/100\text{Å}^\circ.$$

This lamp operating at a temperature of 2150°K provides a radiance of at least 3.3×10^{-4} watts/ster/100Å/cm² at 3800Å (and increases rapidly for the higher wavelengths). Therefore, this lamp would provide a calibration over at least 1/2 of this dynamic range at 3800Å and the complete range for the other wavelengths. Figure 27 illustrates the mechanical layout.

Choice of a standard lamp depends on the radiant power requirements and both electrical and optical stability. Here we will consider optical changes due to vacuum deposition of a tungsten film on the lamp envelope.

The transmission τ is of the deposited film $\tau = e^{-\alpha d}$ where α is absorption coefficient and d is thickness.

$$\text{For 99\% transmission } d = \frac{.01}{\alpha} = \frac{.01}{\frac{2\pi \times .90}{5 \times 10^{-5}}} = 8.4\text{Å}^\circ$$

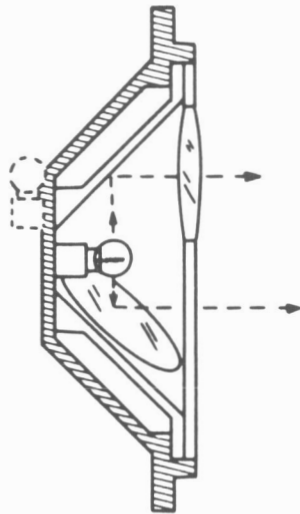


Figure 27

TUNGSTEN LAMP CALIBRATION

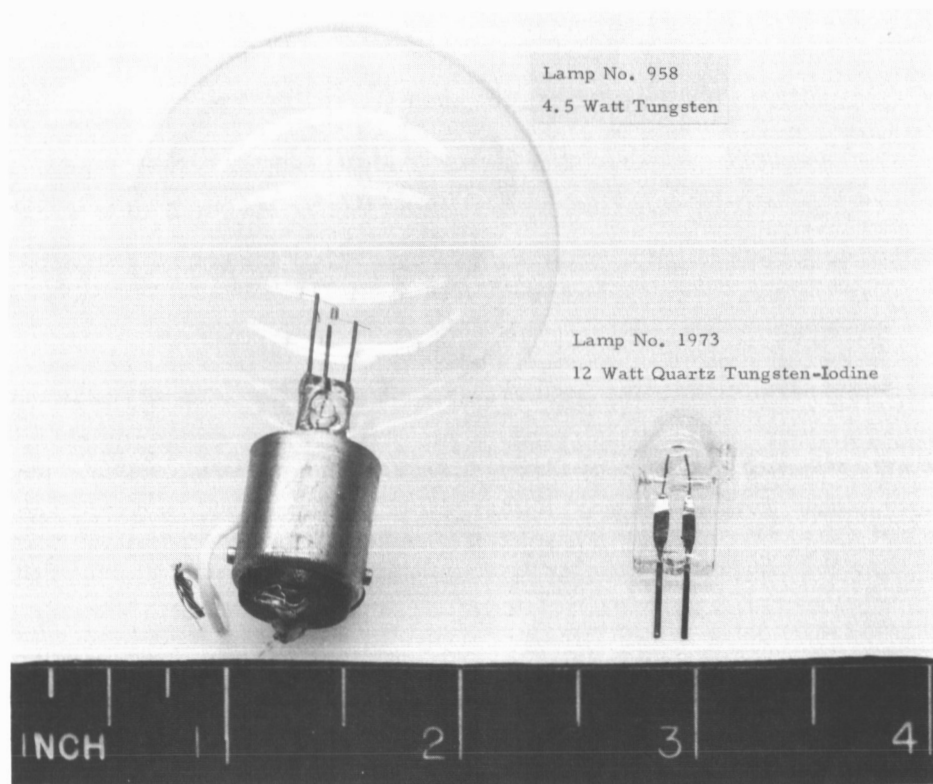


Figure 28

at 5000Å. Little error will result if we assume that this holds true over the entire spectral range of interest.

Consider a tungsten source at temperature T at the center of an evacuated spherical envelope of radius R. The deposited film thickness d will be

$$d = \frac{Ga_F t}{4 \pi \rho R^2}$$

where G is rate of tungsten loss from filament equal to 3.7×10^{-9} gm/cm² sec. at 2500°K.

a_F = filament area

t = time

ρ = tungsten density

Tentative numbers for a tungsten filament lamp of 5 - 6 watts power, filament area 5×10^{-3} cm², filament temperature 2500°K, and bulb radius of 2.5cm. Limitation to 1% transmission loss then gives permissible lamp operation of 360 hours.

Non uniform deposition of tungsten on various regions of the glass envelope may, however, give relative changes in intensity in the various channels of the photopolarimeter which are of the order of a few tenths of a percent. Since this would not be permissible because of the requirement on polarization accuracy, it is recommended that a 12 watt General Electric tungsten iodine cycle lamp be used in the in-flight calibrator. A photograph of this lamp, together with a candidate tungsten bulb, is given as Figure 28 .

b) Solar Calibrator Unit

The sun calibration can be performed with the polarimeter in some "parked" position where it views the three fixed barrels of the calibrator. The spacecraft must then be orientated to view the sun. The calibrator (Figure 29 , shows one of the barrels) consists of an aperture (with a neutral density filter) and a lens Lc. The aperture is in the first focal plane of Lc, the combination of the two lenses images the calibrator aperture (A) in the second focal plane (B) of the polarimeter objective. The geometry has been chosen based on the following considerations:

- (a) the total beam cross section is large where it intersects the lenses (to minimize the effect of any particles which may locally contaminate an area of the lens),

- (b) the aperture area of the fibre optics is sufficiently overfilled, and
- (c) enough clearance is allowed at lens L_p to compensate for a pointing error ϕ . (See below).

Effect of a Pointing Error ϕ : Figure 29 shows the imaging properties of the system. Since the intensity distribution across the aperture is uniform, the corresponding distribution across B is also quite uniform. If a pointing error ϕ is made, it is evident from the diagram that the image of the aperture in the plane B is not altered (rays represented by the dashed lines) if a sufficient clearance of $1.5 \tan \phi$ inches is provided as shown. However, the intensity across the aperture A is reduced by the factor $\cos \phi$ which corresponds to a decrease in the intensity of 1/10% for an error of 2° .

Any gradual degradation of the internal calibrator unit (tungsten source) could be compensated for by an intercalibration with the solar unit provided a reasonable number of sun calibrations are possible.

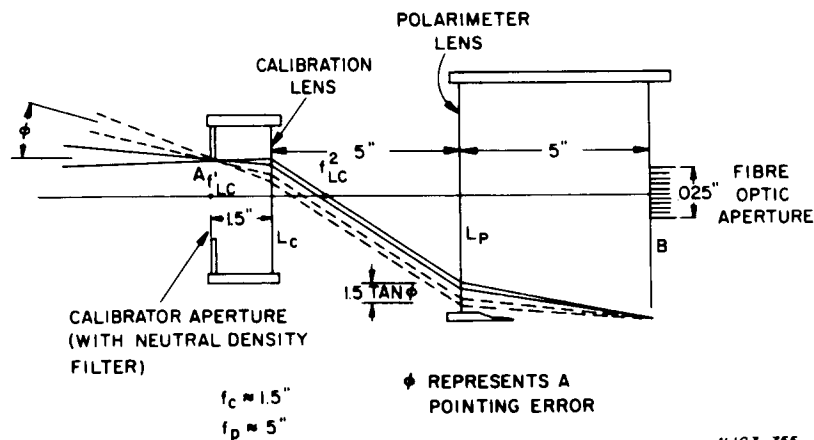


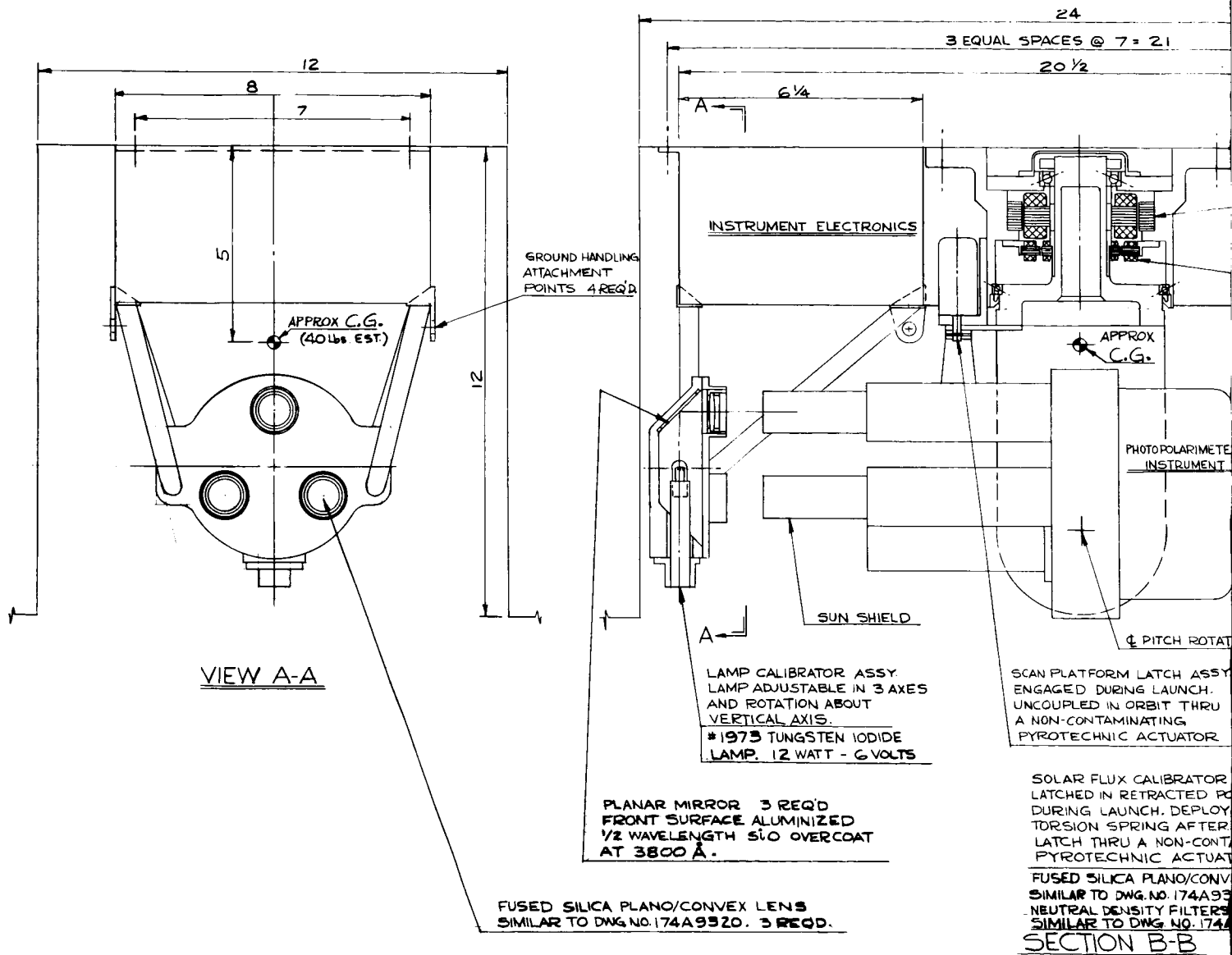
Figure 29

Drawing 895D192 shows the general mechanical arrangement for deploying the solar calibrator.

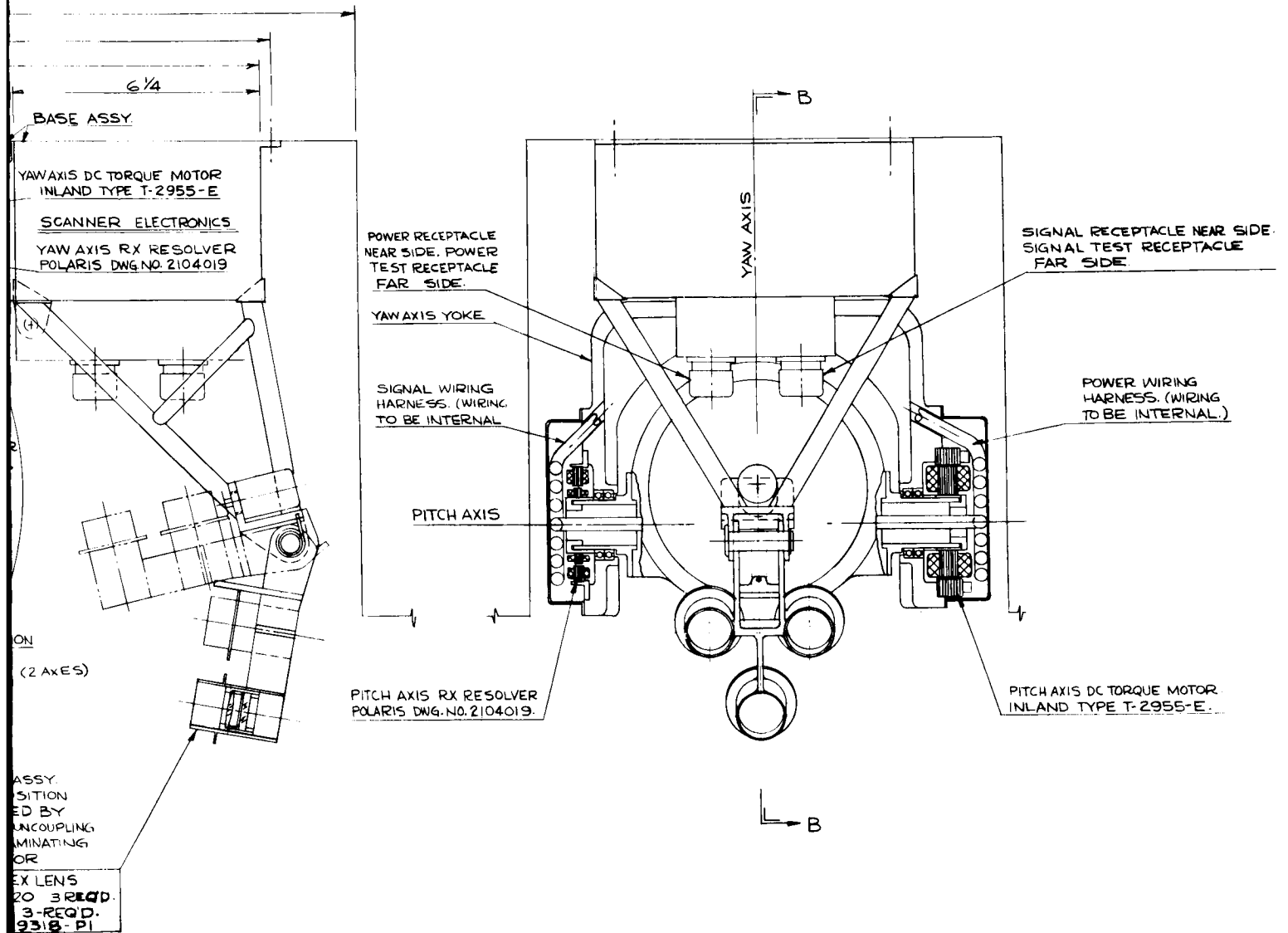
- c) Calibrations Based on an Integrating Sphere Method (Solar and Tungsten Lamp). Comparison with Imaging Systems

The feasibility of using a single integrating sphere as an alternate method for the solar calibration as well as the tungsten lamp calibration is discussed. The considerations outlined below indicate that the same sphere could be used for both calibrations; the correct intensity to provide a solar calibration in the middle of the calculated dynamic range can be obtained with a reasonable aperture area; the intensity provided by this unit used with a tungsten lamp would be $\sim 1/5$ that obtainable with the imaging system, however, with increased lamp power it could provide a calibration over a portion of the

FOLDOUT FRAME



FOLDOUT FRAME

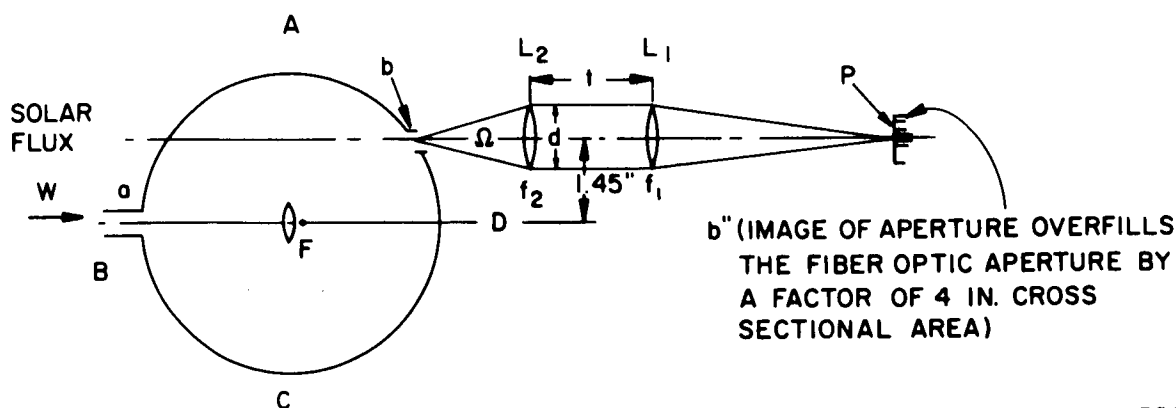


Dwg. 895D192, General Layout

3800Å range and over a reasonable range at 6000Å. It may be worthwhile to consider these systems if difficulties are encountered in the stability of the imaging systems (the imaging system places a rather stringent requirement on the positional stability of the filament - the sphere approach does not have this drawback). However, any change in the reflectivity of the sphere's surface produces a large change in output intensity.

Solar Calibration - In Figure 30 the quantities are defined as follows:

- d = diameter of matching lens used
- t = separation of the lenses
- L_1 = objective lens of polarimeter $f_{L_1} = f_1$
- L_2 = matching lens $f_{L_2} = f_2$
- a = area of input aperture
- S = surface area of sphere
- r = diffuse reflectivity of the interior surface
- b = area of output aperture
- Ω = solid angle subtended by the matching lens
- P = area of the fibre optic aperture
- W = solar constant (watts/in²/μ)



N103-756

Figure 30

Assume the energy aW (watts/ μ) incident on the diffuse Lambert reflector at 0, provides a uniform illumination of:

$$\frac{a W r}{(1/2)S} \text{ watts/in}^2/\mu$$

over the hemisphere ABC. After the first reflection from the surface ABC, the complete sphere interior has the uniform illumination:

$$\frac{a W r^2}{S} \text{ watts/in}^2/\mu$$

The intensity incident on an area b (after successive reflections) is:

$$\frac{b a W r^2}{S} + \frac{b a W r^3}{S} + + \dots = \frac{b a W r^2}{S(1-r)}$$

The radiance $R(b)$ of this surface element is:

$$R(b) = \frac{a W r^2}{\pi S(1-r)} \text{ watts/in}^2/\text{sterad}/\mu.$$

(The areas of the holes have been assumed $\ll S$)

The aperture area b must be matched to the fiber optic area P using a matching lens L_2 .

Evidently,
$$b = \left(\frac{f_2}{f_1} \right)^2 P.$$

The solid angle
$$\Omega = \frac{\pi d^2}{4 f_2^2}$$

The energy accepted by the instrument is proportional to
$$b \Omega = \frac{\pi d^2 P}{4 f_1^2},$$

i. e. the focal length f_2 used, will determine the area b viewed by the instrument, but the product $b \Omega$ will be independent of f_2 .

For $f_1 = 4''$, $d = 0.75''$, $P = 0.049 \text{ in}^2$

$$\underline{b \Omega = 1.35 \times 10^{-3} \text{ in}^2}$$

It is required that the energy flux at 3800 \AA (for example) provided by the integrating sphere be conveniently located in the calculated dynamic range

of intensities expected from the targets. Referring to (PIR No. 023, Dynamic Range Calculations) a convenient power is 2.8×10^{-5} (watts/ μ)* and the solar flux at this wavelength is ~ 0.9 watts/in²/ μ . E s c, the energy received by the instrument from the solar calibrator should also be 2.8×10^{-5} watts/ μ .

$$E s c = 2.8 \times 10^{-5} = R_b (b \Omega) = \left(\frac{a}{s} \right) \frac{W r^2 (\Omega b)}{\pi (1-r)}$$

from this equation with $r = 0.95$ we obtain

$$\frac{R_a}{R_s} = 0.13 \text{ where } R_a \text{ and } R_s \text{ are the radii of the aperture } a \text{ and the sphere } s \text{ respectively.}$$

In order to accomodate the three barrels, it appears that a sphere radius $R_a = 2.5''$ is required. The radius of the solar flux aperture is then fixed at:

$$R_a = 0.32'' \text{ and}$$

the radius of the exit aperture b is $\approx 0.125''$ to ensure that the fiber optics aperture is overfilled.

Tungsten Calibrator

Referring to Figure 30, again, F represents the filament lamp mounted close to the center of the same sphere used for the solar calibration.

A_f = filament area

B_f = radiance of filament watts/in²/sterad/ μ

We wish to compare the efficiency of this arrangement with the imaging system.

Assume that all the energy emitted by the lamp (4π steradians) illuminates the hemisphere ADC.

Energy emitted by filament = $4 \pi (A_f B_f)$ watts/ μ . Neglecting the fact that \sim one-half the radiation emitted by lamp is attenuated by the factor r on reflection from the screen at 0, and taking into account the fact that the geometry prevents radiation from reaching the f.0. aperture directly (before the first surface reflection) the radiance of the aperture b is given by:

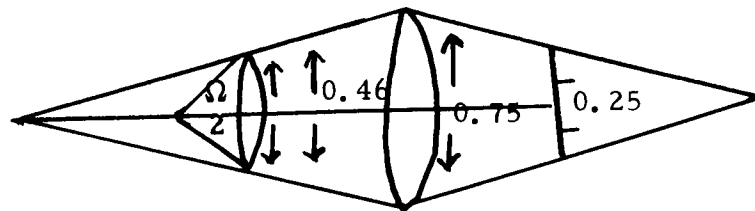
$$R_b = \frac{4 (A_f B_f) r}{S (1-r)}$$

*-This power corresponds to a point in the dynamic range where the signal could be conveniently recorded with the step attenuator both in and out of position.

$$\begin{aligned} \text{Energy received by instrument} &= R_b b \Omega \\ &= 5.25 \times 10^{-3} (A_f B_f) \text{ for the sphere of radius 2.5 inches.} \end{aligned}$$

Comparison with Imaging System

The Figure represents the geometry of the imaging system as presently conceived.



$$\Omega = \frac{\pi (0.23)^2}{4}; \quad \text{Transmission } T = \frac{1}{4} = \frac{\text{area of beam cross-section}}{\text{area of fiber optic aperture.}}$$

Energy Received by the instrument

$$= \Omega T (A_f B_f) = 1.04 \times 10^{-2} (A_f B_f).$$

The integrating sphere is approximately 1/5 as efficient as the imaging systems.

Comparison of Integrating Sphere and Imaging Systems

Integrating Sphere -

- Advantages:
- (a). does not require accurate positional stability of the filament
 - (b). only one matching lens required for each barrel
 - (c). small polarization.

- Disadvantages:
- (a). due to $\frac{1}{(1-r)}$ term in expression for emergent intensities, a variation in r from 0.95 to 0.94 results in a change of ~ 25% in intensity. Therefore, the reflectivity of the surface must be very stable.

Imaging System

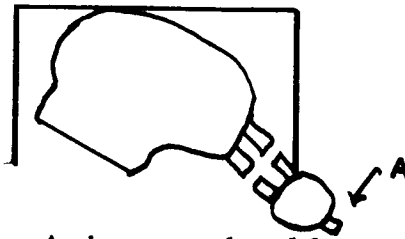
- Advantages:
- (a) can provide more intensity from same lamp
 - (b) small physical size
 - (c) a one % change in reflectivity of mirrors produce only a one % change in intensity.

Imaging System

Disadvantages: (a). Focussing methods require positional stability of the lenses.

Conclusion: It appears that the reflectivity stability requirement of the interior surface of the integrating sphere may be difficult to achieve.

Operation of the Integrating Sphere:



Solar: the aperture A is opened and lamp turned off.
Spacecraft oriented towards the sun.

Tungsten Calibration: The aperture A is closed and the calibration performed with lamp on.

C. Scan Platform

1. Preliminary Selection

The three basic approaches for the scan platform drive considered were (1) DC Direct Drive, (2) DC Geared Drive, and (3) AC Geared Drive. It was concluded that the DC Direct drive has the most overall merit for the following reasons.

- (1) It alone affords the desired level of position accuracy by eliminating backlash.
- (2) Its use results in the most compact and clean cut unit.
- (3) Its results in a set of gimbals with the least weight, being approximately 4 lbs. lighter than geared units.
- (4) Application of the direct drive to the polarimeter requires the least functional modification to already flight proven torque motors, resolvers and control circuitry.

A summary of the specific requirements for a scan platform capable of adequate performance in the S046 Experiment was formulated and is shown in Table V. Also tabulated on this same sheet is the comparative performance which can be expected from each of the approaches.

The range of travel provided by all three drives is limited only by the harness (flexible cable) arrangement. Since no more than 180° of travel is needed, slip rings will not be used.

The direct drive provides a wide range of scan rates without mechanical changes because gearing is not involved.

The gear trains of both geared drives (both of Nimbus origin) would require modification to meet the $5^{\circ}/\text{sec}$ slew rate requirement.

The accuracy capability of the direct drive system exceeds that of the geared drive approaches. This is partly due to the limitation of back lash and partly due to relative accuracy of resolvers and potentiometers. The resolver also offers higher reliability as a position sensor, since there are no sliding contacts to develop high resistance or introduce electrical noise. It is apparent that the desired accuracy can most easily be obtained with the direct drive technique.

TABLE V
SCAN PLATFORM SELECTION CHART

REQUIREMENTS	A DIRECT DRIVE	B) NIMBUS II SAD ACTUATORS	C) D. C. GEARED TORQUER DRIVES
1. <u>SCAN RANGES</u> Pitch (+90° to - 60° from Nadir) Yaw (+4° from Velocity Vector)	+ 90 to - 90 Limited only by harness	+ 90 to - 90 Limited only by harness	+ 90 to - 90 Limited only by harness
2. <u>SCAN RATE</u> Pitch - 20°/second max .30°/second min 50°/second slew Yaw - 1 cycle/90 minutes	50°/sec	.04°/sec to .30°/sec	.04°/sec to .30°/sec
3. <u>ACCURACY</u> Pitch & Yaw + 0.2°	+ 0.2°	1.0°	.6°
4. <u>TORQUE</u> Pitch - 100 in. oz. min Yaw - 100 in. oz. min	124 in. oz. (Peak stall)	465 (with)	720
5. <u>POWER</u> Maximum - 30 Watts/gimbal	Stall - 42 max Scan Average -.5	Stall -8.4 max Average Scan 3.0	Stall 11.1 max Average Scan 0.5
6. <u>WEIGHT</u> Maximum - 14 lbs. Wt. on Platform - 15 - 20 lbs.	14 lbs.	18 lbs.	18 lbs.
7. <u>SIZE</u> 1' x 1' x 2' compartment	10" high, x 10" wide x 7" lg.	11 1/4" high, 11 1/2" wide x 8" long	Same as AC Drive
8. <u>LIFE IN ORBIT</u> Operating Time - 10 hours Total Time - 14 days Shelf Life - 2 years	Believed to be adequate based on performance on classified programs.	15 months continuous demonstrated on Nimbus II	Life Tests on Nimbus back up not run, design goal 10,000 hours
9. <u>REQUIRED MODIFICATIONS</u>	- Uses components from existing flight proven hardware.	1. Change gear ratio of Motor gearhead to 4800:1 2. Redesign gearbox 3. Reselect pot	1. Redesign gearbox to provide lower gear ratio. 2. Reselect pot.

The torque of 100 in. oz. is easily obtained by all these drives. The geared drives can provide torques greatly in excess of requirements and might need protective slip clutches to avoid damage to the platform in case of limit switch failure. This feature of course adds additional complexity to the drive. Geared drives offer the advantage of being self locking to hold the gimbal in whatever position it is in when the motor is turned off. However it is expected that the preloaded bearing friction will be from 10 to 15 in. oz. This torque level should be sufficient to keep the instrument from moving when unenergized in a zero gravity field.

The power requirement for a DC torquer in normal tracking mode becomes very low with a pulse modulated supply. It is calculated to be .5 watts per gimbal for the direct direct drive approach and would be similar for the DC geared unit. Stall power levels however are high and this power supply must be designed to limit maximum power input.

In the weight category only the direct drive is estimated to meet the desired weight of 14 lbs. for the platform. The extra gears and gear boxes on the other two driver create additional weight.

In size, the direct drive again offers an advantage in making the gimbals more compact. With the shorter platform more generous clearances between instrument and compartment walls can be obtained.

Relative budgetary costs of the three types were estimated and showed no major differences.

The large quantities of torque motors and resolvers (approximately 5000), purchased by the General Electric Ordnance Department and used on many missile and satellite vehicles, constitute an important experience factor in the selection of the platform drive. In respect to both design and manufacturing capability, GEOD is undoubtedly the optimum GE source.

2. Gimbal System - Mechanical Description

a) Design Philosophy

Realizing the need for a gimbal assembly with high reliability, components have been selected that have proven themselves in other missile and satellite programs. The integration of these components to form a gimbal assembly was made with simplicity in mind. The number of basic components (torque motors, bearings, resolvers, etc.) has been kept to a minimum by using the same units on both axes. This factor increases the reliability of the system.

The two most critical components in this gimbal assembly are the torque motors and the bearings, since they present the only contact between parts which have relative motion. The torque motor brush-commutator configuration has undergone extensive testing for other satellite programs and has also experienced large numbers of space flights. The bearings have also been tested and flown under the same conditions.

b) Description of the Gimbal Assembly

The gimbal assembly is a two axis unit (see dwg. 985D192). The gimbal mount, which contains the yaw axis torque motor, resolver and bearings is mounted directly to the support structure on the spacecraft. The bearings for this axis have been spread apart to give them a wheel base of 2 inches. These bearings are preloaded. The yaw gimbal is free to rotate inside the gimbal mount. Attached to the yaw gimbal shaft are the torque motor and resolver rotors and the inner race of the bearings.

Stops are provided to limit the travel of the yaw gimbal to ± 4 degrees from center.

The single piece yaw gimbal also provides for the mounting of the pitch gimbal torque motor and resolver stators and the outer races of their associated bearings. The pitch gimbal is supported in the yaw gimbal by DF duplex bearing. The bearings on the resolver end position the gimbal in an axial position while those on the torque motor end are free to permit axial float. Stub shafts on each side of the pitch gimbal are provided to permit assembly. These are attached to the pitch gimbal.

The pitch gimbal provides for the mounting of the photopolarimeter. A latching mechanism is provided to lock the pitch gimbal with respect to the yaw gimbal.

c) Description of Components

Torque Motor

The torque motors will be purchased from Inland Motor Corp., Radford, Va. The motors are a DC motor with 4 brushes and commutators. GE Ordnance Department has purchased over 5,000 similar motors from Inland. These motors have been used on both the Polaris MK 1 and MK 2. The Inland motor has also been used by the Ordnance Department on other guidance systems and satellite programs. This basic type of motor was used as a back up for the Nimbus Paddle Drive. For this program extensive tests in a vacuum were conducted for NASA to determine the optimum configuration and materials to be used in the DC motor. The optimum combination proved to be a silver graphite brush with a gold commutator. The gold on the standard commutator is .005 in. thick plated on copper. The gold plate is adequate and has been used in all past applications, but it was found that the relatively hard silver graphite brush does scrape through the gold plate and exposes small areas of the copper bar. Under

high relative humidity conditions copper oxide forms and increases the brush to commutator resistance.

Tests have been conducted on inlaid gold commutators and these proved to be equal in life but not susceptible to corrosion. The torque motor proposed has the characteristics shown in Table VI.

Bearing and Lubricants

The bearings that will be used on this sytem are identical to those used on past satellite applications and have also undergone extensive tests in vacuum conditions.

The bearings utilize an integral seal to retain the lubricant. The bearing is lubricated with a 25% fill of GE G-300 silicone grease. The grease is strained so that there are no particles larger than 35 microns. Phenolic-laminated retainers are used and these are impregnated with a silicone oil GE F-50. Balls and races are a 440C stainless steel. The bearing has a temperature range from -100°F to $+200^{\circ}\text{F}$. As can be seen in Drawing the bearings have been covered on one side, while on the other side the clearances between the shaft and the housings have been reduced to a minimum to retard outgassing. This method was used on the Nimbus Paddle Drive which has been in operation for over 1 year.

In recent years research has continued on solid film lubricant for space applications. Although these appear to be quite promising, they have not been proven to the extent of the grease lubricants.

Resolvers

The resolver is an RX unit which will produce gimbal position. The resolvers to be used are a pancake unit. They do not employ any slip rings and therefore, do not present any problem in a vacuum application. The resolver used for this application is presently being used in Polaris MK 2. It has the following electrical characteristics:

Primary	115V 800 cps
Secondary	28.8 V
Phase Shift (no load)	$+2.0 \pm .5$ deg.
Primary Power	1.0 watt
Output Impedance	$40 + j$

TABLE VI

INLAND MOTOR CAT. NO. T-2955-D

DC Resistance (ohms)	16.2
Peak Voltage (volts)	34.5
Torque Sensitivity (#-ft/amp)	.40
Back EMF (volts/rad/sec)	.54
Inductance (henries)	17×10^{-3}
Maximum Operating Temperature ($^{\circ}\text{F}$)	310

The friction torque for the gimbal system pitch axis will be as follows:

	Nominal (in-oz)	Maximum (in-oz)
Bearings	10	16
Torque Motor	1.5	2.5
Wire Bundle	<u>2</u>	<u>4</u>
TOTAL TORQUE	13.5	22.5

The yaw axis will be somewhat less.

The motor has a capability of

$$.40 \text{ #ft/amp} \times \frac{26\text{V}}{16} \times 192 = 124 \text{ (in-oz) at maximum applied voltage.}$$

This provides a factor safety under worst case friction conditions of

$$124/22.5 = 5.5$$

Under nominal conditions the torque motor will consume

$$\frac{13.5 \text{ in oz}}{.40 \times 192 \frac{\text{in oz}}{\text{amp}}} = .178 \text{ amps}$$

$$\text{or } I^2 R = (.178)^2 (16.2) = .5 \text{ watts}$$

This is exclusive of AC ripple produced by the servo, but this is negligible.

Construction of Structural Members

The majority of parts will be machined from wrought aluminum stock. Two exceptions to this will be the yaw and pitch gimbals. These will be fabricated by welding aluminum and then machined.

Wiring

Since gimbal freedom is limited in this application slip rings are not required. The wire will be MIL-W-16878 (double wrapped teflon).

The scan platform and the mechanical housing have been combined to provide a weight reduction and to simplify the electrical interface between the instrument and the scan platform. The electrical leads can be brought through the scan platform to the inside of the housing without the use of external connectors and harnesses and the platform can be checked out for performance using a dummy load mounted in the housing.

Latching Mechanisms

A latching mechanism will be employed to hold the gimbal system in the position shown in Drawing 895D192. This will be actuated by a linear solenoid. It appears as though only one is required to latch the pitch gimbal since the freedom on the yaw is limited to only ± 4 degrees.

Two areas which require further study are Electromagnetic Interference (EMI) generation and details of caging the mechanism during powered flight. Caging or latching the instrument in orbit may not be required if the bearing preload provides sufficient torque loading in comparison with vehicle accelerations.

D. Pitch Scan Function Generator

1. Introduction

The purpose of this section is to describe the design features and operation of the pitch scan function generator. This generator programs the position of the pitch gimbal in order to track an earth fixed target from a low altitude orbit. The generator is a self contained all electronic analog computer operating within the pitch servo loop. The computer has three modes of operation: Initial Condition, Operate, and Calibrate.

2. Simplified Block Diagram

Equations

Equation (1) of Section II-F can be written in the alternate form

$$\sin z = \frac{\eta}{h/R + \eta^2/2} \cos z.$$

where $u = h/R$ and

h is orbit height

R is radius from earth center to target

z is the zenith angle

η is the angle from vehicle to target at the center of the earth.

$\sin z$ and $\cos z$ are obtained from resolvers mounted on the pitch axis of the platform. The ratio h/R must be set in by potentiometer for the particular orbit and target height.

Equation (2) of Section II-F relates η to time as

$$\eta = g(t-t_0) + \eta_0 \quad \text{where}$$

g is the integration gain constant and

η_0 is the angle η at time t_0 .

Figure 31 is a block diagram showing how the equations are mechanized.

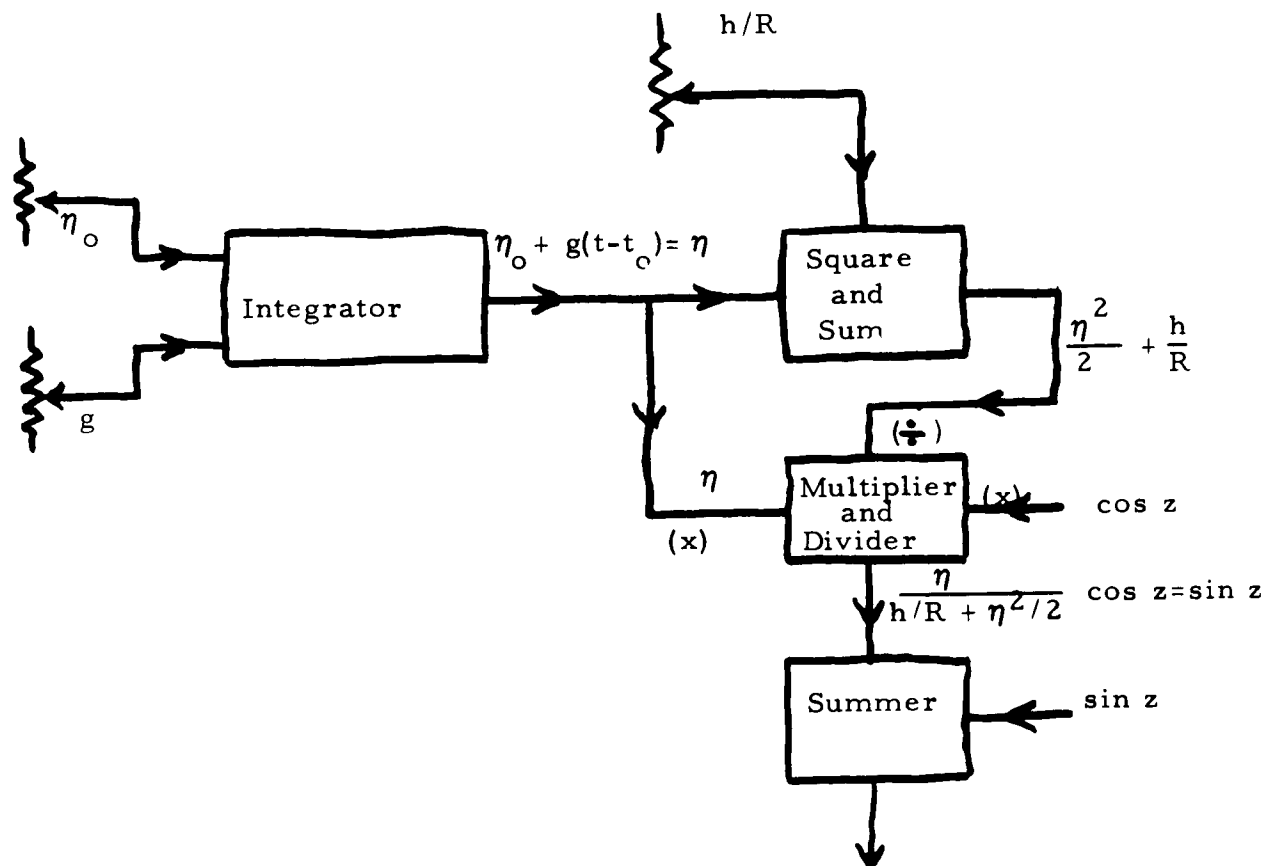


Figure 31

Servo Error

The initial angle η_0 and the gain g are set by potentiometers and the integrator output is $\eta_0 + g(t-t_0) = \eta$. η goes to a squaring circuit where it is squared and then summed to h/R which is also set by potentiometer.

η also goes into one of the multiplying terminals of the multiplier and divider and $\cos z$ goes into the other multiplying terminal. The value $\frac{\eta^2}{2} + \frac{h}{R}$ goes in to the divider terminal. The output of the multiplier-divider therefore is

$$\frac{\eta}{h/R + \eta^2/2}, \quad \cos z = \sin z$$

This value is summed against $\sin z$ from the resolver and any inequality produces a servo error to drive z toward equality.

3. Triangle Waveform Generator

Figure 32 is the schematic of the circuit which generates a precision symmetrical triangular waveform of 20 volts peak to peak. This waveform is used in the squaring circuit to be described in section e. The waveform generator also has a square wave output which is used in the multiplier-divider to be described in section f.

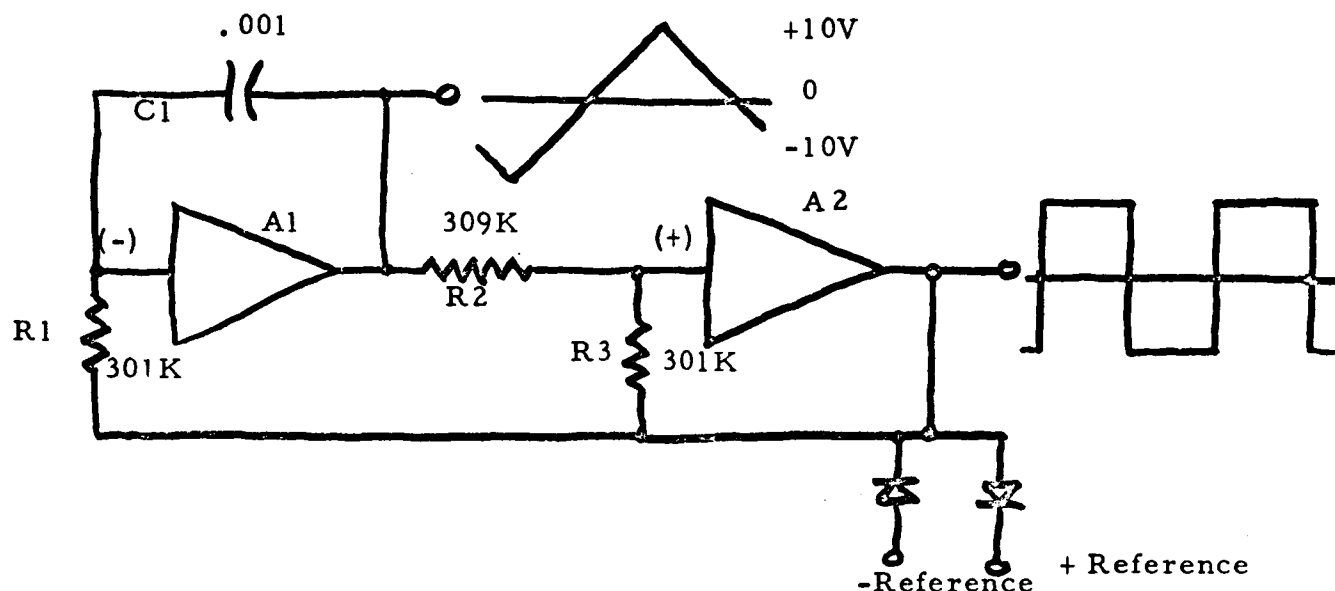


Figure 32

Amplifier A1 is an integrator and amplifier A2 is a threshold. Assume the integrator output is at + 10 volts and the threshold output is -Ref. The current through R2 will just equal the current through R3 so the threshold input will begin to swing (+). Because the amplifier A2 is hooked up in the non-inverting connection its output also goes (+). The output is regenerative coupled to the input through R3 so the threshold goes to + Reference. Now the current into the integrator through R1 is from the + Reference voltage at the threshold output so the capacitor C1 charges causing the output of the integrator to go (-). When the integrator output reaches (-) 10 volts, the current through R2 equals that through R3 so the threshold input starts to go (-) and the output then regenerative goes to (-) Reference. Now the integrator input current through R1 comes from the (-) Reference so the integrator output goes (+). When it reaches +10 volts the cycle repeats.

The output of the integrator is a precision triangle waveform of 20 volts peak to peak, symmetrical about zero volts.

4. Integrator

Figure 33 is the electrical schematic of the circuit that generates the angle η as a function of time.

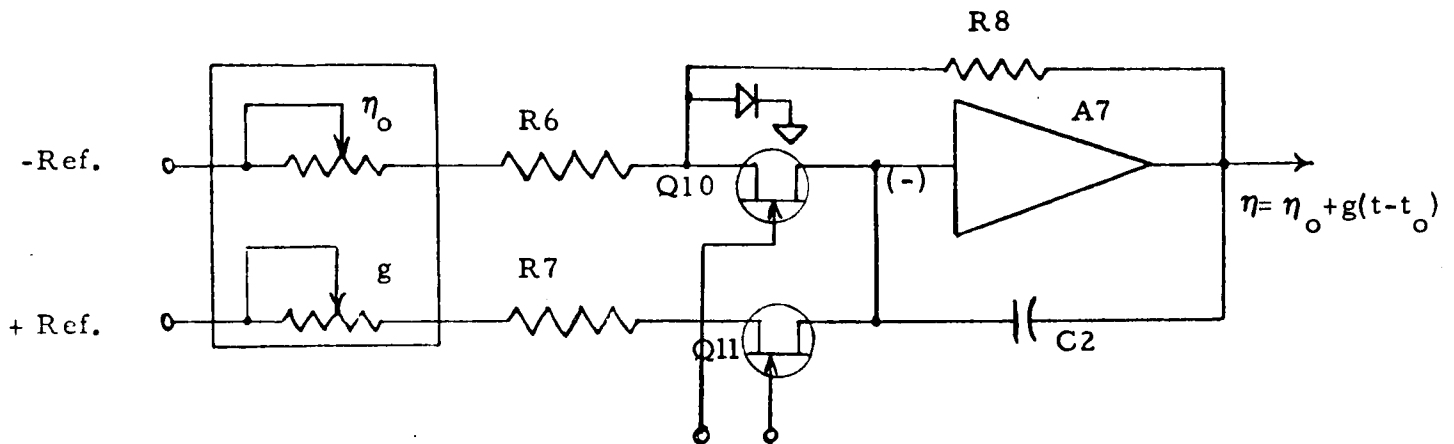


Figure 33

Operational amplifier A7 is an integrator in the "operate" mode with C2 the integrating capacitor. In the "Initial Condition" mode, field effect switch Q11 is open and field effect switch Q10 is closed. Potentiometer η_0 sets in the initial angle for η . In "operate", switch Q10 opens first then Q11 closes. The output now integrates time from t_0 at a rate g set in by potentiometer g .

The design range of the η integrator is ± 10 volts where 10 volts represents 0.1 radian.

5. Squaring Circuit

Figure 34 is the circuit that squares η and sums it with h/R .

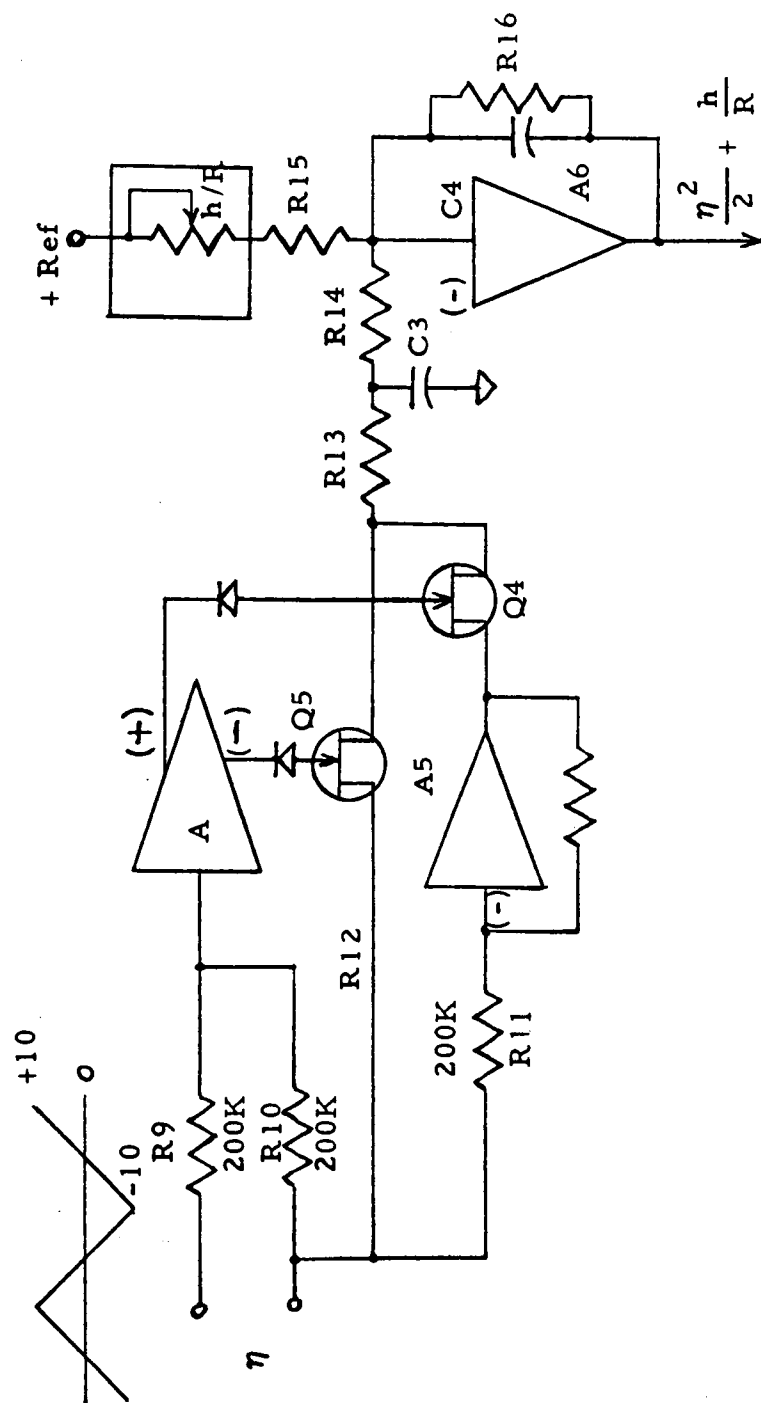


Figure 34

Amplifier A consists of transistors Q1, Q2, and Q3 shown in the overall schematic (902D930). Q4 is driven by the non-inverting output and Q5 is driven by the inverting output. If in Figure 34 we assume $\eta=0$, the triangle wave will drive Q4 and Q5 on and off with a 50% duty cycle. Q4 being on when the triangle wave is + and Q5 being on when the triangle wave is (-).

If η is slightly +, then Q4 will be on more than 50% of the time and Q5 will be on less than 50% of the time. Consider the switches as variable gain devices. At 50% duty cycle their gain is 1/2. At 0% it is 0 and at 100% it is 1. Note that switch Q4 follows the inverter A5 so it switches - signals.

Figure 35 shows one-half of the triangle waveform and the signal

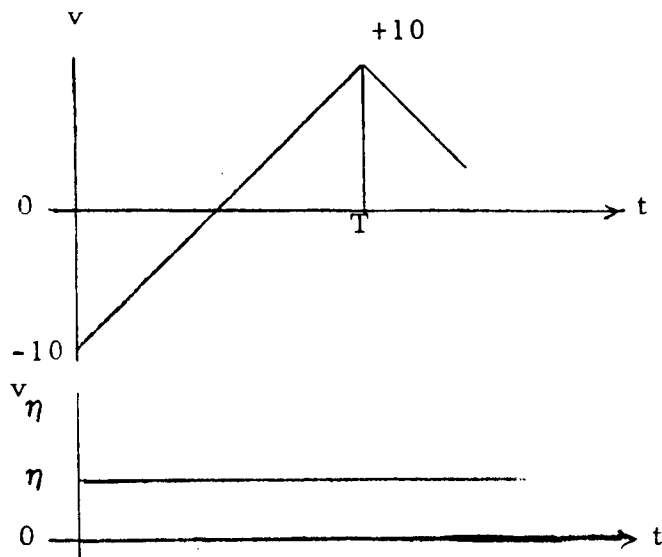


Figure 35

The equation for the triangle here is

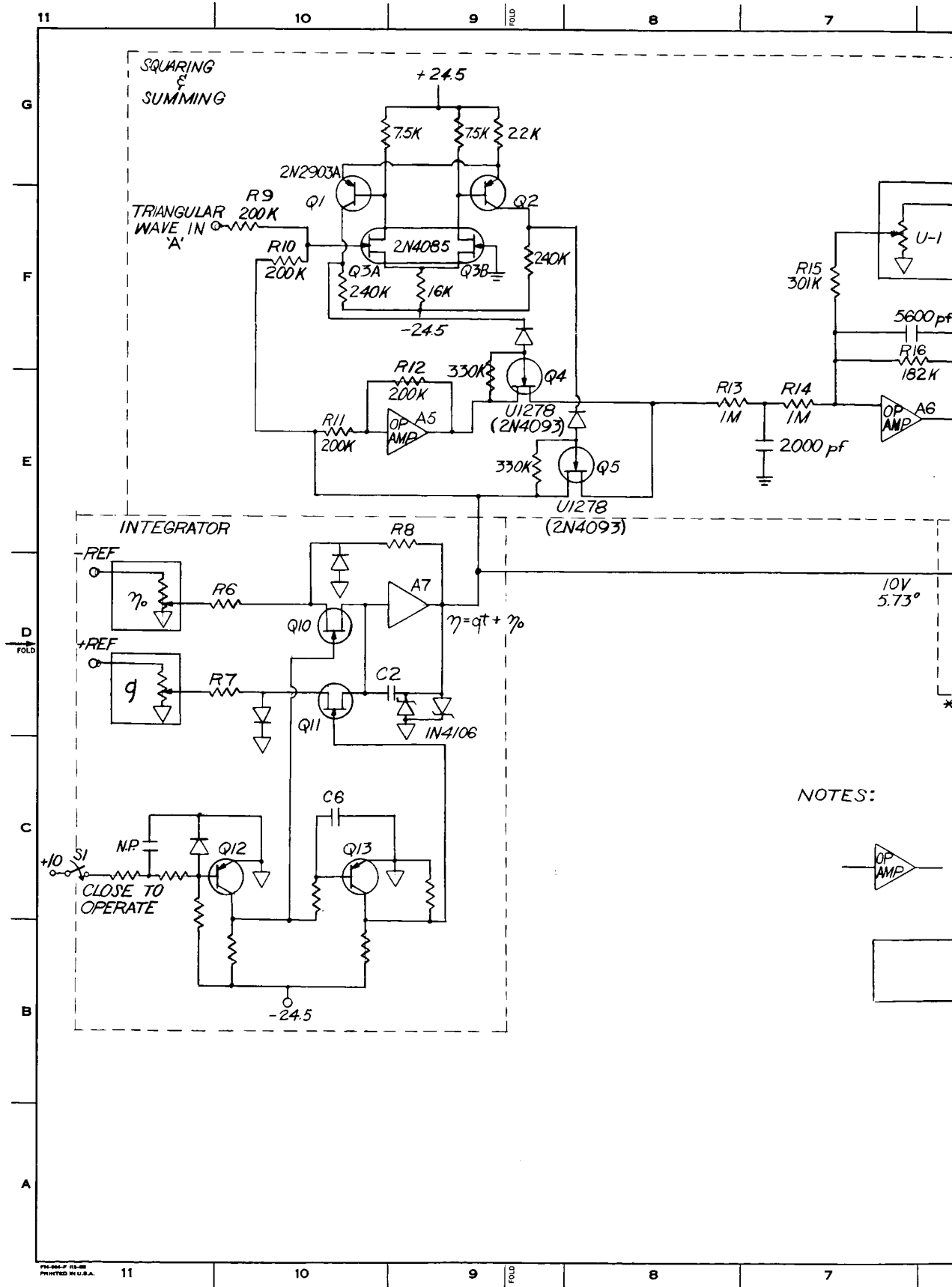
$$v = -10 + \frac{2t}{T} (10) \quad -10 \leq v \leq +10$$

Current into amplifier A is the sum of input currents through R9 and R10, or,

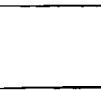
$$I = \frac{v}{200K} + \frac{\eta}{200K} \quad \text{For } I = 0, \quad 10 - \frac{2t_o}{T} (10) = \eta$$

or $t_o = \frac{T}{20} (10 - \eta)$. From Figure 34 it is seen that if $I < 0$, Q5 is on and if $I > 0$, Q4 is on. Now the gain of Q5 is $\frac{t_o}{T}$ and that of Q4 is $\frac{T - t_o}{T}$ because the gain is the ratio of on time to total time. The average voltage on R13 now becomes $V_{avg} = \eta G5 - \eta G4 = \eta (G5 - G4)$.

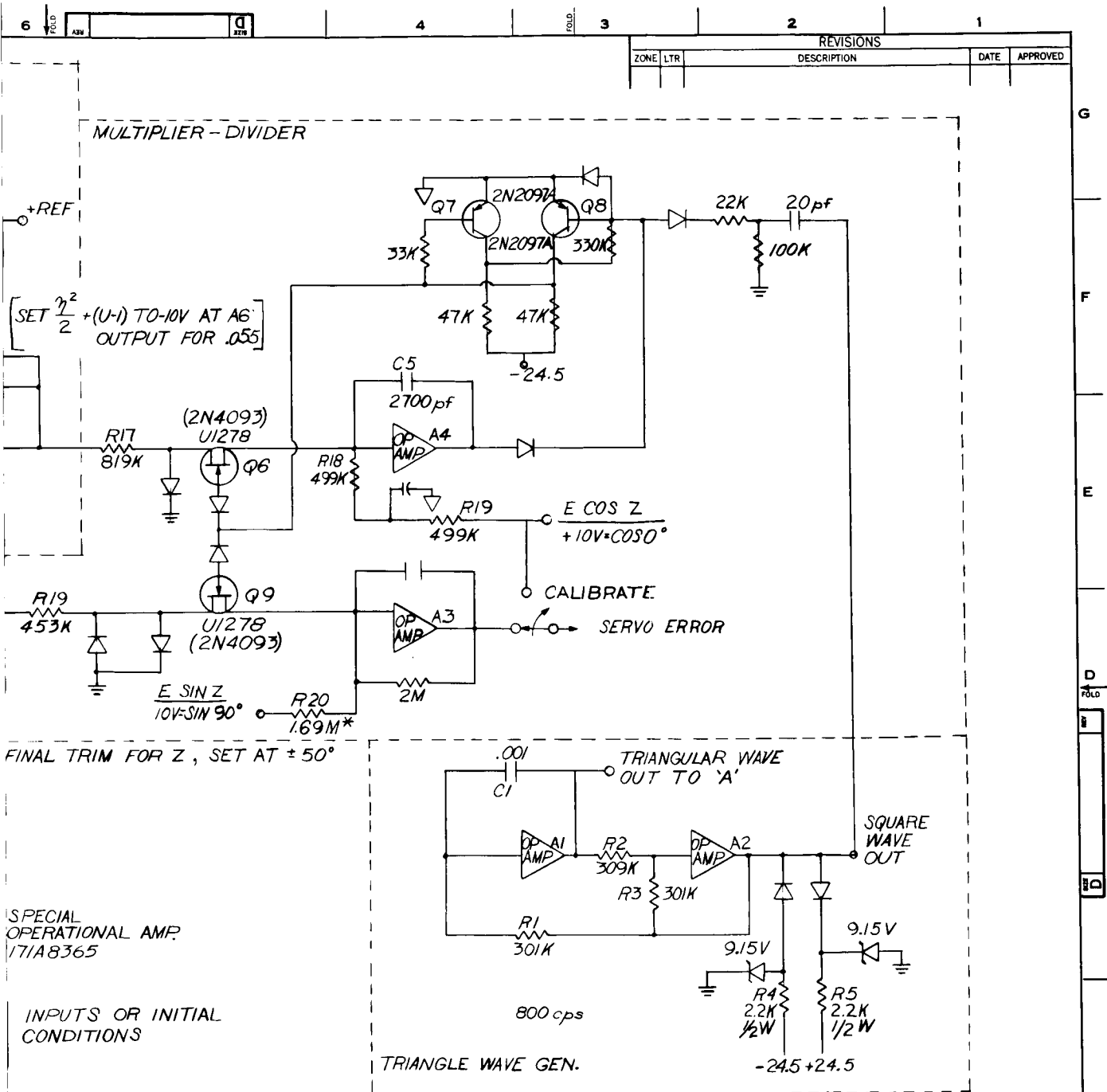
FOLDOUT FRAME



NOTES:



FOLDDOUT FRAME



UNLESS OTHERWISE SPECIFIED DIMENSIONS ARE IN INCHES— TOLERANCES ON: 2-PLACE DECIMALS ± 3-PLACE DECIMALS ± ANGLES ± FRACTIONS ± MATERIAL—		SIGNATURES DRAWN G.B. MALLOY CHECKED TESTED REWORK DATE		DAY 4	MO 1	YR 68
ALL SURF. ✓		GENERAL ELECTRIC DEPT LOC				
S046 EXPERIMENT SCAN SERVO FUNCTION GENERATOR SCHEMATIC						
SIZE D		CODE IDENT NO. 15227		902D930		
SCALE		SHEET 1 OF 1				

$$G_4 = 1 - \frac{10}{20} + \frac{\eta}{20}; \quad G_5 = \frac{10}{20} - \frac{\eta}{20}.$$

$$V_{avg} = \eta \left(\frac{1}{2} - \frac{\eta}{20} - 1 + \frac{1}{2} - \frac{\eta}{20} \right) \quad \text{or} \quad V_{avg} = -\frac{\eta^2}{10} \quad .$$

The squaring circuit has a 10 volt output for $\eta = 0.1$. Resistors R13, R14, R15 with potentiometer $\frac{h}{R}$, and R16 are scaled so that at amplifier A6 output, 10 volts represents $\frac{\eta^2}{2} + \frac{h}{R} = .055$.

6. Multiplier - Divider

A simplified diagram of the multiplier-divider is shown in Figure 36.

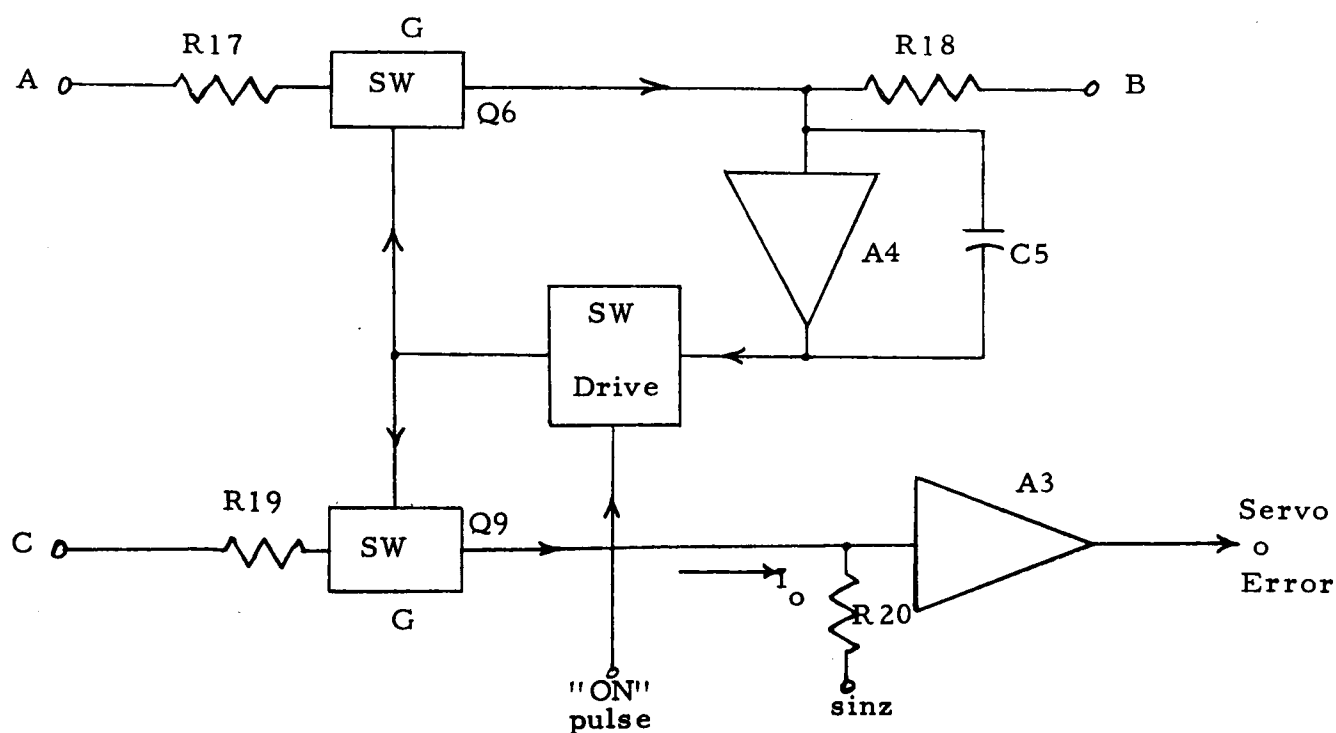


Figure 36

The block labeled sw is a switch whose gain is the ratio of on time to total time. Assume $R_{17} = R_{18} = R_{19} = R_{20}$. Current into amplifier A4, $I = \frac{AG}{R_{17}} + \frac{B}{R_{18}}$. This current must be zero average so $\frac{B}{R_{18}} = -\frac{AG}{R_{17}}$ or $G = -\frac{B}{A}$.

Note that $I_o = \frac{C}{R_{19}} G$ or $I_o = \frac{-C}{R_{19}} \frac{B}{A}$. In this circuit $A = \frac{\eta^2}{2} + \frac{h}{R}$,

$B = \cos z$, and $C = \eta$. Therefore $I_o = -\frac{1}{R_{19}} \frac{\frac{\eta \cos z}{2}}{\frac{\eta^2}{2} + \frac{h}{R}}$. Referring to

section 2, this is $-\sin z$. Amplifier A3 sums I_o and $\sin z$ to get

$I_{\text{error}} = I_o - \frac{\sin z}{R_{20}} = \frac{1}{R_{19}} \frac{\frac{\eta \cos z}{2}}{\frac{\eta^2}{2} + \frac{h}{R}} - \frac{\sin z}{R_{20}}$ which is brought to zero

by the servo. Therefore we get $\sin z = \frac{\frac{\eta \cos z}{2}}{\frac{\eta^2}{2} + \frac{h}{R}}$

The assumption of $R_{17} = R_{18} = R_{19} = R_{20}$ was for simplification. These resistors are not equal but are determined by scaling so in the actual circuit each current is a voltage divided by its resistance. Criteria for value selection are given above, and the circuit diagram with actual values is shown in drawing 902D930.

The switch drive consists of Q7 and Q8 hooked up as a bistable multivibrator. To turn the switches "ON" requires a (-) pulse on the base of Q8. This is furnished by differentiating the square wave output of A2 in the triangle wave generator circuit. The switch stays "ON" until the average current $\frac{AG}{R_{17}}$ equals the average current $\frac{B}{R_{18}}$ where the output of A4 going (+) turns "OFF" the switches by driving the base of Q8 (+). The output of A4 always goes (+) when the switches are "ON" because A is (-) and $|A| > |B|$ (Figure 6). Also, the output of A4 goes (-) when the switches are "OFF" because B is always (+).

7. Computer Operation

Scaling

The value of η is taken as $-0.1 \text{ radian} \leq \eta \leq +0.1 \text{ radian}$. At the output of the η generator $+0.1 \text{ radian}$ is $+10 \text{ volts}$ and $(-) 0.1 \text{ radian}$ is -10 volts .

The value of η^2 at R13, Q4, and Q5 is +.01 and is scaled to +10 volts (see section IV). The value of $\frac{\eta^2}{2} + \frac{h}{R}$ is + .055 max and is scaled to (-) 10 volts at the output of A6.

The scale for $\cos z$ is $v = 10 \cos z$ and the scale for $\sin z$ is $v = 10 \sin z$.

The frequency is set (but not limited to) to 800 cycles per second for the triangle waveform generator. This value was chosen in the event it may be used to excite the inverter for driving the resolver windings.

Trim Requirements

For the best accuracy it is necessary to trim the values of several resistors. Each potentiometer (η_o , g, U-1) has a series resistor in the wiper lead (R6, R7, R15) which is adjusted to align the electrical response to the dial and to the reference voltages. These voltages are given in the scaling section.

With a fixed η and $\frac{h}{R}$ which gives about $\pm 50^\circ$ for z ,

Resistor R20 is trimmed to null the output of amplifier A3. A set of values might be $\eta = \pm .04$, $\frac{h}{R} = .03$, and $z = 52.4^\circ$. This takes out variations in switches

Q6 and Q9 as well as variations in resolvers and the resistors in the multiplier-divider circuit. If a slightly different value for R20 is found for $\pm 50^\circ$ then use the average value. In no case should this difference exceed $\pm 0.1^\circ$ in z .

Operating Modes

(a) Initial Conditions

In this mode S1 (902D930) is open and switch Q10 is closed with Q11 open. The initial angle η_o , gain g, and orbit height ratio U-1, for the particular target and orbit, is set in . The instrument will be pointing at the angle z_o computed for that particular η_o and U-1.

(b) Operate

In this mode S1 is closed which first opens Q10 and slightly later (a few milliseconds) closes Q11. The reason for the delay in closing Q11 is not to disturb η_o during the switching transient when both Q10 and Q11 might be momentarily closed. This delay is accomplished by C6 in the base circuit of Q13.

The integration starts immediately to furnish η and the computer continuously furnishes the servo with error information about z . η and tracking will continue until the mode is changed, z reaches a limit or η reaches 0.12 radian where the η generator saturates.

(c) Calibrate

This is a stow mode which switches the servo from the multiplier-divider output to the $10 \cos z$ terminal where null at 90° is the only stable angle. Placed here is the internal calibrator lamp which may be turned on for calibration of the instrument.

(d) Test Results

The function generator circuit was tested by applying as inputs $\cos z$ and $\sin z$. Normally, η would be generated by an electronic integrator and $\cos z$ and $\sin z$ would be provided by the demodulated output of a resolver mounted on the instrument pitch axis. For the test setup, η was generated by a regulated direct current supply and $\cos z$ and $\sin z$ were generated by the 10 turn precision potentiometers shown in the photograph in Section IV G4.

The output of the scan function generator circuit is an error voltage derived from a comparison of the computed $\sin z$ with the $\sin z$ generated by the resolver. This error voltage is used to drive the DC torque motor which moves the scan platform and the resolver. During the test, the error signal was used to determine when the computed $\sin z$ equaled the resolver (potentiometer) generated $\sin z$. A comparison of η with the value obtained from a mathematical solution based on the $\sin z$, U and $\cos z$ values applied to the breadboard circuit provided a direct indication of the system accuracy. Measured and calculated values for $U=1.03$ are shown in the Table below.

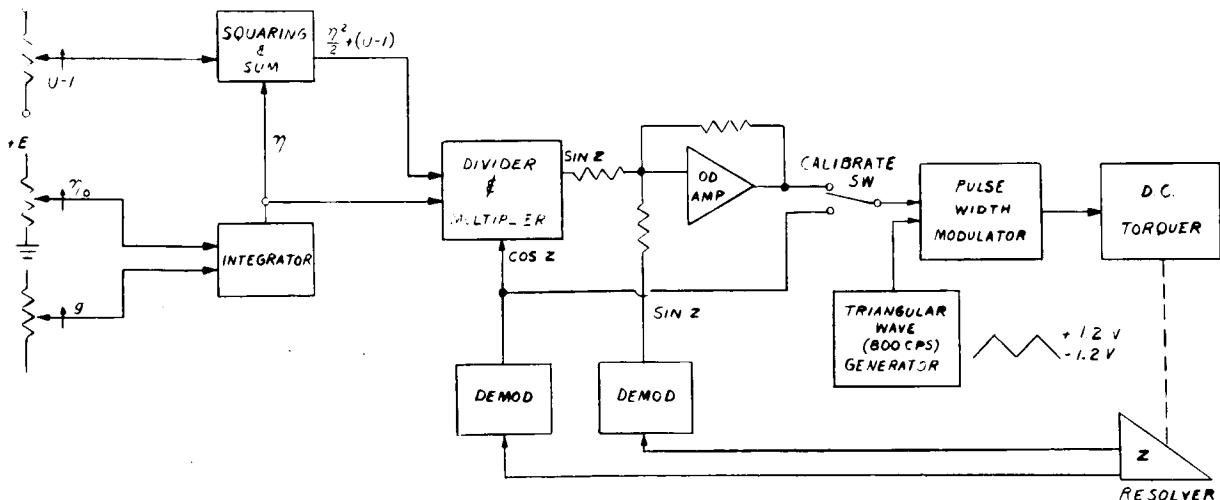
<u>z</u> <u>Error</u>	<u>η</u> <u>Calculated</u>	<u>η</u> <u>Measured</u>	<u>$\cos z$</u> <u>Calculated</u>	<u>$\sin z$</u> <u>Calculated</u>	<u>z</u> <u>Degrees</u>
.000°	-.0550	-.0550	.497	.868	60.2
.044°	-.0500	-.0501	.530	.848	58.0
.066°	-.0400	-.0401	.610	.792	52.4
.096°	-.0300	-.0301	.712	.702	44.6
.000°	-.0200	-.0200	.834	.552	33.5
.000°	-.0100	-.0100	.949	.316	18.4
0	0	0	1	0	0
.000°	.0100	.0100	.949	-.316	-.18.4
.000°	.0200	.0200	.834	-.552	-33.5
.000°	.0300	.0300	.712	-.702	-44.6
.066	.0400	.0401	.610	-.792	-52.4
.000°	.0500	.0500	.530	-.848	-58.0
.000°	.0550	.0550	.497	-.868	-60.2

The error amounts to less than 0.1 degree and is equivalent to one digit in the third place when setting in values for $U-1$, $\cos z$ and $\sin z$. This is also the limit of the instruments used for the breadboard test therefore the error indicated when combined with an equivalent instrumentation error places the actual error to no more than ± 0.2 degrees.

Tests verified that large variations ($\pm 20\%$) in resolver excitation voltage do not affect the performance of the computer.

8. Scan Servo

Drawing 125C 1823 shows the scan platform servo arrangement and its interconnections with the scan function generator. The error signal is amplified and fed to a pulse width modulator whose output is a pulse which has a percent on time proportional to the DC input signal. This pulse is fed to a DC torque motor which moves the scan platform and the resolver. The resolver output is demodulated, filtered and fed back to the function generator. Drawing 125C1824 (next page) shows the circuit for the scan servo amplifier and demodulator.



Dwg. 125C1823, Scan Servo Block Diagram

E. S046 Experiment System

1. Experiment Layout

The preliminary design general layout for the S046 experiment is shown on Drawing 895D192*. The initial weight estimate of 40.0 pounds detailed below is conservative since no major weight reduction work has been attempted during the preliminary design phase. Another subsequent section established an initial power profile for the experiment based on information available at this time. Thermal control power requirements cannot be established until the location of the experiment has been established and the thermal environment defined by the integrating contractor.

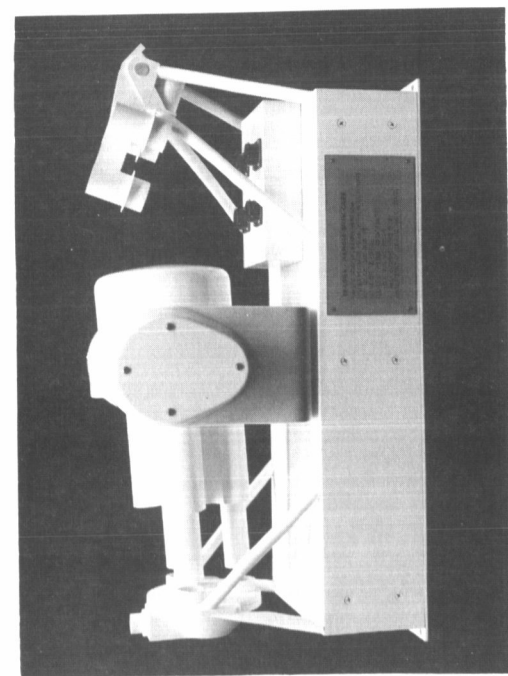
A significant feature of the arrangement of the S046 experiment is the combining of the scan platform base assembly with the electronics housings to provide a common base for the S046 package. The arrangement is such that the yaw axis elements can readily be eliminated from the design if the carrier vehicle can provide this yaw function. The scanner electronics, in one end of the base assembly, is packaged in separate modules for each of the two axes, and one of these can be eliminated if yaw axis rotation is not required. Electrical connections for the S046 experiment package are located such that they are accessible for installation after the package is mounted in the carrier vehicle.

The solar flux calibrator assembly is pivoted in order to permit the unit to be mounted within the available space. A pyro technic-mechanical device is used in combination with a torsion spring to provide a reliable, single operation deployment of the solar flux calibrator unit. The unit is located such that it is outside the field of view of the photopolarimeter instrument during normal scanning operations. Solar flux calibration is performed by rotating the instrument, by means of the pitch axis of the scan platform, to a position approximately 15° beyond the maximum scan angle of 60° aft of nadir position. With the instrument in this position the spacecraft is oriented such that the instrument axis is within 2° of the vehicle-sun line.

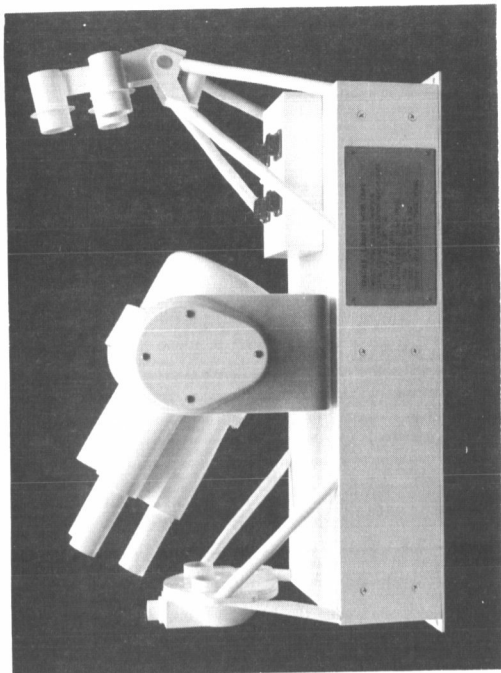
The lamp calibrator assembly is permanently mounted such that the photopolarimeter instrument is in line with the lamp calibrator axis during the normal stowed or caged position of the photopolarimeter instrument. Lamp calibration is performed prior to, and following such scan in order to provide a high degree of confidence in the values of the data obtained.

Figure 37 shows photographs of the mock-up built under the Phase C Contract.

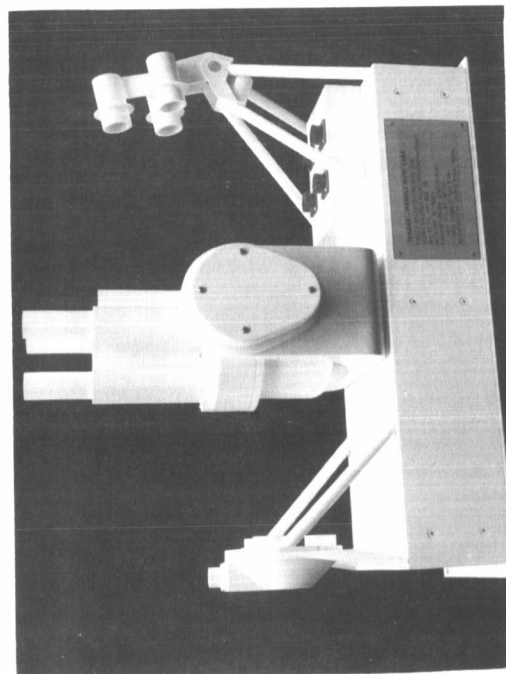
* See p. 83/84



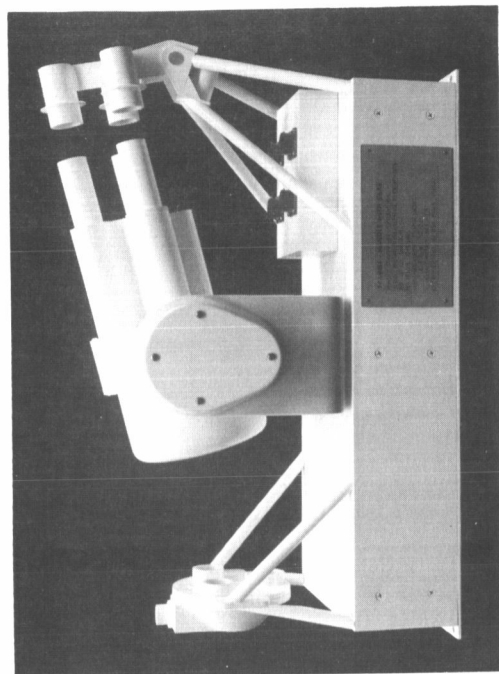
Stowed position-instrument in lamp
calibration position



Standby - ready to start scan



Instrument in nadir position



Sun calibration position

Figure 37

2. Initial Weight Estimates

The following weight estimate is based on information available to date concerning each of the identified components of the experiment package. Mass properties statement, M.S.C. Form 1121 (Rev. Dec. 65) is shown as Figure 38.

1.	Optical/Mechanical Module - based on 8.5 [#] Breadboard without cover and without fiber optics plus .5 [#] =	9.0 [#]
2.	Yoke - based on 2 ft ² of .090" Al @ 1.25 [#] plus 1.5 [#] Torquer plus 1.0 [#] Resolver plus .5 [#] bearing plus .5 [#] miscellaneous =	6.0 [#]
3.	Base structure based on 4 ft ² of .090 Al @ 1.25 [#] plus 30% =	6.5 [#]
4.	Torquer Resolver and Bearings based on 1.5 [#] Torquer plus 1.0 [#] Resolver plus .5 [#] Bearing =	3.0 [#]
5.	Two axis scanner Electronics based on phone call to GE-OD-similar electronics =	5.5 [#]
6.	Function generator and processor electronics based on 6 boards @ 1 [#] /board installed =	6.0 [#]
7.	Sun Calibrator and Bracket ROM estimate =	2.0
8.	Lamp Calibrator & Bracket ROM estimate =	2.0
		<hr/> 40.0 [#]

3. Initial Power Profile

The following power profile is based on information available to date concerning each of the identified components of the experiment package.

The power profile curve shown as Figure 39.

PREPARED BY: D.E. LEE

DATE: 11-29-67

FIGURE 38

MASS PROPERTIES STATEMENT

PAGE NO. 2 of 2
 REPORT NO. UCLA PIR
No. 049

CODE	DESCRIPTION	CCA NUMBER	CONTROL WEIGHTS (POUNDS)	CURRENT WEIGHT (POUNDS)	CHANGE SINCE LAST REPORT (POUNDS)	BASIS FOR CURRENT DATA			STORAGE LOCATION	ICD NUMBER	DIMENSIONS (INCHES)		
						E.	C.	A.			L.	W.	H.
	Optical/Mech. Module			9.0				✓					
	Scanner Yoke			6.0			✓						
	Base Structure			6.5			✓						
	Yaw Torquer/Hydrology			3.0			✓						
	OD Electronics			5.5			✓						
	MSD Electronics			6.0			✓						
	Sun Calib. & Bkt			2.0		✓							
	Lamp Calib. & Bkt			2.0		✓							
				40.0									

<u>Item</u>	<u>Power (Watts)</u>	<u>Duration (Sec.)</u>	<u>Energy (Watt-Sec.)</u>
1. Calibration Lamp	12	1440	17280
2. Beam Selector Drive	3	540	1620
3. Electronics & Scanner Platform (EST)	5	540	2700
4. Start & Stop Platform (6)	30	0.06	2
5. Operate Neutral Density Filter (15)	4.5	7.5	34
Total Energy =			<u>21636</u>
			=
			6 Watt Hour

Assumptions:

1. Calibration lamp requires 15 minute warmup.
2. Beam Selector drive and all electronics are operational in about 1-5 seconds.
3. Calibration through three apertures can be accomplished within 30 seconds after instrument and scanner are energized.
4. Scan Platform moves to Standby (+60°) position for 60 seconds prior to scan.
5. Scanner acceleration and deceleration at full power (30 watts) will proceed in steps from closed (4) to open (1) during first calibration and will proceed in two steps to the maximum density position (3) and return to open (1) two times during the scan. It will then return to closed (4) in steps during the final calibration prior to instrument shut down. Position profile for the ND filter as described above is as follows: 4 - 3 - 2 - 1 --- 2 - 3 - 2 - 1 --- 2 - 3 - 2 - 1 --- 2 - 3 - 4. Based on the above assumptions, the total power for 100 scans will be 100 x 6 watt hours = 0.6 KWH.

F. Ground Support Equipment

1. General Description

A four foot diameter integrating sphere shown in drawing 902D928 has been procured for permanent retention in the laboratory. The procedure for using the sphere for checkout of the photopolarimeter has been developed during system tests of the experiment breadboard. It will form the basis for Pre Delivery Acceptance and Pre Installation Acceptance of the S046 equipment and will be available for verification of equipment calibration on either a routine or unscheduled basis.

The Ground Support Equipment Mobile Checkout Stand will consist of a four foot diameter integrating sphere with a six ampere tungsten iodide lamp and the electrical and mechanical equipment necessary to command and integrate the S046 experiment package. This equipment will include a mounting fixture, a polarimeter control panel, a polarimeter monitor panel, and a calibration control panel. A removable polarimeter simulation panel will be included if further studies indicate that it is needed. The simulator would be used to verify GSE circuits or for trouble shooting within the flight vehicle or launch facility circuits.

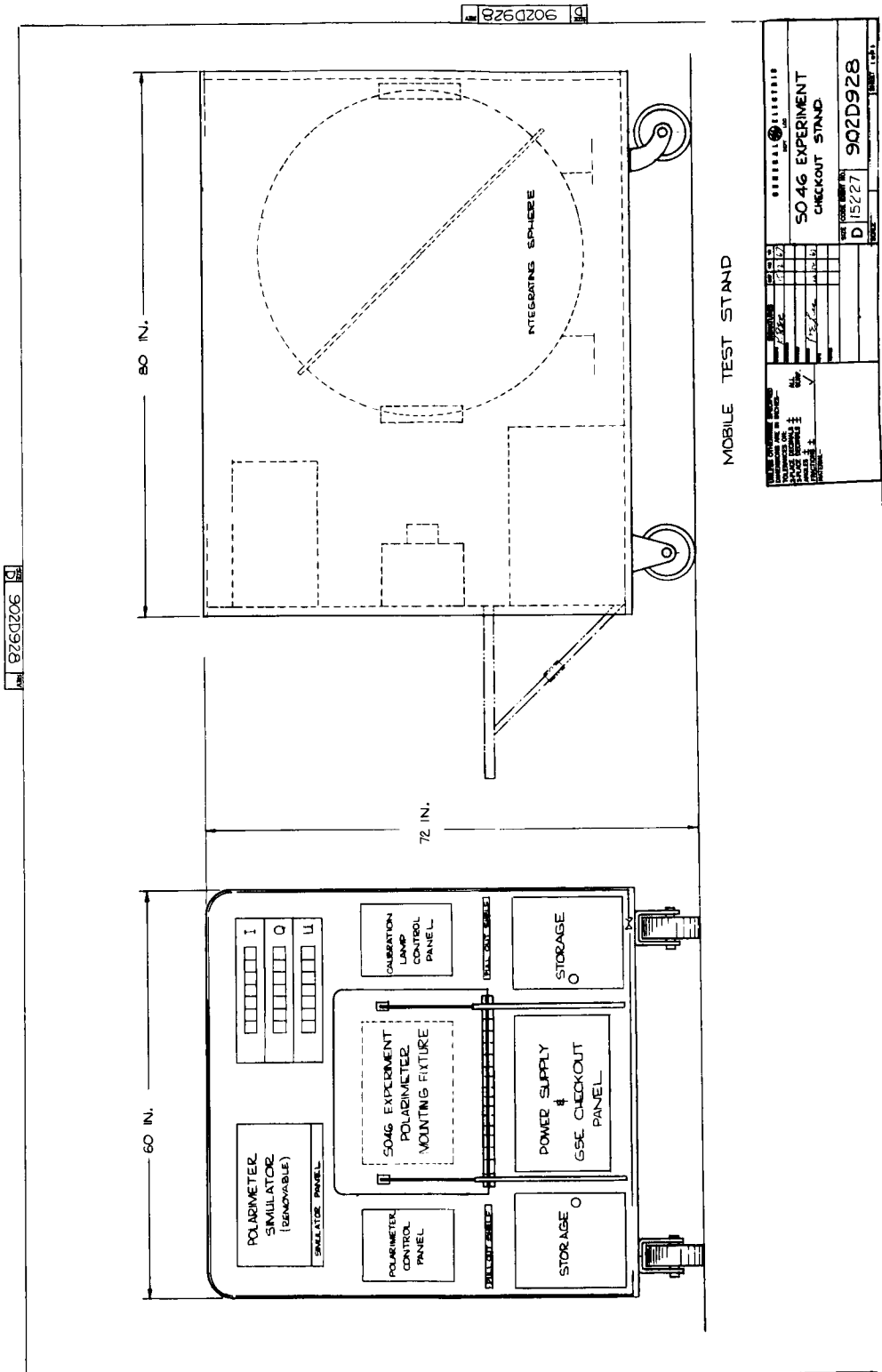
The GSE Mobile Test Stand will be mounted on a portable chassis meeting the requirements of MIL-M-008090E, Type I, Class 1, suitable for manual transport in a laboratory or shop area. Storage space will be provided for cable assemblies, special tools, instruction manuals and spare parts as needed.

2. System Requirements

The ground support equipment will provide inputs to, and accept outputs from the S046 polarimeter experiment package, and will be used to check out and calibrate the instrument. The ground support equipment will provide: polarimeter control capability; polarimeter mounting fixture which contain rate and position detectors; stabilized tungsten light source with intensity stable to $\pm 0.1\%$; telemetry processor and display to separate, hold and display the I, Q, and U parameters. Displays are also required to indicate the color being observed, the state of the neutral density filter drive and all of the housekeeping functions. Power supplies for the polarimeter instrument, the calibrated light source and all the electronic equipment are to be located in the ground checkout stand.

3. Subsystem Requirements

a) Mechanical



MOBILE TEST STAND

902D928 5046 EXPERIMENT CHECKOUT STAND	
D 15227 902D928	902D928

o Size - Maximum overall size of the ground support equipment checkout stand will be 60 inches wide x 72 inches high x 80 inches long.

o Weight - The maximum weight of the checkout stand will be 600 pounds.

o The checkout stand will be mounted on wheels.

o The ground support equipment will be fitted with an integrating sphere 48 inches inside diameter.

o A target 7 inches in diameter will be provided inside the sphere at which the instrument can be aimed.

o The GSE shall be capable of measuring the instrument pitch axis position and position rate and comparing these measurements with the specifications for various scan programs.

b) Optical

o The light source inside the integrating sphere will be a quartz-tungsten-iodine lamp operated at a filament temperature of $3080^{\circ}\text{K} \pm 50^{\circ}\text{K}$.

o The light source will be stabilized so that the intensity does not vary more than $\pm 0.1\%$ short term and $\pm 0.5\%$ long term.

o The target will be flat white with a reflectivity of greater than 0.8 and will be illuminated such that the intensity across the target will not vary more than 0.2% from one side to the other when the target is employed with an aperture 0.1 inch in diameter.

o The residual polarization of the light reflected from the target will be less than 0.2%.

o The polarization of the light reflected from the target will be adjustable to one of three different levels as follows: 1) Minimum polarization less than 0.2%, 2) Light polarization $10\% \pm 1\%$, 3) Maximum polarization $95\% \pm 5\%$.

o The absolute intensity of the dominant polarization component will be maintained for the three steps as follows: 1) 100% to -0.2%, 2) 100% to -0.2%, 3) 100% to -65%. The short term and long term variations of the intensity of the dominant polarization component must be within the limits of $\pm 0.1\%$ in a previous paragraph.

c) Electrical

o Electrical Input Power Requirements

- (a) Voltage 115 VAC 60 cps
- (b) Power Requirements 600 watts maximum

o Electrical Output Power Requirements

- (a) Voltage 24 VDC
- (b) Power Requirement 50 watts maximum

o Signal Data Requirement

- (a) Buffer storage must be provided for the following data requirements.

- (1) Signal amplitude 0-10V 10 bits 120 bits per second
- (2) Scale 0-10V 2 bits 24 bits per second
- (3) Polarity 0-10V 1 bit 12 bits per second
- (4) Filter position 0-10V 2 bits 8 bits per second
- (5) Pitch angle 1-10V 10bits 10 bits per second
- (6) Yaw angle 0-10V 5 bits 5 bits per second
- (7) Spectral identification 1-10V 2 bits 8 bits per second

- (b) Displays must be provided for each of the above signals as follows:

- | | | |
|-----------------------------|---|-----------------|
| (1) Signal amplitude | - | Decimal Digital |
| (2) Scale | - | Lights |
| (3) Polarity | - | Lights |
| (4) Filter position | - | Lights |
| (5) Pitch angle | - | Decimal Digital |
| (6) Yaw angle | - | Decimal Digital |
| (7) Spectral identification | - | Lights |

G. Photopolarimeter Breadboard Tests

1. General Description

Certain portions of the S046 Preliminary Design were subject to test in the laboratory in order to obtain test data which would further guide the design effort. Principle portions of the experiment which were mocked up and tested were:

- (1) Optical and mechanical module
- (2) Signal processor, exclusive of logic and automatic gain switching
- (3) High voltage power supply
- (4) Scan function generator

A breadboard version of the photopolarimeter instrument was available at the beginning of the contract. The earlier breadboard had shown feasibility for the general design approach. Because of the many potential problems involved in the design of a new type of instrument, a more detailed version was constructed and tested during the Phase C contract. This instrument is nearly identical to that shown in the inboard profile drawing number 902D929. The principal difference is that, in the breadboard instrument the individual barrel axes are tilted to the extent that they cross approximately 4-1/2 feet in front of the device. This was done in order that the three barrels would view the same portion of the laboratory light source in the calibration tests that were performed. Figure 40 is a front view of the photopolarimeter showing the optical module, phototube and associated electrical connections.

A beam selector disk rotates at the rate of 4 revolutions per second and a Geneva mechanism advances a color filter disk 90° once per beam selector disk rotation. Values of I, U, and Q are thus obtained in each of four colors once per second. Figure 41 shows the mechanical portion of the photopolarimeter with the beam mixer in place. The Geneva movement can be seen adjacent to the beam selector drive motor.

A number of problems were originally encountered due to electrical transients and pickup in the signal processor. These problems were, however, solved and the resultant circuit changes led to the final processor circuit diagram shown in the previous section on electrical design. Subsequent tests of the signal processor showed short term stability consistent with the specification of measuring 5% polarization with an accuracy of .05%. Measurement of noise was consistent with predictions on the basis of photoelectron statistics and stability of electronic amplification as discussed in the previous section on noise and measurement errors. Figure shows the overall polarimeter test setup and associated electrical test equipment. Figure 42 shows the overall test setup including the four foot

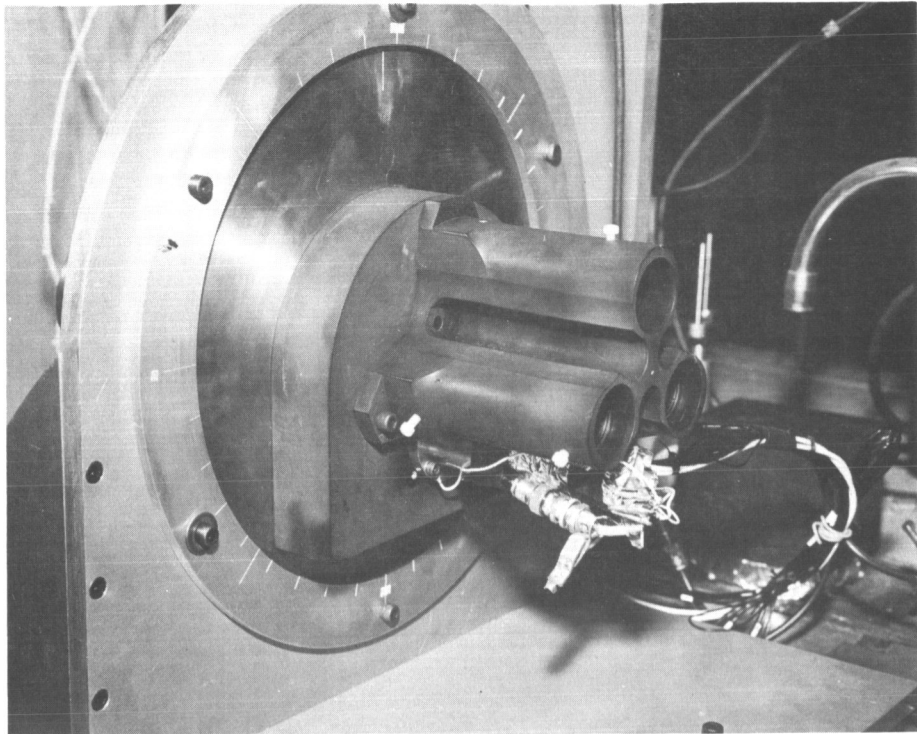


Figure 40. Front view of photopolarimeter

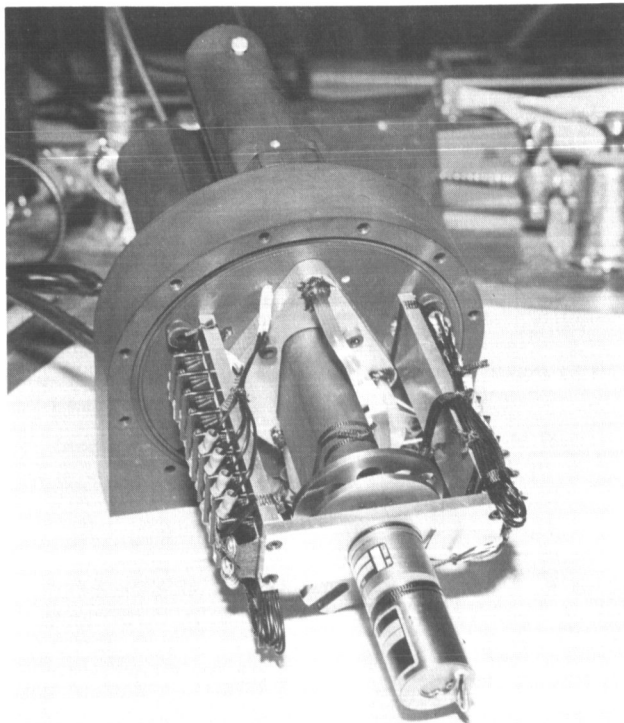


Figure 41. Mechanical portion of photopolarimeter with beam mixer in place

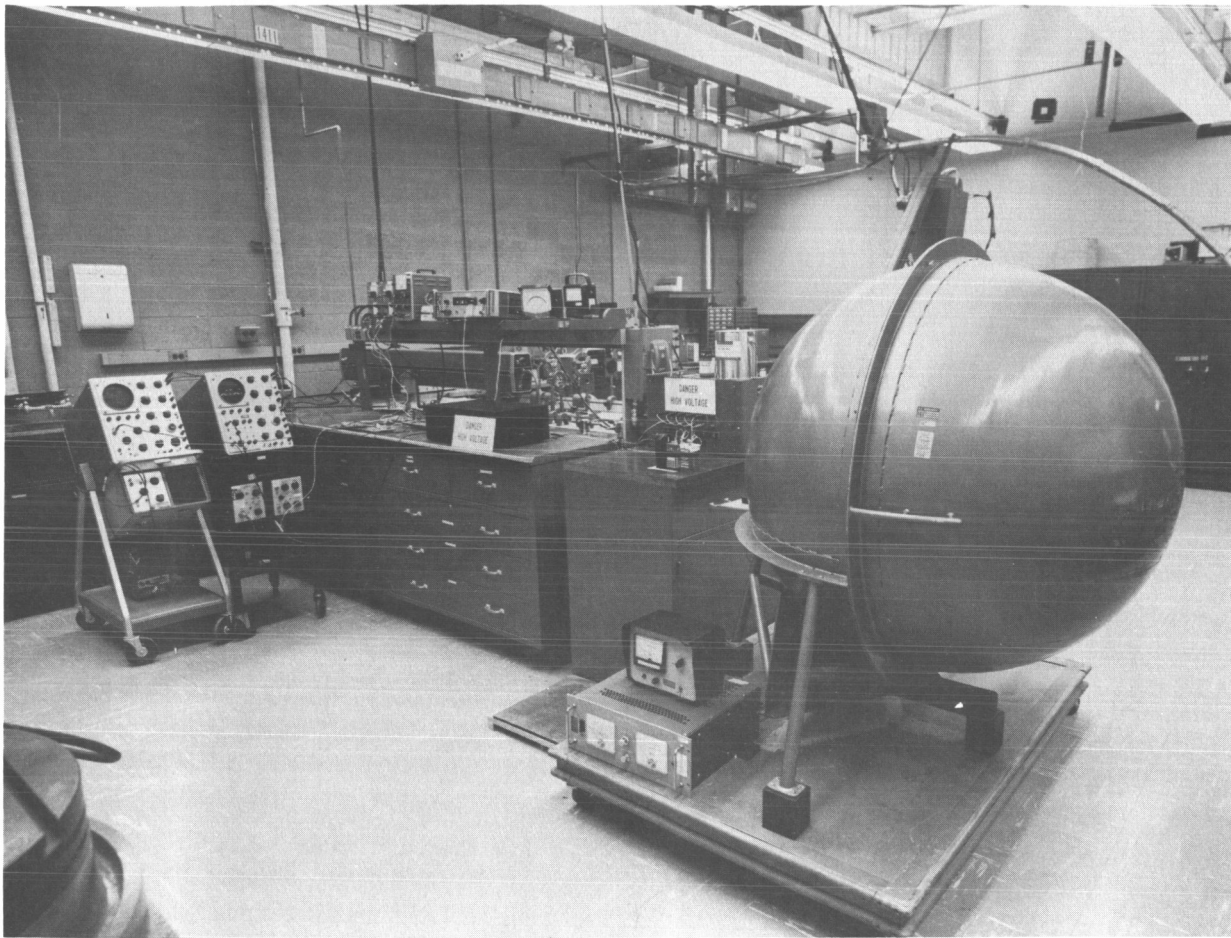


Figure 42. Overall test setup including the four-foot integrating sphere

integrating sphere. The original photopolarimeter breadboard is shown under test on the laboratory bench.

The electronic logic and automatic gain switching were not represented in the electronic breadboard since these represent standard circuitry for which no unusual problems are expected.

Synchronization between beam selector wheel and signal processor switching was accomplished by a miniature light source and a photodiode.

Measurements were made of optical transmissions for various components and were consistent with expectations. Some of these results have been already given in the previous section on optical design. The only optical component used in the breadboard failing to meet specification requirements was the beam mixer which was hastily assembled because of the failure of timely delivery of the Bausch and Lomb model. The model used to operate the beam selector wheel and color filter drive was of the same type recommended in the preliminary polarimeter design and proved adequate for the task. A normal temperature rise was observed. The Geneva movement used was a commercially available model obtained from PIC, Inc. A second unit was life-tested to 6 million cycles with a load simulating the moment of inertia of the color filter wheel. This mechanism has been discussed in the previous section on mechanical design.

2. Beam Trimming Procedure

For the initial breadboard tests, the relative intensities of the three separate beams being compared required trimming in order that the instrument readings would better approximate the true values of the Stokes parameters Q and U . The subsequent trimming of the optical channels which we have denoted as B and D (same notation as original UCLA RFP) was complicated by the presence of residual polarization from the integrating sphere. The Stokes parameters Q and U of the integrating sphere source was assumed small but non-vanishing.

Let us assume that the B and D beams have not been trimmed, but that there is no orientation error of the two prisms (B -prism oriented at precisely 90° and D -prism oriented at precisely 135° relative to the vertical). Denote the value measured by the untrimmed instrument corresponding to the Stokes parameter Q as q . Assume that the optical signal from the B barrel is fB , where for a perfectly trimmed instrument $f = 1$. The instrument will then give a reading

$$q/2 = I/2 - fB.$$

Likewise assume that the D barrel gives a phototube current gD relative to I , where for a perfectly trimmed instrument $g = 1$. The instrument will then read, instead of $U/2$,

$$u/2 = I/2 - gD.$$

It is assumed that polarized beams have been approximately trimmed so that the source polarization is not negligible. We assume no prism orientation errors and can use the results from Chandrasekhar, page 29, to write the intensities which would be measured by the B and D barrels, neglecting the trim mismatch.

$$I_{\psi} = A \cos^2 \psi + B \sin^2 \psi + \frac{U}{2} \sin 2\psi \quad (|V| < 1)$$

$$\text{For } \psi = \frac{\pi}{2}, \quad I_B = B$$

$$\text{For } \psi = \frac{3\pi}{4}, \quad I_D = \frac{A}{2} + \frac{B}{2} - \frac{U}{2} = \frac{I-U}{2}.$$

Now suppose that the barrels are not trimmed relative to the I barrel, i.e.

$$I_B = fB$$

$$I_D = \frac{g}{2} (I-U)$$

How do we determine the constants f and g by using the instrument with a source having some unknown (linear) polarization? Let the values measured for the intensity in the B & D channels be denoted by fI_B and gI_D respectively. It is more convenient at this stage to write the Stokes parameters as:

$$Q = A - B = I_l - I_r$$

Using the double angle trigometric identity we obtain

$$(1) \quad \begin{aligned} Q &= IP \cos 2\psi = I - 2B \\ U &= IP \sin 2\psi = I - 2D \end{aligned}$$

We now consider that the instrument is rotated through an angle α , counter-clockwise looking toward the source. For a perfectly trimmed instrument, new values for Q and U would now be measured. We denote these new values by a prime and from equations (1) can immediately write

$$(2) \quad \begin{aligned} Q' &= IP \cos 2(\psi + \alpha) = IP [\cos 2\psi \cdot \cos 2\alpha - \sin 2\psi \sin 2\alpha] \\ U' &= IP \sin 2(\psi + \alpha) = IP [\sin 2\psi \cdot \cos 2\alpha + \cos 2\psi \sin 2\alpha] \end{aligned}$$

In matrix form the transformation law for Q and U is

$$(2a) \quad \begin{bmatrix} Q' \\ U' \end{bmatrix} = \begin{bmatrix} \cos 2\alpha & -\sin 2\alpha \\ \sin 2\alpha & \cos 2\alpha \end{bmatrix} \begin{bmatrix} Q \\ U \end{bmatrix}.$$

The beam intensities in the new coordinate system are given by

$$(3) \quad \begin{aligned} B' &= \frac{I - Q'}{2} \\ D' &= \frac{I - U'}{2} \end{aligned}$$

equations (2) and (3) then give

$$\begin{aligned} B' &= \frac{I}{2} - \frac{1}{2} (Q \cos 2\alpha - U \sin 2\alpha) \\ D' &= \frac{I}{2} - \frac{1}{2} (U \cos 2\alpha + Q \sin 2\alpha) \end{aligned}$$

Assuming now that the instrument trim factors are f and g, the instrument readings corresponding to Q' and U' will be

$$(4) \quad \begin{aligned} q' &= I - 2fB' = (1-f)I + f(Q \cos 2\alpha - U \sin 2\alpha) \\ u' &= I - 2gD' = (1-g)I + g(U \cos 2\alpha + Q \sin 2\alpha) \end{aligned}$$

If we now make two sets of readings, one set for which $\alpha = 0$ and for which we denote measured values with a prime and a second set with an orientation angle $\alpha = 90^\circ$, for which we denote measured values with a double prime, we obtain a set of four equations in four unknowns:

$$(q' - I) \frac{1}{f} - Q = I$$

$$(u' - I) \frac{1}{g} - U = I$$

$$(q'' - I) \frac{1}{f} + Q = I$$

$$(u'' - I) \frac{1}{g} + U = I$$

Adding the first and third of these equations and the second and fourth give the instrument trim factors

$$f = \frac{q' + q''}{2I} - 1, \quad g = \frac{u' + u''}{2I} - 1.$$

Subtraction gives, subsequently, the unknown Stokes parameters

$$Q = \frac{q' - q''}{2F}$$

$$U = \frac{u' - u''}{2g}$$

In all of the above it is assumed that the response of the I-barrel does not change as the instrument is rotated. If this is not verified in initial tests of the instrument, it will be necessary to trim the I-barrel until such a result is obtained before carrying out the final trim procedure outline. After the instrument is trimmed a useful test will be to use it to measure the Stokes parameters from a polarized source (i.e. integrating sphere viewed through polaroid) and then rotating the instrument about its optic axis. The Stokes parameters Q and U , when plotted as rectangular coordinates should describe a circular path of radius P . This circle will be described twice as the instrument is rotated once ($2a$).

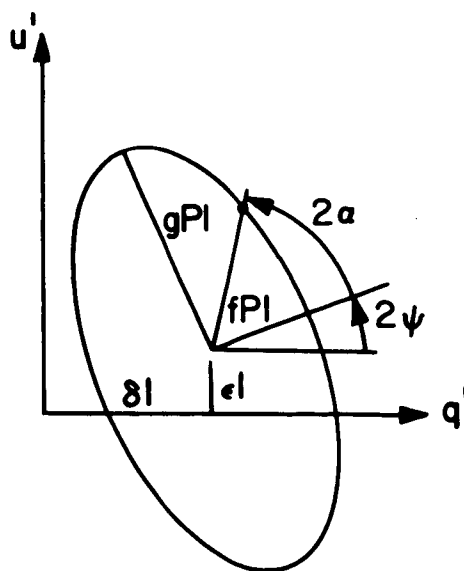


Figure 43. Plot of equation (4)

3. Initial Polarization Measurements and Trimming of the Breadboard Instrument

Based on the assumption that the integrating sphere represents a source of low polarization, the initial trimming was accomplished by masking the objective aperture areas of the B and D channels by the appropriate factors to reduce q and u to low values. In Figure 44, the values of q/I and

u/I obtained as the instrument, viewing the integrating sphere target, was rotated about its optic axis lie within the cross-hatched circle of radius 0.002. An upper limit to the degree of polarization of the source is given by the radius of this circle and is less than 0.2%. The center of the hatched area is displaced from the origin by a very small amount indicating that the initial trim is close to the required final trim.

a) Low Polarization Source

A glass plate placed between the instrument and the integrating sphere and inclined at an angle of 32.7° to the optical axis was used to produce a partially polarized radiation flux. Assuming an index of refraction of 1.5 for the glass, application of the Fresnel equations predicts a degree of polarization of 4.1%. The values for q/I and u/I obtained as the instrument was rotated are shown in Figure 44. The locus obtained is approximately circular (described twice as the instrument makes a single revolution); the center is near the origin as expected since the initial trim is close to the required value and the radius is ~ 0.04 . The measured value for the polarization is in agreement with the estimated value. The slight departures of the locus from a perfect circle is probably related to the lack of parallelism among the individual barrels.

b) Completely Plane Polarized Source

A sheet of polaroid film was used to approximate a perfectly plane polarized source. The parameters q and u obtained as a function of angular rotation of the instrument are plotted in Figure 45. The curve is almost circular, the radius is slightly less than unity as might be expected for a polaroid film and slight trim errors.

4. Scan Function Generator Breadboard

Figure 46 shows a photograph of the breadboard test setup and photographs of oscilloscope traces for the signals at various points of the circuit. Data on numerical performance for this setup has already been discussed in the previous section on electrical design.

U/I vs Q/I OBTAINED BY ROTATION OF PHOTOPOLARIMETER

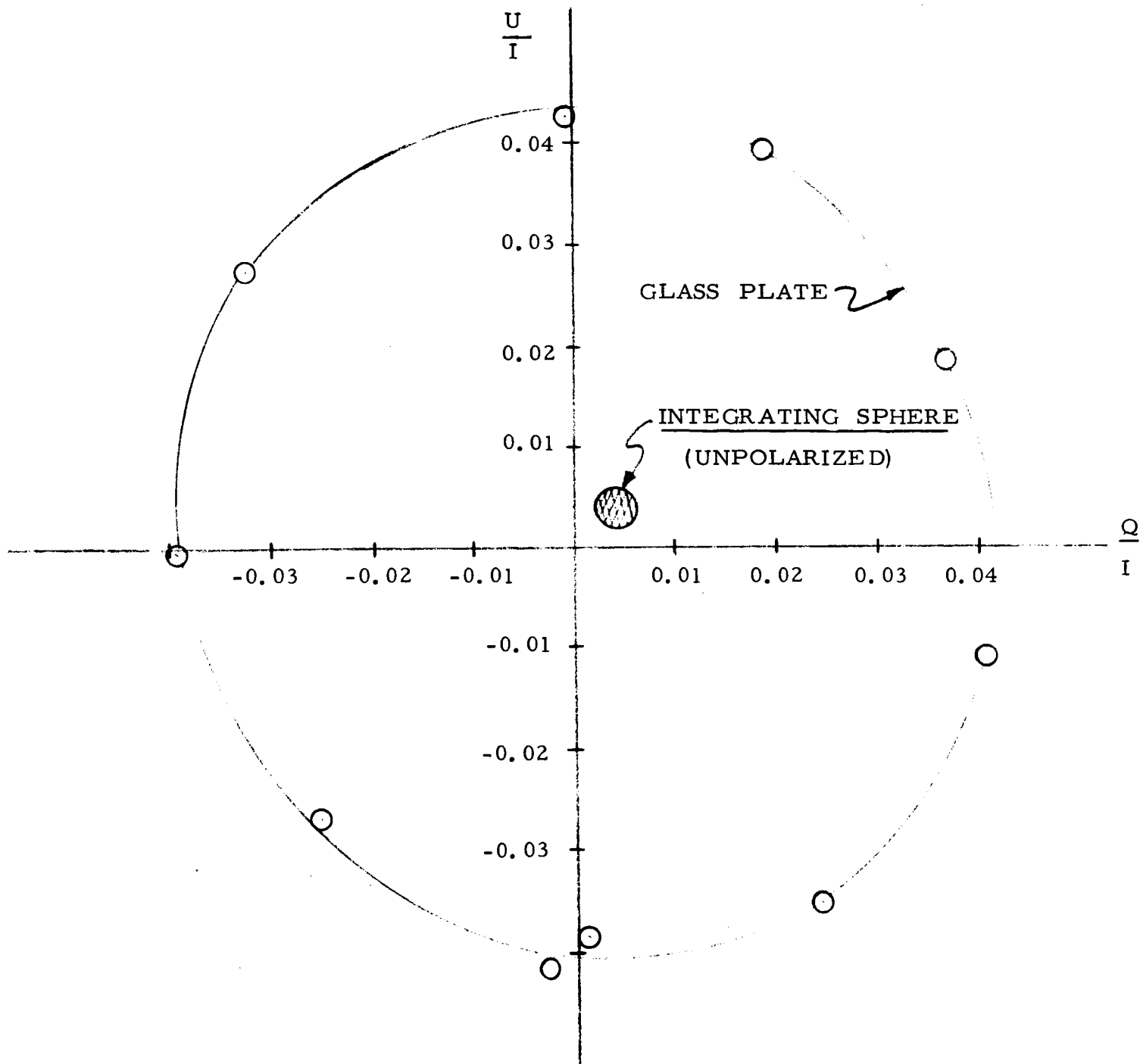


Figure 44

U/I vs Q/I OBTAINED BY ROTATION OF PHOTOPOLARIMETER

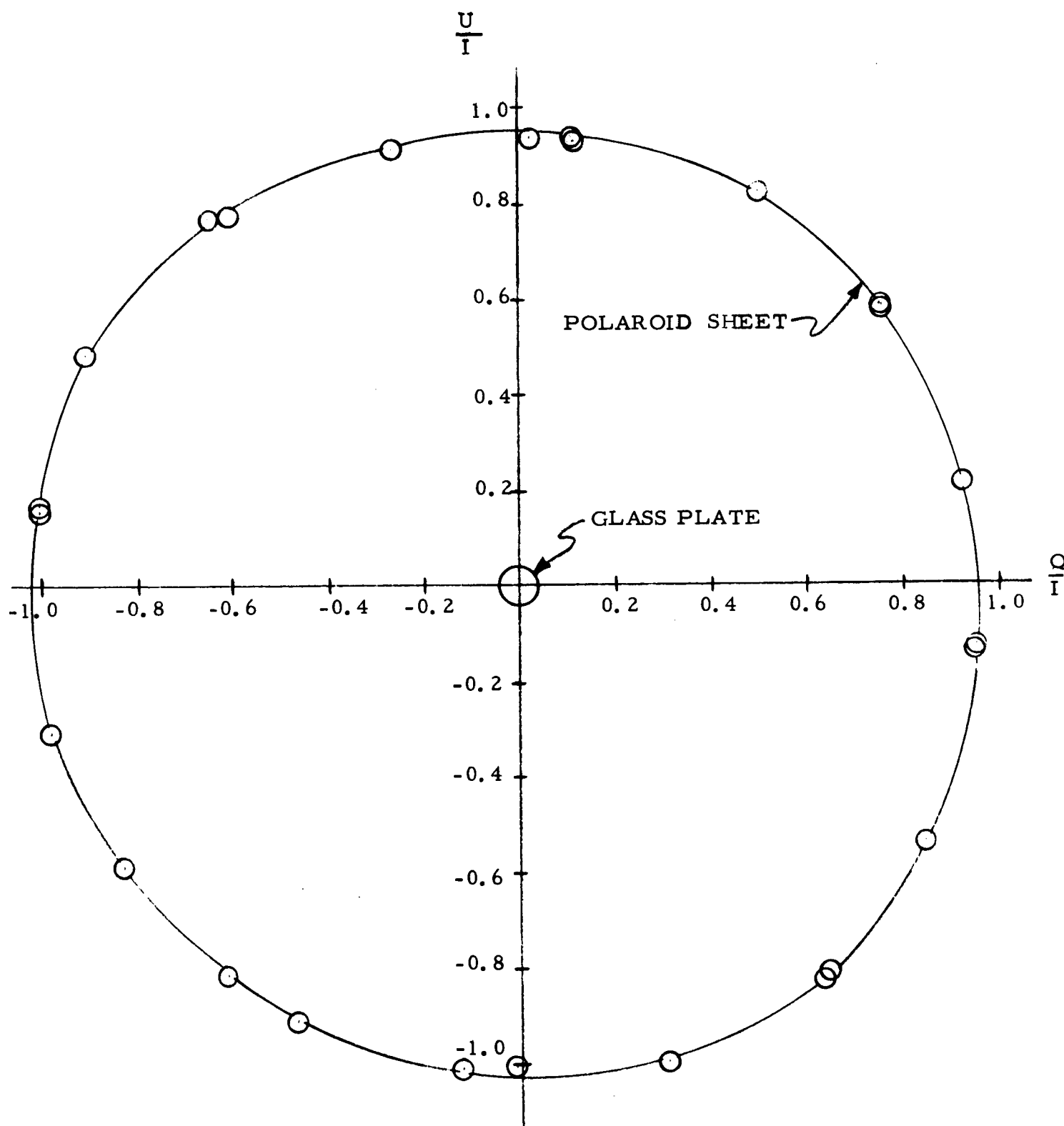
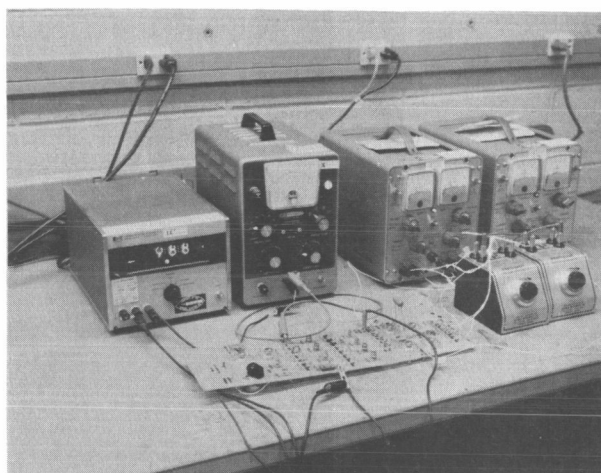
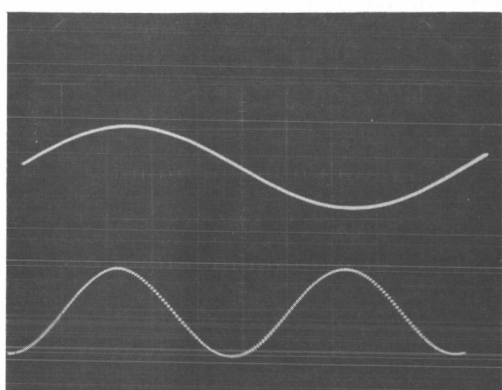


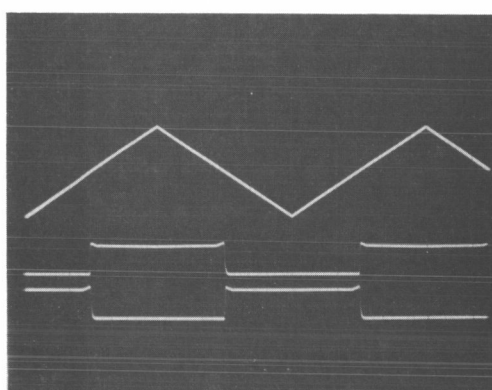
Figure 45



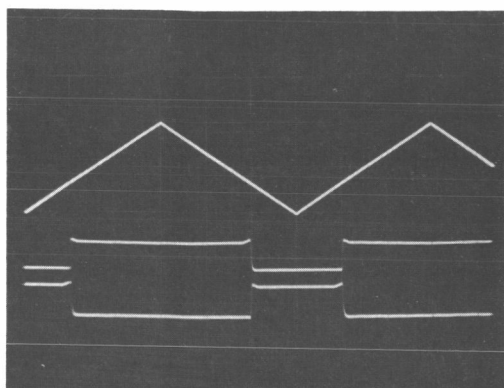
SCAN FUNCTION GENERATOR BREADBOARD TEST SETUP



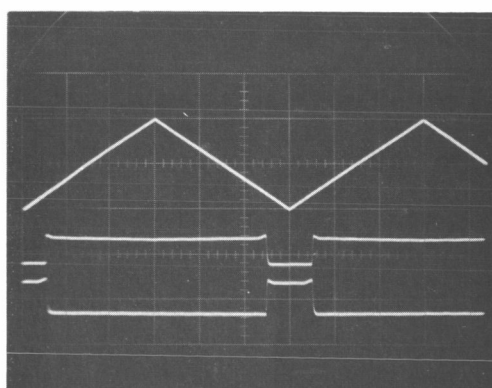
a. $\frac{1 - \cos 2\theta}{2}$ OUTPUT OF SQUARING
CIRCUIT FOR $\sin \theta$ INPUT



b. REFERENCE TRIANGLE WAVEFORM
INTERNAL OSCILLATOR & TIME
CONTROL SWITCH DRIVERS FOR
 $\eta = 0$



c. REFERENCE TRIANGLE WAVEFORM
INTERNAL OSCILLATOR & TIME
CONTROL SWITCH DRIVERS FOR
 $\eta = 0.0333$



d. REFERENCE TRIANGLE WAVEFORM
INTERNAL OSCILLATOR & TIME
CONTROL SWITCH DRIVERS FOR
 $\eta = 0.0667$

Figure 46

V. DOCUMENTATION

A. Preliminary Engineering Specifications

The S046 Experiment End Item specification was rewritten to be in accordance with the draft copy dated November 20 of the Apollo Applications Program Mission AAP-1A General Experiment Specification. Initial work on the specification was in accordance with the content and format of NPC 500-1 and Supplement 1, thereto, dated December 11, 1964. The General Experiment specification was useful in the preparation in the End Item Specification and appears to be more applicable to the experiment than the NPC 500-1 document.

A ground support equipment top specification based on the mission AAP-1A General Experiment specification draft copy dated November 20, 1967 was written. The specification incorporates the S046 experiment checkout stand drawing 902D928 and was prepared on a paragraph by paragraph deviation basis from the General Experiment specification.

Individual specifications have been prepared for component parts or subsystems which are expected to be purchased items. The function generator specifications, which was originally expected to be a separate document, has been combined with the electrical section of the Scan Platform specification since there appears to be both technical and economic advantages to combining these two items. The separate specification for the photopolarimeter instrument was deleted since the instrument is adequately defined in the experiment End Item specification.

Copies of all completed specifications have been delivered to UCLA/NASA. These are listed as follows:

- S046 End Item Specification
- GSE Specification
- Photopolarimeter Instrument Spec. (See Note 1)
- Scan Platform Specification
- Function Generator Spec. (See Note 2)
- In-Flight Calib. Spec.
- Beam Mixer Assembly
- Motor, Gearhead
- High Voltage Power Supply

Note 1 Photopolarimeter Instrument Specification has been adequately defined in the End Item Specification. A separate specification is therefore not required.

Note 2 The Function Generator has been incorporated into the Scan Platform Electronics and it is therefore specified in the electrical portion of the Scan Platform Specification.

B. Management Plans

The management documents specified in UCLA RFP AL 7532 and GE Proposal N-10768 were redefined to be specific sections of a "Management Plan" with each section prepared and issued separately. Section 8.2 of the Apollo Applications Program Mission AAP-A1 General Experiment specification identifies additional sections of a Management plan which were not included in the Phase C contract. Sections of the management plan being supplied in this contract can be identified with their respective sections of the Management plan defined in the General Experiment specification. These sections are listed as follows:

Management Plan Sections

- A Engineering Plan
- B Manufacturing Plan
- C Quality Control Plan
- E Reliability Plan
- F Configuration Management Plan
- G Integrated Test Plan
- H Training Plan
- I Documentation Plan
- J Schedule
- K Cost Plan

The configuration management plan, although not specified as a requirement in the RFP, was prepared to define the organizational and documentation requirements established by the Apollo Configuration Management manual, NPC 500-1 and MSC supplement No. 1. It is in general agreement with the section 7 of the general experiment specification, although it was prepared prior to receipt of this document.

The documentation plan recommends a documentation program based on Exhibit B and C of the UCLA RFP AL 7532, and incorporates the documentation requirements of section 8 of the Apollo Applications Program General Experiment specification draft copy dated October 16, 1967. The November 20 issue of the general experiments specifications has minor revisions which may affect the documentation plan.

C. Functional Plans

A Phase D test plan was written using information supplied by sections 6 and 8 of the General Experiment specification, draft dated November 20, 1967 and Exhibit D of the UCLA RFP AL 7532. The plan identifies the type of qualification and acceptance tests to be provided for the S046 Experiment package and subsystems where necessary. A requirement for the pre-installation and pre-launch test specifications and procedures is identified in accordance with sub-paragraphs of section 6 in the General Experiment specification.

A Reliability Plan and Training Plan were prepared in accordance with the requirement of the UCLA RFP AL 7532 and paragraphs 4-b and 4-c of the GE Proposal N-10768.

A Facilities Plan was developed as a portion of the manufacturing section of the management plan. These plans were coordinated with the development of the cost plan in order to provide a realistic basis for defining the S046 Experiment acquisition phase. The Facilities plan was incorporated into the manufacturing section in accordance with the Phase C Management Plan submitted with Monthly Progress Report No. 1.

The GSE Development plan is considered to be a portion of the Engineering section of the Management Plan as stated in the Phase C Management plan submitted with the Monthly Progress Report No. 1.

The Ground Operations describes ground checkout operations. These are to be rather simple and straightforward, with field checkout requirements being limited to verification of continued operational status for the S046 experiment package and system compatibility tests of the package with the carrier vehicle, Apollo Spacecraft and Launch control system wiring.

D. Technical Reports

A total of forty technical reports were produced during the phase C contract and are listed below with the report number, author, and report titles. These have been delivered to UCLA/NASA as appendices to the Monthly Progress Reports. Essential results of these reports as they influence the preliminary design, have been summarized in this final report.

<u>Number</u>	<u>Title</u>	<u>Author</u>
UCLA-001	Lubricant Deposition on Optical Surfaces	Frost
UCLA-012	Photomultiplier Selection	Stockhoff

<u>Number</u>	<u>Title</u>	<u>Author</u>
UCLA-014	Illumination of a Photomultiplier Cathode by a Fiber Optics Bundle	Stockhoff
UCLA-016	Lubrication Optics Test	Lee
UCLA-017	System Dynamic Range Considerations	Frost
UCLA-018	Solar Calibrator Unit	Shaw
UCLA-020	Photomultiplier Gain Stability in the Presence of Anode Current	Napaluch
UCLA-021	High Voltage Supply Regulator for S046 Experiment	Napaluch
UCLA-022	Calibration Source	Shaw
UCLA-023	Dynamic Range Calculations	Halsey
UCLA-024	Investigation of an Alternate Mechanism to the Geneva Drive for Rotating the Filters	Pater
UCLA-027	Identification of Optical Elements	Halsey
UCLA-028	Acceleration and Shock Characteristics of Geneva Mechanism	Frost
UCLA-029	Color Filters	Halsey
UCLA-031	Preliminary Design Definition	Lee
UCLA-032	Effects of Thin Oil Films on Optical Components	Shaw
UCLA-034	Meeting to Discuss Lubricant-Optics Interaction Problem	Frost
UCLA-035	Scan Platform (Preliminary Selection)	Stanhouse
UCLA-036	Meeting with Ordnance Department on Scan Platform for Experiment S046	Stanhouse
UCLA-037	Beam Mixing Uniformity Requirements	Frost

<u>Number</u>	<u>Title</u>	<u>Author</u>
UCLA-039	A Method for Planned Mixing of the Three Input Beams	Lee
UCLA-040	Fiber Optics-Photomultiplier Tests	Stockhoff
UCLA-041	Intensity Uniformity Requirements for Beam Mixer Unit	Shaw
UCLA-043	Optimum Phototube Gain, Dynamic Range of Processed Signals, and Value for Pre-amplifier Feedback Resistor	Frost
UCLA-045	Calibrations Based on an Integrating Sphere Method (Solar and Tungsten Lamp). Comparison with Imaging Systems	Shaw
UCLA-046	Beam Mixer Specification	Frost
UCLA-047	Initial Breadboard Tests and Beam Trimming	Frost
UCLA-049	S046 Experiment-Initial Weight Estimates	Lee
UCLA-051	S046 Experiment Initial Power Profile	Lee
UCLA-052	High Voltage Power Supply Design Reference: PIR UCLA-20-21	Napaluch
UCLA-053	The Pitch Scan Function Generator for the S046 Experiment	Napaluch
UCLA-054	Statistical Noise Limitations and Other Measurement Errors for S046	Frost
UCLA-055	Non-Linearities, Maximum Permissible Phototube Currents, Required HV Regulation	Frost
UCLA-056	Internal Calibration Standard	Frost
UCLA-057	Spurious Polarization Due to Window and Lens	Frost
UCLA-058	Color Filters	Halsey
UCLA-059	Advanced Breadboard Optical System	Halsey

<u>Number</u>	<u>Title</u>	<u>Author</u>
UCLA-060 Revision A	Breadboard Trim and Initial Polarization Measurements	Shaw and Stockhoff
UCLA-061	Electronic Gain Settings and Gain Overlap Regions	Frost
UCLA-062	S046 Processor, Gain Change and Polarity Control Circuits	Napaluch

E. Preliminary Design Review

The Preliminary Design Review called for under terms of the Phase C contract, was held at General Electric Space Sciences Laboratory on December 4 and 5, 1967, and the minutes of the review were mailed to UCLA/NASA on 15 December 1967.

The objective of the Preliminary Design Review was to establish the correctness of the design approach. Areas considered were:

- o Comparison of the design with the requirements
- o Examination of the basic analyses and tradeoffs
- o Examination of interfaces
- o Recognition and definition of problem areas
- o Evaluation of the test results on the breadboard instrument
- o Establishment of action items and recommendations

Action Items Recommended

- o More detail to be provided on preliminary design drawings of the inflight calibrator, the scan platform mechanisms, and the general deployment mechanism for the in-flight calibrators.
- o Circuit diagrams for electronics to be included in final report together with explanations of circuit operation.
- o Minimum orbit height adjustment to scanner mechanism to be changed from 150 nautical miles to 125 nautical miles.
- o In-orbit time to be changed from two weeks to four weeks and an alternate in-orbit condition of 40 hours operating time and 52 weeks total time to be added.
- o Possible sensitivity of total intensity channel to source polarization due to lack of complete depolarization of fibre optics and polarization sensitivity of photomultiplier needs resolution.
- o S046 end item specification format to be changed to conform to specimen furnished by Mr. Hergert.

These action items have now all been accomplished.

Conclusions, Recommendations

It is recommended that the Final Design for the S046 Experiment be based on the Preliminary Design, where supported by test results as reported herein. In several areas where engineering tradeoffs have not been made based on testing, it is recommended that detailed choices of components be left open until the final design. Examples of choices left open in the present preliminary design are the following:

- o Coherent vs "scrambled" beam mixer
- o Phototube type
- o Detailed choice of discrete motion mechanism for color filter
- o Detailed mechanical configuration required for weight reduction

REFERENCES

1. Sekera, Z. (1966) - "Scattering Functions for Rayleigh Atmospheres of Arbitrary Thickness", RAND R-452 PR.
2. Sekera, Z. (1963) - "Radiative Transfer in Planetary Atmospheres with Imperfect Scattering", RAND R-143-PR.
3. Arking, A., and Potter, J., Private communication.
4. Sekera, Z. (1966) - "Determination of Atmospheric Parameters from Measurement of Polarization of Upward Radiation by Satellite or Space Probe", RAND Report RM-5158-PR.
5. Pellicori, S.F., and Gray P. R., Applied Optics 6, 1121 (1967).

APPENDIX
(PIR 2290-41)

	<u>Page</u>
Introduction	1
I. Spherical Earth, Circular Orbit	2
A. Vehicle Ground Track	2
B. Scan Platform Pointing Direction	2
C. Great Circle Vehicle - Target Separation as Function of Time	3
D. Out-of-Plane Pointing Angle ξ	5
E. Summary of Pointing Requirements	5
F. Required Nadir Angle z as Function of Time	6
II. Correction for Earth Oblateness	6
A. Correction to Tracking Rate	6
B. Conversion of Geodetic Latitude to Geocentric Latitude L_T .	7
III. Correction for Target Height	8
IV. Correction for Orbit Eccentricity	8
V. Generalized Block Diagram of Scanning Mechanism	

GENERAL ELECTRICMISSILE AND SPACE DIVISION
PHILADELPHIA**PROGRAM INFORMATION REQUEST / RELEASE**

NO.

2290-41

FROM R. T. Frost, Space Physics Section Room M9533 - Ext. 3517		TO Dr. T. A. Hariharan UCLA	
DATE SENT	DATE INFO. REQUIRED	PROJECT AND REQ. NO.	REFERENCE DIR. NO.
SUBJECT Scan Platform Requirements - UCLA Photopolarimeter			
INFORMATION REQUESTED / RELEASED <u>Introduction</u> <p>The purpose of this memo is to derive the tracking requirements for a scan platform in order to track an earth fixed target from a satellite in low altitude orbit. We will restrict our attention to the case where targets are used which pass directly under the vehicle track. This restriction simplifies the problem considerably and is permissible in the case of Meteorological Experiment #8 of the APSA package of experiments. Instead of precise analytical expressions for the required tracking angles it was desired to derive simple and useful expressions which would be valid to an accuracy of 0.1° or so and which would best lend themselves to mechanization of the scan mechanism. These expressions are summarized in Section E on page 5. Effects of orbit inclination, precession, eccentricity, period, target latitude and height and earth oblateness are included. It is found that all of these effects can be combined to two or three rate adjustments.</p>			
DISTRIBUTION H. Blau, A. Petty, E. Gray, G. Wouch, D. Lee(4), Prof. Sekera, Dr. Hariharan, C. Boman(Farrelley)			PAGE NO. 1 OF 9 CONT. ON

I. Spherical Earth, Circular Orbit

A. Vehicle Ground Track

The true anomaly ψ of the vehicle, measured from the ascending node Ω is (1) $\psi = 2\pi t/T$ radians, where time is reckoned from time of crossing the ascending node and t and T are in the same units. To most simply derive the required geometric relationships, it is helpful to project the orbit plane onto the celestial sphere as a great circle. The North pole projects as the point N, the line of nodes as the point Ω , and the vehicle and target positions as the points V and T. It is then easy to visualize the problem in terms of spherical trigonometry. See Fig. 1.

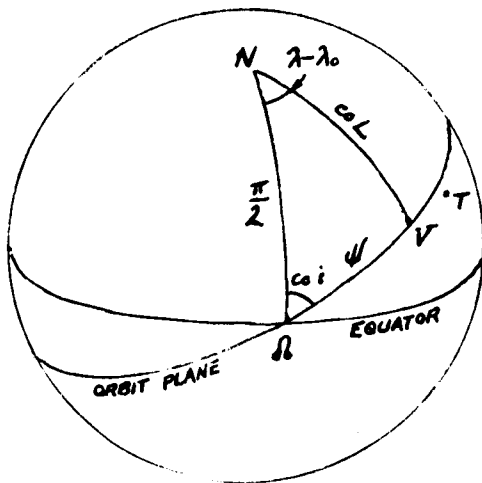


Fig. 1

The vehicle latitude L and longitude λ are given by (2) $\begin{cases} \sin L = \sin \psi \sin i \\ \tan (\lambda - \lambda_0) = \tan \psi \cos i \end{cases}$ where i is the orbit inclination.

The angle $\lambda - \lambda_0$ is chosen in the same quadrant as ψ for inclinations less than 90° and the longitude λ_0 of the ascending node Ω is given by $\lambda_0 = \Lambda + (\omega + \Omega)t$ (3) Λ is the longitude of the ascending node at $t = 0$

ω is the sidereal angular velocity of the earth, $\frac{366.25}{365.25} \times 15^\circ/\text{hr}$ and

$$\dot{\Lambda} = \frac{(8.6^\circ/\text{day}) \times \cos i}{a^2(1-e^2)^2} \quad \begin{matrix} \text{(orbit semimajor axis} \\ \text{a in earth radii)} \end{matrix}$$

e is the orbit eccentricity and i the inclination.

Ω is the rate of precession of the line of nodes

B. Scan Platform Pointing Direction

In the local horizon coordinates of the vehicle, the pointing direction in zenith angle z and azimuth ζ required to intercept a target located at a fixed latitude and longitude L_T, λ_T can be found from the plane triangle determined by the vehicle, target, and earth's center as: (4) $\frac{\sin(z + \eta)}{h + R} = \frac{\sin z}{R}$

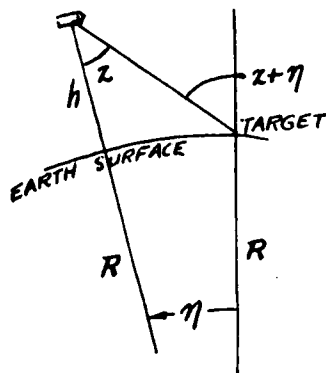


Fig. 2

where h is the orbit height and R the earth's radius. η is given by:

$$(5) \cos \eta = \sin L \sin L_T + \cos L \cos L_T \times \cos (\lambda - \lambda_T) \quad \text{and} \quad \text{(See Fig. 2)}$$

$$(6) \sin \zeta = \cos L_T \sin (\lambda_T - \lambda) / \sin \eta.$$

We wish to display the form of $z(t)$ in terms of departures from a simple flat earth model, and the variations $Z(t)$ in terms of departure from the orbit plane. It is somewhat easier to effect these expressions in terms of the "orbital" coordinate system ψ , rather than in terms of the earth-fixed coordinates L, λ . The foregoing analysis is required, however, in computing the ground track of the vehicle and thus determining which of the pre-selected target areas will pass beneath the vehicle position in a given orbit.

C. Great Circle Vehicle-Target Separation as Function of Time

The trajectory of the target projection on the celestial sphere during the scan is well approximated by a great circle*. The great circle arc between the target position and its position when it passes beneath the orbit plane is given by

$$\cos \beta = \sin^2 L_T + \cos^2 L_T \cos(\omega + \Omega)(t - t_T) \quad (\text{See Fig. 3})$$

t_T is the time at which the target passes beneath the vehicle.

The foregoing expression is well approximated during the scan interval by

$$(7) \quad \beta = (\omega + \Omega)(t - t_T) \cos L_T = \omega'(t - t_T) \cos L_T$$

We now consider, on the celestial sphere, the intersection I of the target projection track and the vehicle projection track. (Fig. 4). The angle α at which the tracks intersect is given by

$$(8) \quad \cos \alpha = -\cos i / \cos L_T \quad (\text{See Fig. 5})$$

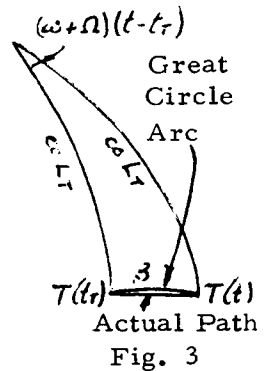


Fig. 3

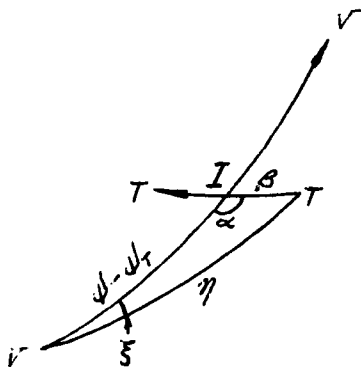


Fig. 4

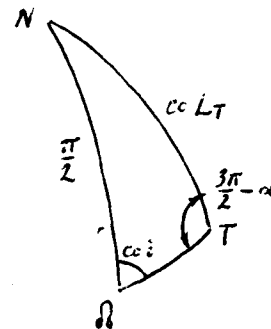


Fig. 5

The vehicle anomaly ψ , relative to the point where the target passes directly beneath the vehicle, is given by (9) $\psi - \psi_T = 2\pi \frac{t - t_T}{T}$ where t_T is the time at which the target passes beneath the vehicle.

*The maximum departure between the actual small circle path and the great circle arc for moderate latitudes is approximately $1/2 \times 10^{-4}$ rad = 0.005° during a given scan.

The separation angle η between vehicle and target is then given by:

$$(10) \quad \cos \eta = \cos(\psi - \psi_r) \cos \beta + \sin(\psi - \psi_r) \sin \beta \cos \alpha$$

Using (8) we obtain

$$\cos \eta = \cos(\psi - \psi_r) \cos \beta - \sin(\psi - \psi_r) \sin \beta \cos i / \cos L_r$$

We note that $\psi - \psi_r \lesssim 10^{-1}$ and $\beta \lesssim 10^{-2}$

To good approximation,

$$(11) \quad \eta = (\psi - \psi_r) \sqrt{1 + 2 \frac{\beta}{\psi - \psi_r} \frac{\cos i}{\cos L_r}} = (\psi - \psi_r) \sqrt{1 + \frac{\omega' T}{\pi} \cos i} \quad \text{where we have used (7) and (9).}$$

In the absence of earth rotation, we would have $\eta = \psi - \psi_r = 2\pi \frac{t - t_r}{T}$

The maximum correction in tracking rate $\dot{\eta}$ occurs for zero inclination for which the tracking rate is increased by the factor $f = \sqrt{1 + \frac{2}{n} \cos i} = \sqrt{1 + \frac{2}{n}}$

where n is the ratio $\frac{2\pi}{T}/\omega'$ of orbital angular rate to the rate of rotation of Earth with respect to the precessing orbit plane. (n is approximately the number of orbits per day). For $T = 90^{\text{min}}$, $n \approx 16$ and $f \approx 1.06$.

We note that, in the approximation given by (11), the separation angle η is a linear function of time.

$$(12) \quad \eta = f \cdot 2\pi \frac{t - t_r}{T}$$

The time rate $\dot{\eta}$ depends upon the inclination i and, through the orbital period T , on the orbit height.

As an example, for a 30° inclined, 90 minute orbit, the difference in the time rate $\dot{\eta}$ to that for zero inclination is given by a factor of approximately

$$\frac{\sqrt{1 + \frac{2}{16} \cos 30^\circ}}{\sqrt{1 + \frac{2}{16}}} = \frac{1.108}{1.124} = 1 - \frac{1}{2} \frac{0.016}{1.062} = 0.992$$

For an inclination of 90° , however, the rate is 6% lower than for zero inclination.

D. Out of Plane Pointing Angle

The out-of-plane angle ξ (see figure 4) is given by $\sin \xi = \sin \beta \sin \alpha / \sin \eta$

The smallness of ξ, β and η allows the expansion

$$(13) \quad \xi \approx \frac{\beta}{\eta} \sin \alpha = \pm \frac{\omega' T \cos L_r}{2 \pi f} \sqrt{1 - \left(\frac{\cos i}{\cos L_r} \right)^2} = \pm \frac{\cos L_r}{nf} \sqrt{1 - \left(\frac{\cos i}{\cos L_r} \right)^2}.$$

We note that, to excellent approximation, the out-of-plane angle ξ doesn't change during a given scan, but does depend upon orbit inclination i and target latitude L_r . The maximum required out-of-plane azimuth occurs for the maximum α , i. e. for minimum $\frac{\cos i}{\cos L_r}$ or for $L_r = 0$. For $i = 30^\circ$, we have

$$\xi = \pm \frac{\sin i}{nf} \approx \pm \frac{1}{2n\sqrt{1 + \frac{13}{n}}} \approx \pm .03 \approx \pm 2^\circ \quad \text{The + sign applies when the vehicle}$$

is south of the target; the - sign when it is north. Since in-plane tracking will thus lead to angular errors which are sizeable unless the target is near the nadir, it would be advisable to bias the scan axis of the instrument by an amount ξ dependent upon the target latitude. It is suggested that incremental steps of 0.25° or 0.50° would be sufficient.

E. Summary of Pointing Requirements

The design of the scanning mechanism is governed by equations (4), (12) and (13). For convenience, we summarize these here:

$$(4) \quad \sin (z + \eta) = (1 + u) \sin z$$

$$(12) \quad \eta = \frac{f}{T} 2 \pi (t - t_r)$$

$$(13) \quad \xi = \pm \frac{\cos L_r}{nf} \sqrt{1 - \left(\frac{\cos i}{\cos L_r} \right)^2} \quad \text{where we have introduced the parameters}$$

$$u = \frac{h}{R} = \text{ratio of orbit height } h \text{ to earth radius } R$$

$f = \sqrt{1 + \frac{2}{n} \cos i}$ = ratio of rate $\dot{\eta}$ to its value for a non-rotating earth and a non-precessing orbit plane.

n is the ratio $\frac{\omega' T}{2\pi}$ of angular rate $\dot{\psi}$ to the rotation rate of Earth with respect to the precessing orbit plane.

F. Required Nadir Angle z as Function of Time

The output of the scan mechanism is of course the desired nadir angle $z(t)$ and azimuth ξ in the local horizon system of the vehicle. ξ is measured with respect to the orbit plane rather than with respect to the local north direction..

Trigonometrical relations other than (4) relating z and η are of course possible. The relation (4) is convenient, however, for it allows a rapidly convergent power series expansion for $\tan z$ in which the leading term gives the "flat earth" approximation. We re-write (4) as

$\sin z \cos \eta + \cos z \sin \eta = (1 + u) \sin z$ and exploit the fact that $\eta \leq 10^{-1}$.
 $\sin z \left(1 - \frac{\eta^2}{2} + \frac{\eta^4}{24}\right) + \cos z \left(\eta - \frac{\eta^3}{6}\right) = (1 + u) \sin z$ Noting that $\frac{\eta^4/24}{\eta^2/2} = \frac{\eta^2}{12} \leq 10^{-3}$
 and $\frac{\eta^3/6}{\eta} = \frac{\eta^2}{6} \leq 1.6 \times 10^{-3}$, we drop the last terms in the $\cos \eta$ and $\sin \eta$ expansions and obtain, to sufficient accuracy.

$$(14) \quad \tan z = \frac{\eta}{u + \eta^2/2} = \frac{\eta}{u} \frac{1}{1 + \eta^2/2u} \approx \frac{\eta}{u} \left[1 - \frac{\eta^2}{2u} + \left(\frac{\eta^2}{2u}\right)^2 \right]$$

The third term has a magnitude which never exceeds $\left(\frac{10^{-2}}{2 \times 0.05}\right)^2 \approx 10^{-2}$ but

its neglect would lead to an error Δz in z given by

$$\sec^2 z \cdot \Delta z \leq \frac{\eta}{u} 10^{-2} \text{ or } \Delta z \leq \frac{2 \times 10^{-2}}{4/3} = 0.015 \approx 0.75^\circ \text{ and hence the third term}$$

should be retained.

II. Correction for Earth Oblateness

A. Correction to Tracking Rate

The tracking rate correction for earth oblateness can be made simply by allowing the orbit height h to vary with target latitude L_r . This variation in orbit height affects the parameter $u = h/R$ in formula (4) but doesn't affect the orbit period T .

This should cause no confusion as long as the orbit period is entered separately and is not calculated from $T \sim (1+u)^{3/2}$.

If a^* and b are the equatorial and polar radii of the earth, the variation of h with L_T is expressed as follows:

$$\frac{R^2 \cos^2 L_T}{a^{*2}} + \frac{R^2 \sin^2 L_T}{b^2} = 1$$

For small eccentricities e^* this can be expanded to $R \approx a^*(1 - \frac{1}{2}e^2 \sin^2 L_T) = a^* + \Delta R$

$$u = \frac{h}{R} = \frac{h_0 - \Delta R}{a^* + \Delta R} \approx u_0 - (1+u_0) \frac{\Delta R}{a^*}$$

where u_0 is the orbit height parameter where the orbit crosses the equator. $u_0 = \frac{h_0}{a^*}$

$$(15) \quad u = u_0 + (1+u_0) \frac{e^2 \sin^2 L_T}{2}$$

The earth oblateness is customarily given in terms of

$$\frac{a^* - b}{a^*} = \frac{21.5}{6378.4} = 1 - \frac{b}{a} \approx e^2/2$$

$$\text{whence } \frac{e^2}{2} = 3.37 \times 10^{-3}$$

$$\text{For } L_T = 30^\circ, \sin^2 L_T = \frac{1}{4} \text{ and } u = u_0 + (1+u_0) 0.84 \times 10^{-3}$$

$$= u_0 + 0.88 \times 10^{-3} \quad (u_0 \approx .05)$$

and the oblateness effect is equivalent to a 10.8 km change in orbit height. We have implicitly used L_T every where to represent the geocentric latitude of the target instead of the geodetic latitude.

B. Conversion of Geodetic to Geocentric Latitude

We use the approximate geoid expression

$R = a^*(1 - \frac{e^2}{2} \sin^2 L_T)$ to derive the geodetic latitude ℓ as a function of geocentric latitude L_T . The difference $\ell - L_T$ between the two types of latitude is given by (see Fig. 6)

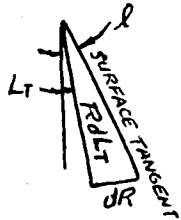


Fig. 6

$$l - L_T = \tan^{-1} \left(-\frac{dR}{R dL_T} \right) \approx \tan^{-1} (e^2 \sin L_T \cos L_T)$$

OR (16) $l - L_T \approx e^2 \sin L_T \cos L_T \approx e^2 \sin l \cos l$

The maximum difference $l - L_T$ thus occurs for $L_T = 45^\circ$, where it attains a value

$$\frac{e^2}{2} = 3.37 \times 10^{-3} \approx 0.00337$$

Since the tracking formulae are simpler when expressed in terms of geodetic latitude, it is recommended that the known geodetic latitude of desired targets be converted to geocentric latitude through the use of expression (16)

III. Correction for Target Height

Since cloud tops may be viewed up to perhaps 10 mi., this should be allowed for in a similar manner through the parameter u . For a target height h_T above the geoid, the change in u is

(16) $u = - (1+u) \frac{h_T}{R}$ the orbit period being of course left unchanged.

IV. Correction for Orbit Eccentricity

From the Kepler's Third Law, $(1+u)^2 \dot{\psi} = \text{constant}$ where u is the orbit height $\frac{h}{R}$ without correction for earth oblateness or target height.

Kepler's 3rd law may be written $\dot{\psi} = \frac{2\pi}{T} \left(\frac{a}{r} \right)^2 \sqrt{1-e^2}$

This is to be compared with the expression $\dot{\psi} = \frac{2\pi}{T}$ used in expression (12) where a circular orbit was assumed.

For the general case, we see that the fractional variation in $\dot{\psi}$ from its value for a circular orbit can be written as

$$\frac{\Delta \dot{\psi}}{\dot{\psi}} = -2 \frac{\Delta r}{r}$$

Since it is expected that the orbit achieved will give $\Delta r \lesssim 5$ mi, we expect

$\frac{\Delta \dot{\psi}}{\dot{\psi}} \lesssim -2 \frac{5}{4000} \approx -0.0025$. This is small enough that the cumulative error in z resulting

from neglect of orbit eccentricity would be $\sim .0025 \times 120^0 \frac{4}{3} \approx 0.4$ and might be considered negligible. However, since the rate $\dot{\eta}$ must in any event be adjusted for T and i, we can use the same adjustment to compensate for the variation of $\dot{\psi}$ in an eccentric orbit.